Monitoring and Modeling Changes in the Atmospheric Aerosol Properties and Surface UV radiation over the Northeast Asia

APN Project 2002-14

Final Activity Report

ADEMRC

(ADvanced Environmental Monitoring Research Center)

APN

(Asia-Pacific Network for Global Change Research)

Final Activity Report for APN Project

- **Project Title : Monitoring and Modeling Changes in the Atmospheric Aerosol Properties and Surface UV radiation over the Northeast Asia**

- **Project No. : APN 2002-14**

- **Abstract**

During the study period UV-B broadband instruments were used to monitor the surface UV variation at Mongolia and Kyoto. MFR and UVMFR (Gwangju) were used to monitor the spsectral aerosol optical depth at visible and wavelength range, respectively (Gwangju, and RSR at Gwangju, Ulaanbaator). Two intensitve aerosol sampling were conducted from 23 July to 1 August, and from 5 to 16 November at four measurement sites (Gwangju, Kyoto, Ulaanbaator, and Beijing). Chemical characteristics of aerosols and backward trajectory were analysed. Radiative transfer model was also used to investigate the aerosol effect on the surface UV radiation.

- **Project Information**

This project was leaded by Prof. Young J. Kim

Advance Environmental Monitoring Research Center (ADEMRC), Kwangju Institute of Science and Technology, 1-Oryongdong, Buk-gu, Gwangju 500-712, Republic of Korea
Tel:82-62-970-3401, Fax:82-62-970-3404, yjkim@kjist.ac.kr

APN Funding

US$60,000

Participating countries

Korea, Japan, China, Mongolia

- **Introduction**

  Atmospheric aerosol particles influence the Earth's radiation balance directly and indirectly and affect human health. The radiative forcing by anthropogenic aerosol particles due to the combined effects is estimated to be in the range between -0.4 and -3.0 W/m2 on a global scale. There is substantial uncertainty in the magnitude and spatial distribution of the radiative forcing by aerosols. This uncertainty significantly limits our ability to assess the effect of natural and human induced changes in the chemistry of the atmosphere on global climate.

  Increased UV radiation has effects on human health, in particular human skin disease and has effects on biosphere. Thus it is necessary to monitor aerosols and UV radiation at ground stations. The spatial and temporal variations of aerosol are affected by regional meteorological conditions. Because emitted air pollutants have effects not only on originating country but also the neighbor nations, it is not national problems but an international issue. Therefore there exists need for international collaboration on characterizing atmospheric aerosols and their impact on UV radiation in the Northeast Asia.

- **Activities Conducted**

  1. Chemical and physical properties of aerosols over the Northeast Asia.

  Aerosol samples were collected with aerosol samplers such as PM2.5 cyclone and MOUDI (Micro-Orifice Uniform Deposition Impactor). The collected samples were analyzed to determine aerosol mass, ionic, and elemental composition, organic carbon and elemental carbon (OC/EC), and aerosol size distribution. We had conducted the intensive sampling twice over four countries simultaneously in August and November, 2002.

  2. Aerosol radiative properties over the Northeast Asia region

  By using RSR plus MFRSR (Multi-Filter Rotating Shadowband Radiometer) AOD was monitored to investigate the changes in atmospheric aerosol loading in the Northeast Asia. From October, 2002

spectral AOD measurement at UV wavelength range began using Ultravilet MFR. We monitored the atmosphere of four countries from 2000 and making a database to do a model of atmospheric transfer.

3. Surface UV radiation.

The changes in UV radiation were monitored by UV-A and UV-B radiometers at ground stations. UV-B radiometers are located at Gwagnju, Ulaanbaatar, and Kyoto. Measured aerosol and UV data are to be analyzed to characterize the impact of atmospheric aerosols on UV radiation and to provide information on atmospheric compositions changes.

4. Radiative transfer modeling

The radiative transfer modeling was performed to investigate the effects of aerosols, clouds and ozone on the atmosphere transmission of UV radiation. The modeling of air mass back-trajectory analyses were also done by using the HYsplit program which covers major anthropogenic source and downwind regions.

.

- **Outcomes and Products**

-Conference presentations

UV Irradiance monitoring and effects of aerosol optcial depth on the ground-based measurement of ultraviolet irradiance at Kwsangju, Korea, Young J. Kim, Jeong E. Kim, Seong Y. Ryu, and Kehinde O. Ogunjobi (SPIE's Third Int'l Asia-Pacific Environmental Remote Sensing Symposium Remote Sensing of the Atmosphere, Ocean, Environment, and Space 2002, 23-27 October 2002, Hangzhou, China)

Spectral Aerosol Optical Depths and Atmospheric Turbidity In Kwangju, South Korea, Ogunjobi Kehinde, Y. J. KIM, J. E KIM and S.Y RYU

Comparisons of carbonaceous specious of PM2.5 aerosol over the Northeast Asia in 2001, Ryu Seongyun, Jeong E. Kim, Young J. Kim, M. Kasahara, S. Guangyu

Surface UV Radiation Comparison over the Northeast Asia, Jeong Eun Kim, Seong Yun Ryu, Kehinde O. Olufunso, Young J. Kim (The 4th

International Symposium on Advanced Environmental MonitoringDecember 4-6, 2002, Jeju, Korea)

- Web page will be available for access in March 2003.

ADEMRC (Advanced Environmental Monitoring Research Center) will create and maintain a website dedicated to the APN project. Thus all scientific results from the proposed study will be available for immediate dissemination to the scientific community.

.

- **Conclusions**

From the study conducted during the period aerosol chemical and radiative properties were investigated for summer, fall and Asian dust event over the Northeast Asia. Mass and ion concentration was higher in November than in August over the measurement sites. Seasonal variation was not very distinct because insufficient data because of lots of cloudy days during the study period. With the help of backward trajectory and radiative transfer modelling we could trace the air mass for intensitve sampling period, and the aerosol effect on the surface UV irradiance due to atmospheric aerosol loadings.

- **Future Directions**

Aerosol intensive sampling and radiation monitoring will continue over four network sites (Gwangju, Kyoto, Mongolia and Beijing) in order to get the sufficient database to reduce the uncertainty in predicting aerosol forcing on the climate.

Atmospheric aerosol particles influence the Earth's radiation balance directly and indirectly and affect human health. The radiative forcing by anthropogenic aerosol particles due to the combined effects is estimated to be in the range between -0.4 and -3.0 W/m2 on a global scale. There is substantial uncertainty in the magnitude and spatial distribution of the radiative forcing by aerosols. This uncertainty significantly limits our ability to assess the effect of natural and human induced changes in the chemistry of the atmosphere on global climate.

Increased UV radiation has effects on human health, in particular human skin disease and has effects on biosphere. Thus it is necessary to monitor aerosols and UV radiation at ground stations. The spatial and temporal variations of aerosol are affected by regional meteorological conditions. Because emitted air pollutants have effects not only on originating country but also the neighbor nations, it is not national problems but an international issue. Therefore there exists need for international collaboration on characterizing atmospheric aerosols and their impact on UV radiation in the Northeast Asia.

I. Chemical properties of aerosols over the Northeast Asia

1 Introduction

Atmospheric aerosols are significant source of direct and indirect global climate forcing. There is a natural aerosol component consisting mostly of soil dust, sea salt, biogenic sulfates, and organic matter that is geographically and seasonally variable; it plays a fundamental role in cloud formation processes, and also makes a small-amplitude direct radiative forcing contribution (Lacis and Mishchenko, 1995). These are two major sources of atmospheric aerosols: widespread surface sources and spatial sources. Widespread surface sources implied the sources at the base of the atmospheric volume (e.g., oceans and deserts) while spatial sources refer to those within the atmospheric volume (e.g., gas to particle conversion and clouds). Additional point sources, such as volcanoes, are globally important in their influence on the stratosphere. Otherwise, due to short tropospheric residence times, aerosols from point sources affect mainly regional and local scales (Jaenicke, 1993). Northeast Asia is an important source region of all major tropospheric aerosols. The fast economic development, the large area of desert, and the intensive forest and agriculture fires in this region contribute to 1/4 to 1/3 of global emissions of SO_2, organic matter, soot, and dust. Northeast Asian aerosols are probably always a mixture of multiple components. For example, mineral dust transported out from the desert can pass major pollution regions where it can be coated and mixed with sulfate and organic aerosols. It can be further mixed with sea salt particles off the coast. Long-range transport of anthropogenic acidic aerosol and organic aerosol has great impacts on not only

regional air quality but also regional climate through radiative balance change.

2 Measurement and analysis

In order to determine chemical properties of aerosol over the Northeast Asia, three intensive samplings were conducted at four measurement sites at Gwnagju (Korea), Beijing (China), Ulaanbaatar (Mongolia) and Kyoto (Japan). Atmospheric aerosols were collected with $PM_{2.5}$ URG cyclone sampler in two intensive periods; 23 July ~ 3 August, and 5 ~ 16 November 2002. To investigate seasonal variation in the chemical properties of aerosol over the Northeast Asia, consecutive 24 hours samplings were conducted and the samples from each intensive sampling were analyzed for ionic compounds (Na^+, NH_4^+, K^+, Mg^{2+}, Ca^{2+}, Cl^-, NO_3^-, SO_4^{2-}). $PM_{2.5}$ particles were collected on the teflon filter and the flow rate was maintained at 16.7 liter per minute by flow-meter. After field sampling the collected particles on the filter were analyzed for anion compounds (Cl^-, NO_3^-, SO_4^{2-}) and cation compounds (Na^+, NH_4^+, K^+, Mg^{2+}, Ca^{2+}) using ion chromatography (IC). Aerosol samples collected on quartz filter were used for analysis of organic carbon (OC) and elemental carbon (EC). For pretreatment of the teflon filter before sampling, the filters were exposed by clean air for 30 minutes and then were dried in a desiccator for 24 hours. After desiccating, the initial filter weight was measured. After sampling, the $PM_{2.5}$ mass concentration was calculated by dividing the measured mass difference by the total air volume. For pretreatment of 47mm diameter quartz filters, all were baked at the same temperature of 550℃ for 12 hours. After backing, the backed filters were placed in the clean room until they have been sealed into prepared petri dishes. In order to extract the ionic

compounds (Na^+, NH_4^+, K^+, Mg^{2+}, Ca^{2+}, Cl^-, NO_3^-, SO_4^{2-}) from the Teflon filter collected particles were placed inside a vial. At first 1ml methanol was added onto the filter face uniformly and then 9ml ultra-pure water was added into vial. However, to prevent chemical oxidation by microbes, 20μl of chloroform was also added. Lastly, the vial containing the sample was systematically shaken for 30 minutes for complete extraction of ionic compounds. Ionic compounds were analyzed by ion chromatography. The IONPAC AS4A-SC column was used for anion column and the IONPAC CS12 column was used for cation column. The anion eluent was 0.35 M Na_2CO_3 + 0.1 M $NaHCO_3$, with flowrate of 2ml/min and cation eluent was 22mN H_2SO_4, with flowrate of 1ml/min. Carbon analyses were carried out at AtmmAA, Calabasas, CA, USA by the selective thermal oxidation method with a MnO_2 catalyst. Elemental specious (Na, Mg, Al, Si, S, K, Ca, Sc, Ti, V, Cr, Mn, Fe, Co, Ni, Cu, Zn, As, Sr, Zr, Se, Pd, Cd, Sb, Ba, Ce, Pb) also were analyzed using ICP-MS.

3 Results

Two intensive samplings of aerosols were conducted at four measurement sites, Gwangju, Beijing, Kyoto, and Ulaanbaatar. Table 1 shows the summary of sampling periods and sites. The mean concentrations of $PM_{2.5}$ mass were increased when it was November (Figure 1). Mean values of 1^{st} intensive sampling period were 21.3 at Ulaanbaatar, 140.1 at Beijing, 18.0 at Gwangju and 40.0 at Kyoto, and during 2^{nd} intensive sampling period, these values were 55.0 at Ulaanbaatar, 128.3 at Beijing, 46.8 at Gwangju, and 25.1 at Kyoto, respectively (Table 2). NO_3^-, SO_4^{2-} and NH_4^+ were major specious over the four sites (Table 3).

Carbonaceous aerosols contain carbon, organic carbon (OC) aerosols are the fraction of carbonaceous aerosols that contain compounds of carbon, whereas elemental carbon (EC) is operationally defined as the light-absorbing component of aerosols. Sources of carbonaceous aerosols are either primary or secondary. Primary sources are emitted as particles ; secondary sources are emitted as gases and undergo chemical or photochemical transformation processes in the atmosphere before forming compounds that have low volatility and may condense to form an aerosol. The natural sources of fine particle carbonaceous aerosols include : (a) primary emissions of particles from natural fires, (b) primary emissions of plant materials injected through abrasion and by direct means, and (c) emissions of organic vapors, which form condensable organics after partial oxidation in the atmosphere. Anthropogenic sources include : (a) primary emission from the burning of biomass, (b) primary emissions from the burning of fossil fuels, from industrial processes and from fugitive source, and (c) emissions of volatile organics from fossil-fuel burning and industrial processes which form condensable organics after particle oxidation. Organic compounds and carbonaceous compounds such as carbonate are also found in the particle emissions associated with sources of dust and sea-salt aerosol, but since most of the mass of these aerosols in associated with larger-sized particles that are radiatively ineffective and small in number (Penner, 1995). Table 4 shows the results of carbon measurement conducted in July and November 2002, the average values over the four countries. The concentrations of organic carbon and elemental carbon in Beijing were the highest when compared to the other sampling sites (Figure 2). The concentration of OC is around 3.5 $\mu g/m^3$ in rural locations and 5 to 20 $\mu g/m^3$ in polluted atmospheres (Seinfeld and Pandis). Table 5 shows the averaged fine

elemental concentrations during the two intensive sampling periods over four sites. Fine elemental specious were also affected by local events and special events such as Asian dust (9~12 November, 2002).

Table 1. Summary of intensive sampling periods and sites

	1st intensive	2nd intensive
Ulaanbaatar, Mongolia	7/23~8/1	11/7~11/16
Beijing, China	7/23~8/2	11/5~11/14
Gwangju, Korea	7/23~8/1	11/5~11/14
Kyoto, Japan	7/23~8/3	11/5~11/14

Table 2. Mean concentrations of $PM_{2.5}$ mass during the two intensive sampling periods over four sites.

($\mu g/m^3$)

	Ulaanbaatar, Mongolia	Beijing, China	Gwangju, Korea	Kyoto, Japan
1st	21.3±3.6	140.1±94.3	18.0±3.2	40.0±14.8
2nd	55.0±20.8	128.3±99.9	46.8±36.0	25.1±16.8

Mean±Std

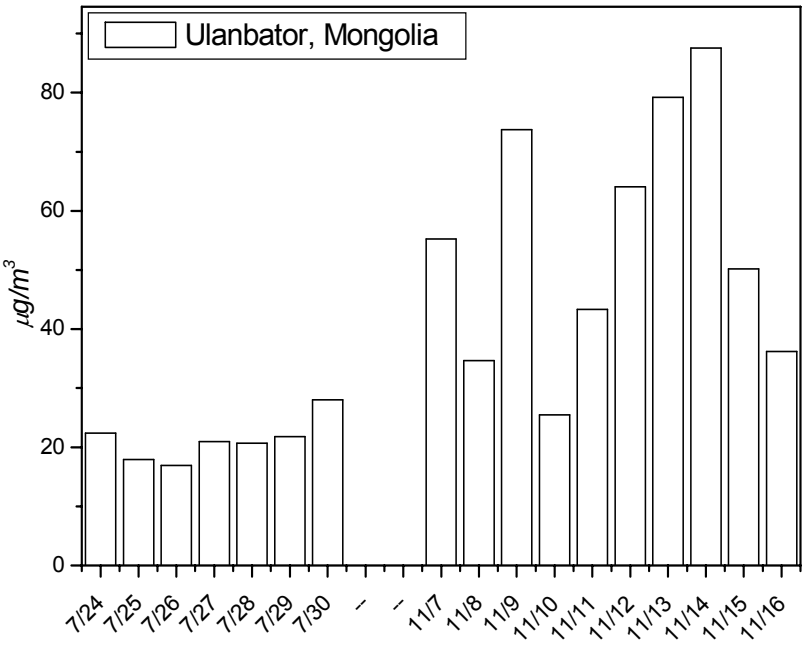
Ulanbator, Mongolia
μg/m3
0
20
40
60
80
7/24
7/25
7/26
7/27
7/28
7/29
7/30
11/7
11/8
11/9
11/10
11/11
11/12
11/13
11/14
11/15
11/16

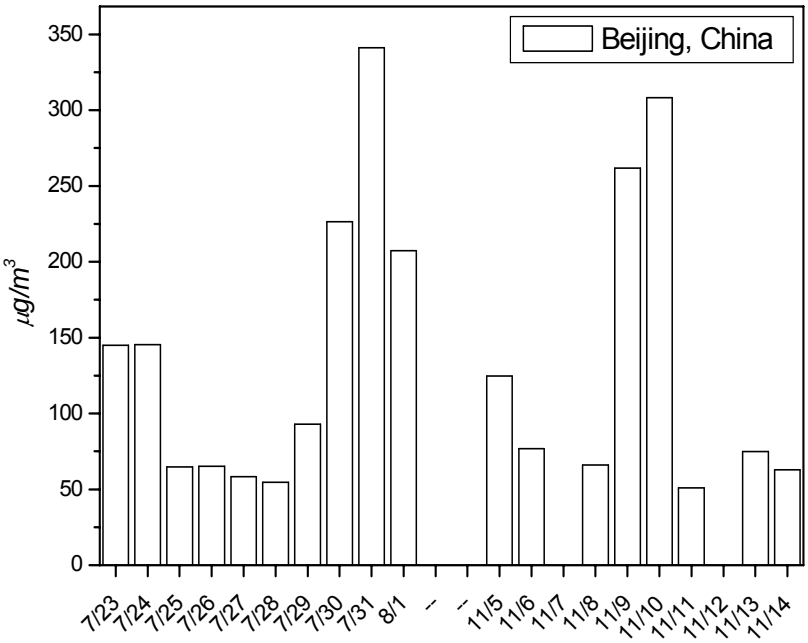
Beijing, China
μg/m3
0
50
100
150
200
250
300
350
7/23
7/24
7/25
7/26
7/27
7/28
7/29
7/30
7/31
8/1
11/5
11/6
11/7
11/8
11/9
11/10
11/11
11/12
11/13
11/14

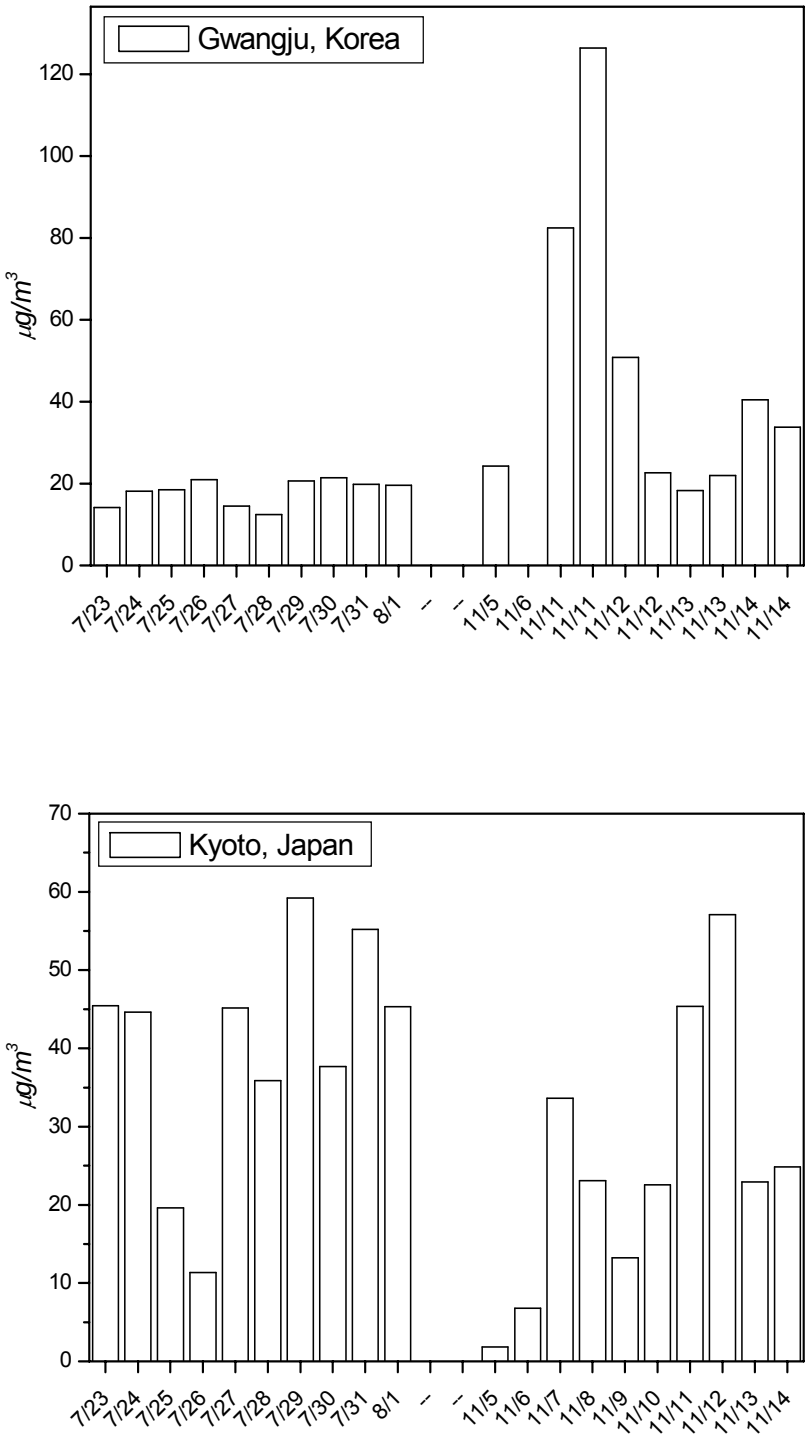

Figure 1. Variations of $PM_{2.5}$ mass concentration during the two intensive sampling periods over four sites.

Table 3. Variations of ionic specious of $PM_{2.5}$ particles during the two intensive sampling periods over four sites.

Ulaanbaatar	Cl^-	NO_3^-	SO_4^{2-}	Na^+	NH_4^+	K^+	Mg^{2+}	Ca^{2+}
11/7	0.951	2.472	5.921	1.230	2.696	0.126	0.090	1.204
11/8	0.712	2.571	4.191	1.117	1.790	-	0.086	1.097
11/9	1.318	4.307	6.099	1.008	3.231	0.114	0.103	1.367
11/10	0.608	0.887	3.342	1.097	1.089	-	0.089	1.117
11/11	0.925	1.534	4.733	1.069	1.893	-	0.096	1.069
11/12	1.132	2.850	6.605	1.091	2.895	-	0.126	1.277
11/13	1.009	2.187	7.806	1.025	3.273	-	0.094	1.784
11/14	1.163	2.701	8.618	1.224	3.806	-	0.097	1.240
11/15	0.786	1.877	5.649	1.155	2.173	-	0.084	1.191
11/16	0.678	1.346	3.534	1.020	1.394	-	0.074	1.020

Beijing	Cl^-	NO_3^-	SO_4^{2-}	Na^+	NH_4^+	K^+	Mg^{2+}	Ca^{2+}
11/5	5.209	15.364	16.898	2.393	8.930	2.879	0.322	2.364
11/6	2.616	12.782	18.798	2.699	9.927	1.632	0.344	2.116
11/7	0.963	0.936	3.432	1.614	0.740	0.216	0.153	1.589
11/8	3.948	2.817	6.716	1.672	3.506	1.541	0.311	2.349
11/9	11.808	30.017	25.547	2.685	22.018	4.244	0.639	4.193
11/10	8.335	29.829	23.416	3.126	16.934	4.004	0.638	6.681
11/11	1.241	1.562	4.641	1.747	1.084	0.365	0.331	2.940
11/12	1.231	1.023	3.720	1.728	1.292	0.327	0.199	1.757
11/13	3.310	5.400	6.603	1.463	3.978	1.160	0.271	2.291
11/14	3.464	4.447	5.875	1.513	3.764	0.858	0.259	2.081

(continued)

Gwangju	Cl^-	NO_3^-	SO_4^{2-}	Na^+	NH_4^+	K^+	Mg^{2+}	Ca^{2+}
11/5	1.580	1.935	3.528	0.129	2.461	0.308	-	0.020
11/6	0.877	4.024	7.504	0.153	3.484	0.539	0.012	0.097
11/11	1.159	6.091	14.406	0.490	5.894	1.649	0.022	0.138
11/11	0.899	3.143	7.256	0.380	2.486	1.251	0.103	0.780
11/12	1.143	1.296	1.607	0.208	0.781	0.386	0.052	0.403
11/12	0.495	1.251	1.225	0.324	1.033	0.181	-	0.004
11/13	0.649	0.855	2.663	0.106	1.295	0.199	0.008	0.107
11/13	0.824	1.412	2.685	0.066	1.582	0.156	0.008	0.069
11/14	2.153	2.275	3.557	0.352	2.606	0.504	-	-
11/14	1.523	2.641	4.027	0.152	2.439	0.448	0.007	0.067

Kyoto	Cl^-	NO_3^-	SO_4^{2-}	Na^+	NH_4^+	K^+	Mg^{2+}	Ca^{2+}
11/5	1.357	-	2.271	1.841	0.414	0.148	0.137	1.217
11/6	1.101	1.036	1.643	1.339	0.317	-	0.090	0.982
11/7	-	3.119	4.958	1.672	1.837	0.448	0.065	1.413
11/8	1.046	1.653	6.045	1.978	1.785	0.380	0.143	1.401
11/9	1.332	-	2.681	2.455	0.508	-	0.108	1.523
11/10	1.056	1.628	4.533	2.125	1.417	0.228	0.144	1.528
11/11	-	4.100	8.470	2.081	2.892	0.400	0.159	1.584
11/12	1.519	2.292	6.319	2.250	1.417	0.550	0.233	2.186
11/13	1.268	1.317	4.038	1.992	1.026	0.280	0.163	1.690
11/14	1.277	1.720	4.393	1.941	1.338	0.299	0.146	1.451

Table 4. Mean concentrations of $PM_{2.5}$ carbonaceous species during the two intensive sampling periods over four sites.

($\mu g/m^3$)

		OC	EC	OC/EC
1st	Ulaanbaatar, Mongolia	2.3±0.7	0.4±0.2	6.6±3.9
	Beijing, China	12.4±4.4	5.4±2.6	2.4±0.4
	Gwangju, Korea	1.4±0.5	0.3±0.1	4.3±1.4
	Kyoto, Japan	5.0±1.8	1.3±0.8	5.0±2.1
2nd	Ulaanbaatar, Mongolia	23.1±10.6	2.6±1.1	8.6±0.8
	Beijing, China	27.6±22.9	6.7±5.9	4.3±0.4
	Gwangju, Korea	12.7±5.6	2.5±1.1	5.6±3.1
	Kyoto, Japan	7.9±3.0	2.5±1.5	3.7±1.3

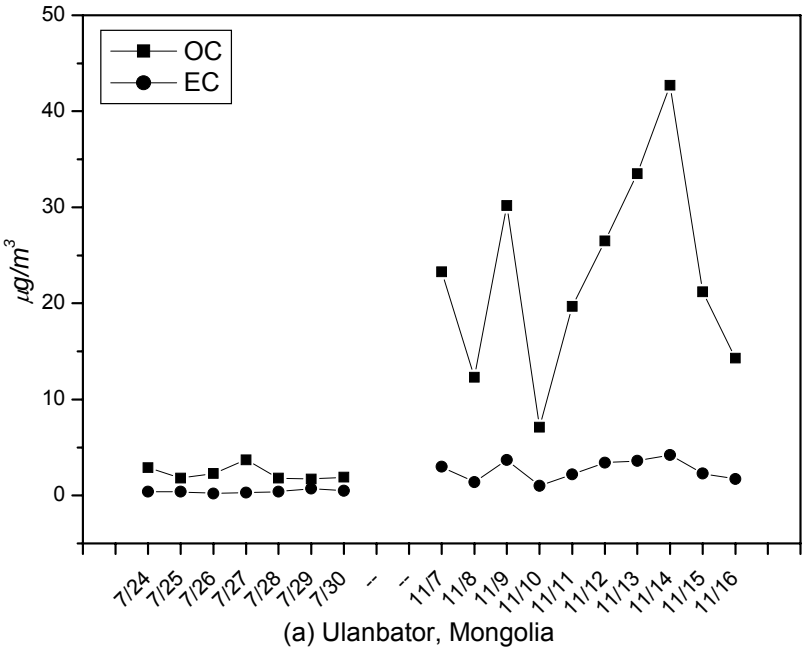

(a) Ulanbator, Mongolia

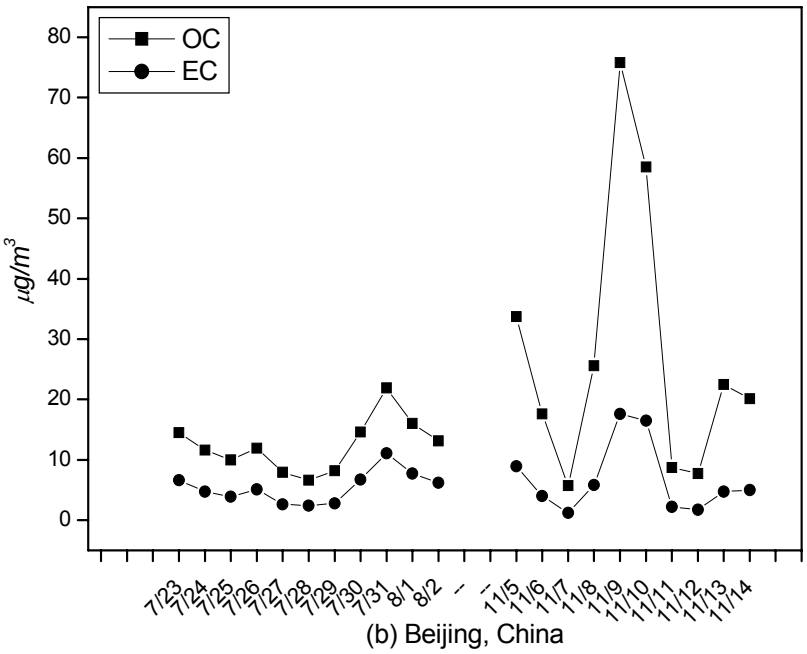

(b) Beijing, China

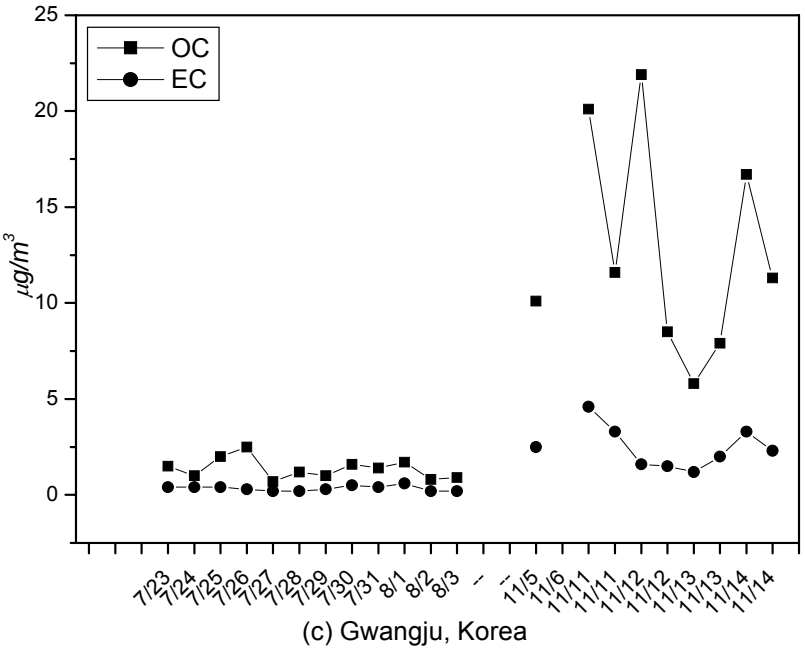

(c) Gwangju, Korea

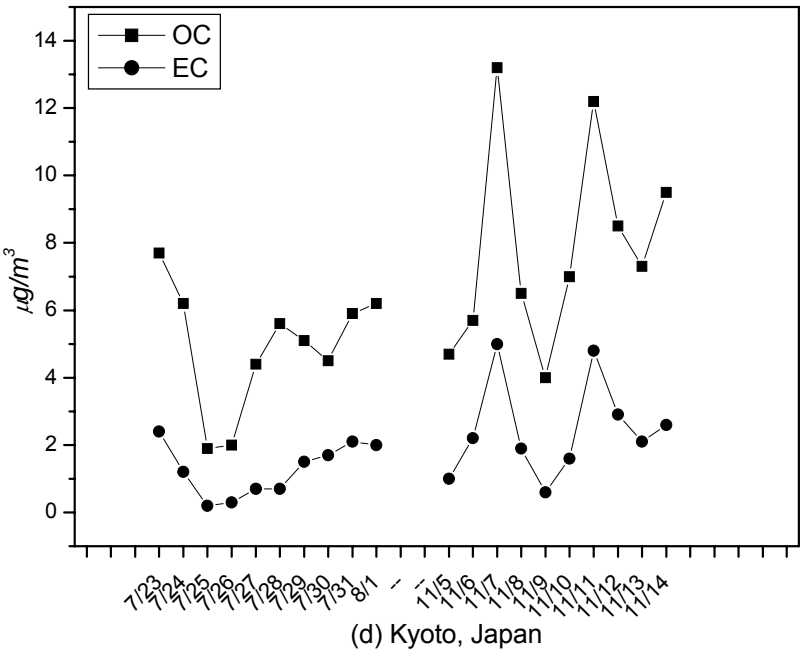

(d) Kyoto, Japan

Figure 2. Variations of OC and EC of $PM_{2.5}$ particles during the two intensive sampling periods over four sites.

Table 5. Averaged fine elemental concentrations measured in four sites during two intensive sampling periods.

(ng/m^3)

Sites	Soil Elements								
	Al	Ca	Fe	K	Mn	Mg	Na	Ti	
Ulaanbaatar	4347.472	6533.317	791.090	1668.679	19.708	2246.448	36130.167	50.697	10
Beijing	4378.842	7488.821	1717.240	4502.781	89.941	2546.051	20133.093	75.596	28
Gwangju	2894.577	4857.104	136.223	1275.535	5.102	1959.739	16789.251	10.192	3
Kyoto	2188.631	3498.577	140.591	886.177	7.340	1385.262	21829.387	16.130	3
1^{st}									

Sites	Soil Elements								
	Al	Ca	Fe	K	Mn	Mg	Na	Ti	
Ulaanbaatar	938.642	2871.716	1192.635	1240.424	29.422	403.622	4799.798	24.887	1
Beijing	6155.344	5601.033	4801.711	5854.279	147.016	1837.383	5151.895	89.951	3
Kyoto	1789.372	3955.504	986.514	1143.854	25.511	964.522	10124.251	21.838	
2^{nd}									

4 Conclusions

Through the two intensive samplings of aerosol over four countries, at Ulaanbaatar, Mongolia, Beijing, China, Gwnagju, Korea and Kyoto, Japan, chemical properties were investigated in this part. Values in November concentrations of mass and ion compounds were higher than values in July over the four measurement sites. The Asian dust from China or Mongolia can affect the atmospheric composition over the Northeast Asia in autumn and winter. Thus the characteristics of aerosols were also affected by the air mass direction. From the carbon analysis, during the 1st intensive period, the mean OC/EC ratios has been observed 6.6 at Ulaanbaatar, 2.4 at Beijing, 4.3 at Gwangju and 5.0 at Kyoto, and during the second intensive period, these values were 8.6 at Ulaanbaatar, 4.3 at Beijing, 5.6 at Gwangju, and 3.7 at Kyoto, respectively. Fine elemental specious were also affected by local events and special events such as Asian dust (9~12 November, 2002).

5 References

S. S. Park, Y. J. Kim and Kochy Fung, PM2.5 carbon measurements in two urban areas; Seoul and Gwnagju, Korea, Atmos. Environ. 36, pp1287~1297 (2002)

S. S. Park, Y. J. Kim and Kochy Fung, Characteristics of PM2.5 carbonaceous aerosol in the Sihwa industrial area, South Korea, Atmos. Environ. 35, pp657~665 (2001)

Peter V. Hobbs, Aerosol-Cloud-Climate Interactions, Academic Press, California,

pp. 1-31 (1993)

R. J. Charlson and J. Heintzenberg, Aerosol Forcing of Climate, John Wiley & Sons, England, pp. 43-72 (1994)

J. C. Chow, Measurement Methods to Determine Compliance with Ambient Air Quality Standards for Suspended Particles, J. Air & Waste Manage. Assoc. 45, pp. 320-382 (1995)

E. Meszaros, T. Bareza, A. Geleneser, J. Hlavay, G. Kiss, Z. Krivacsy, A. Molnar and K. Polyak, Size Distributions of Inorganic and Organic Species in the Atmospheric Aerosol in Hungary, J. Aerosol Sci. 28, pp. 1163-1175 (1997)

S. Hering, A. Eldering and J. H. Seinfeld, Bimodal Character of Accumulation Mode Aerosol Mass Distributions in Southern California, Atmos. Environ., 31, pp. 1-11 (1997)

J. H. Seinfeld and S. N. Pandis, Atmospheric Chemistry and Physics from Air Pollution to Climate Change, John Wiley & Sons, New York, pp. 700-765 (1998)

II. **Aerosol optical depth and solar radiation analysis at Gwnagju and Mongolia**.

1 **Introduction**

Information on the availability of solar irradiance is important for many applications dealing with the exploitation of solar energy. The knowledge of the diffuse fraction of global solar irradiance is a major requirement in estimating the long-term expected values of the output of concentrating solar collectors and also provides a fundamental input to the techniques for estimating radiation on inclined surface. The solar irradiance received at the Earths surface in the visible part of the electromagnetic spectrum (from ~0.4 to 0.7m), apart from its relevance to daily human activities, plays an important role in plant growth and development of higher plants through the processes of chlorophyll synthesis and photosynthesis (Udo and Aro, 1999). This coupled with other useful information that could be derived from comprehensive analysis of diffuse radiation makes the long-term measurement and analysis of the latter desirable. The seasonal variations in the diurnal evolution of global and diffuse solar irradiance at the surface in Gwnagju (Korea) and Ulaanbaatar (Mongolia) are thus presented in detail in this work because no similar scientific information on solar radiation variability about these cities is available in literature. However, considering that the presence of the clouds modifies the global irradiance and taking account that the processes involving clouds tend to be very dynamic, a great variability of instantaneous values is expected. Other important factors affecting the amount of solar radiation reaching the earth's surface is the existence of aerosol particles in the

atmosphere. At urban sites, high aerosol concentration reduces or modifies the total incidence energy and alters the direct-diffuse ratio (Unsworth and Monteith 1972, Repapis et al., 1998, Jacovides et al., 2000). Aerosols are important contributing factor to global climate change through their direct and indirect influences on climate processes on the earth's atmosphere (Intergovernmental panel on climate change (IPCC) 1995; Jacovides et al., 1996; Haywood et al., 1999). Aerosols also play an important role in air quality and environmental health effects (Prospero, 1979; Pinker et al., 2001).

Optical aerosol climatology is a supplementary property used to characterize aerosol, assess atmospheric pollution and make atmospheric corrections to satellite remotely sensed data. The validation of aerosol optical properties derived from satellite requires a good knowledge of the atmospheric transmission at different wavelengths (d'Almeida, 1987). It is therefore apparent that a comprehensive record and analysis of the optical properties of aerosols be performed. The spectral aerosol optical depth at Gwnagju is therefore performed in this analysis. AODs at UV wavelength range were also calculated using UVMFR which is a UV version of MFRSR described by Harrison et al. (1994). This instrument has 2-nm FWHM bandwidth filters centered at 299.2, 304.5, 310.6, 317.1, 323.9, 331.7, and 367.4 nm to measure global, diffuse, and direct irradiance. Measurement began in October at K-JIST in Gwangju, Korea. Measurement is taken every 20 seconds and averaged to 1 minute to record in a data logger.

2 Results and Discussion

Figure 1 shows the daily variation of global and diffuse solar irradiance at Gwnagju, South Korea during the measurement periods of February to December 2002. The figure shows a distinct seasonal pattern with solar radiation increasing gradually from minimum value in January to peak during the summer season. It then decreases gradually until minimum values are reached in December. Also evident in the figure is the increase in daily diffuse radiation to peak values during 23rd to 26th May. This may be attributed to the effect of aerosol in the atmosphere during the spring season. Minimum daily diffuse radiation is also noted in the raining season. This may be due to the clearing of the atmosphere just immediately after rain during this period. Figure 2 shows the daily variation of global and diffuse solar radiating at Ulaanbaatar, Mongolia during March to October 2002. Similar pattern is noted with that observed in figure 1. The maximum daily global radiation at Ulaanbaatar is 328.31 w/m^2 on 14 July 2002 while the maximum diffuse radiation is 153.14 on 12 May 2002.

Figures 3 and 4 show the monthly variation of global and diffuse radiation at both Gwnagju and Ulaanbaatar in 2002. The peak values monthly global radiation were 333.85w/m^2 (June, 2002) and 253.68 (July 2002) w/m^2 at Gwnagju and Ulaanbaatar respectively. An increase in the values of monthly diffuse radiation to a maximum in June was noted in figures 3 and 4 respectively. The monthly diffuse ratio is shown in Figure 5. It shows that the ratio of global to diffuse radiation is higher at Gwnagju than Ulaanbaatar in all months throughout the year.

Figure 6 shows the spectral aerosol optical depth at Gwnagju from June2002 –February 2003 computed from MFR7 radiometer. During this period, higher aerosol optical depths were noted in October fall season. This can be

attributed to biomass burning at the site. The aerosol optical depth decreases to minimum in February 2003. The aerosol optical depth at 510nm wavelength is shown in Figure 7. The maximum value and minimum daily aerosol optical depth were 0.46 and 0.06 respectively.

The computed Angstrom parameter α is shown in Figure 7. Higher Angstrom alpha parameters were observed in September and October respectively, which are typical of biomass burning aerosols.

Figures 9-15 show the diurnal variation of global and diffuse solar radiation for month with similar atmospheric properties at Gwnagju and Ulaanbaatar. Results show a distinct seasonal difference in the diurnal variation at both sites. The daily global and diffuse radiation increases steadily in the early hours and reaches maximum around 1200-1300 hr in the afternoon, and steadily decreases back to minimum at 1700-1900hr depending on the month and season on the year. It is also observed that the available solar irradiance is higher at Gwnagju at all season than Ulaanbaatar. The maximum monthly mean hourly global and diffuse radiation at Gwnagju are 970.79 w/m^2 and 520.71w/m^2 respectively in March, 2002 while The maximum monthly mean hourly global and diffuse radiation at Ulaanbaatar are 205.42 w/m^2 and 56.83 w/m^2 respectively.
AOD data at UV wavelength range under all sky conditions are shown in Table 1 and Figures 17. Figure 16 is an example of daily AOD variation at 6 different UV channels.Table 1 shows the monthly mean of each month and Figure 17 shows daily mean during the study period.

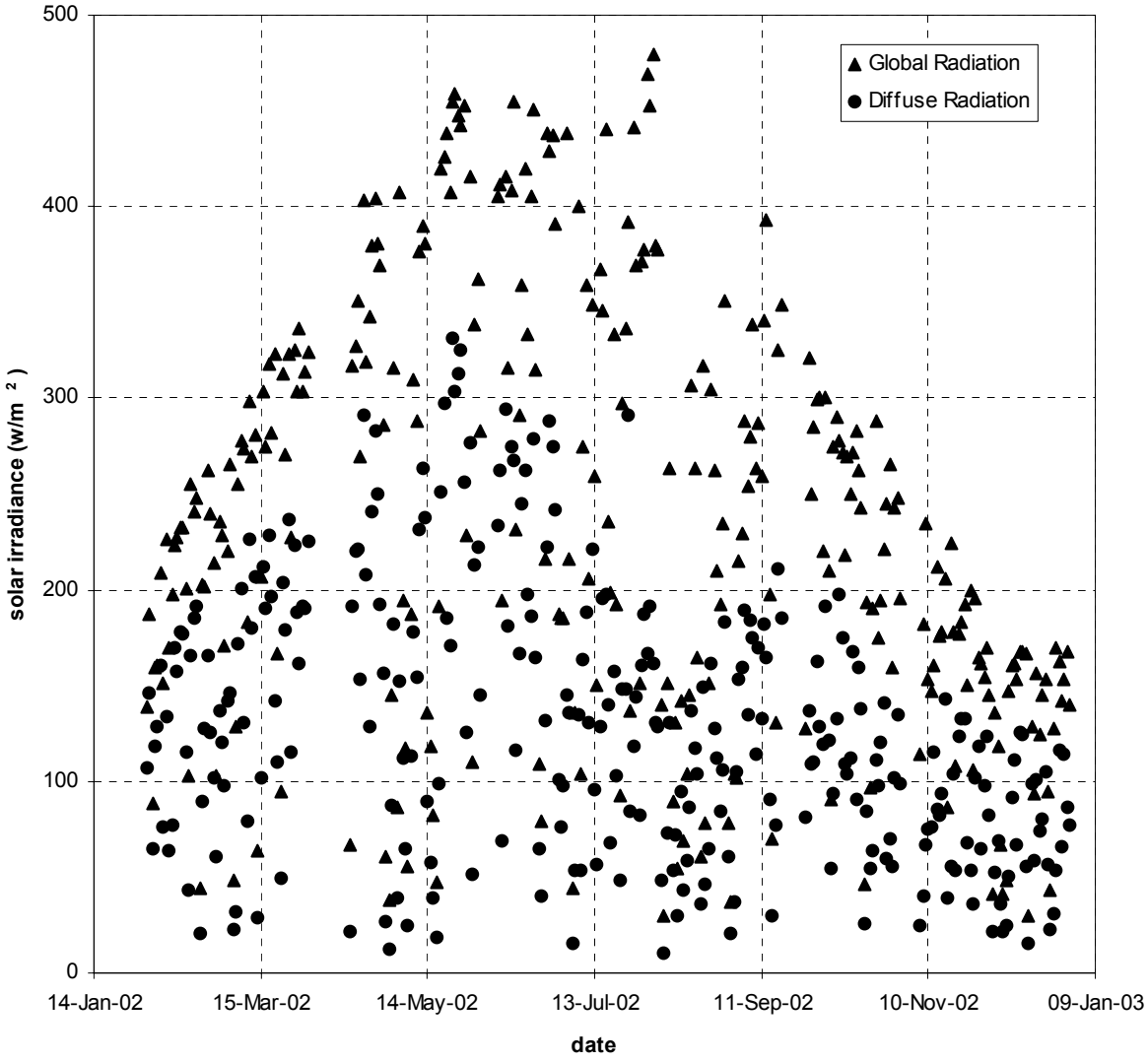

Figure 1. Daily variation of global and diffuse solar radiation at Gwnagju, Korea from February to December 2002.

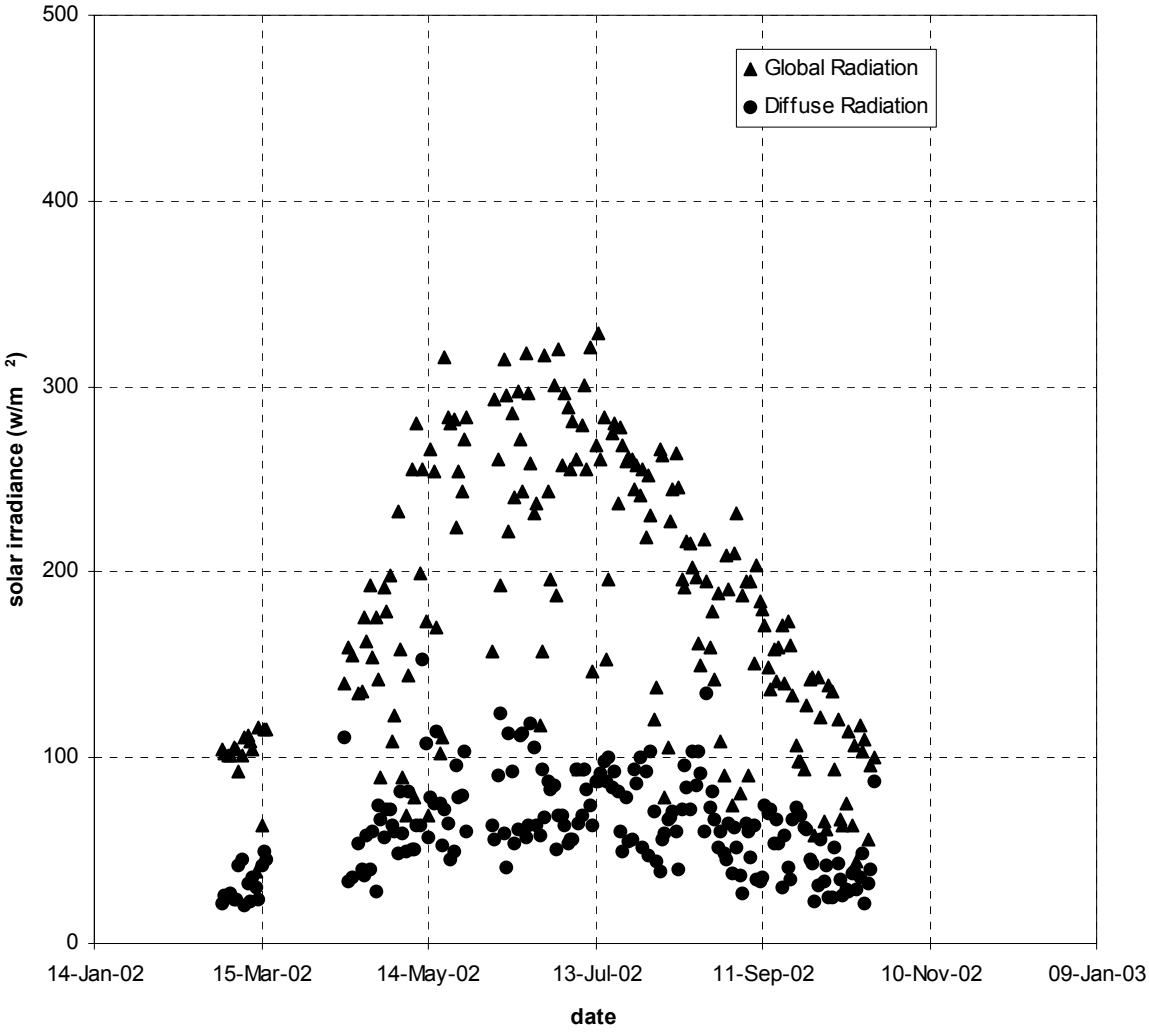

Figure 2. Daily variation of global and diffuse solar radiation at Ulaanbaatar, Mongolia from March to October 2002.

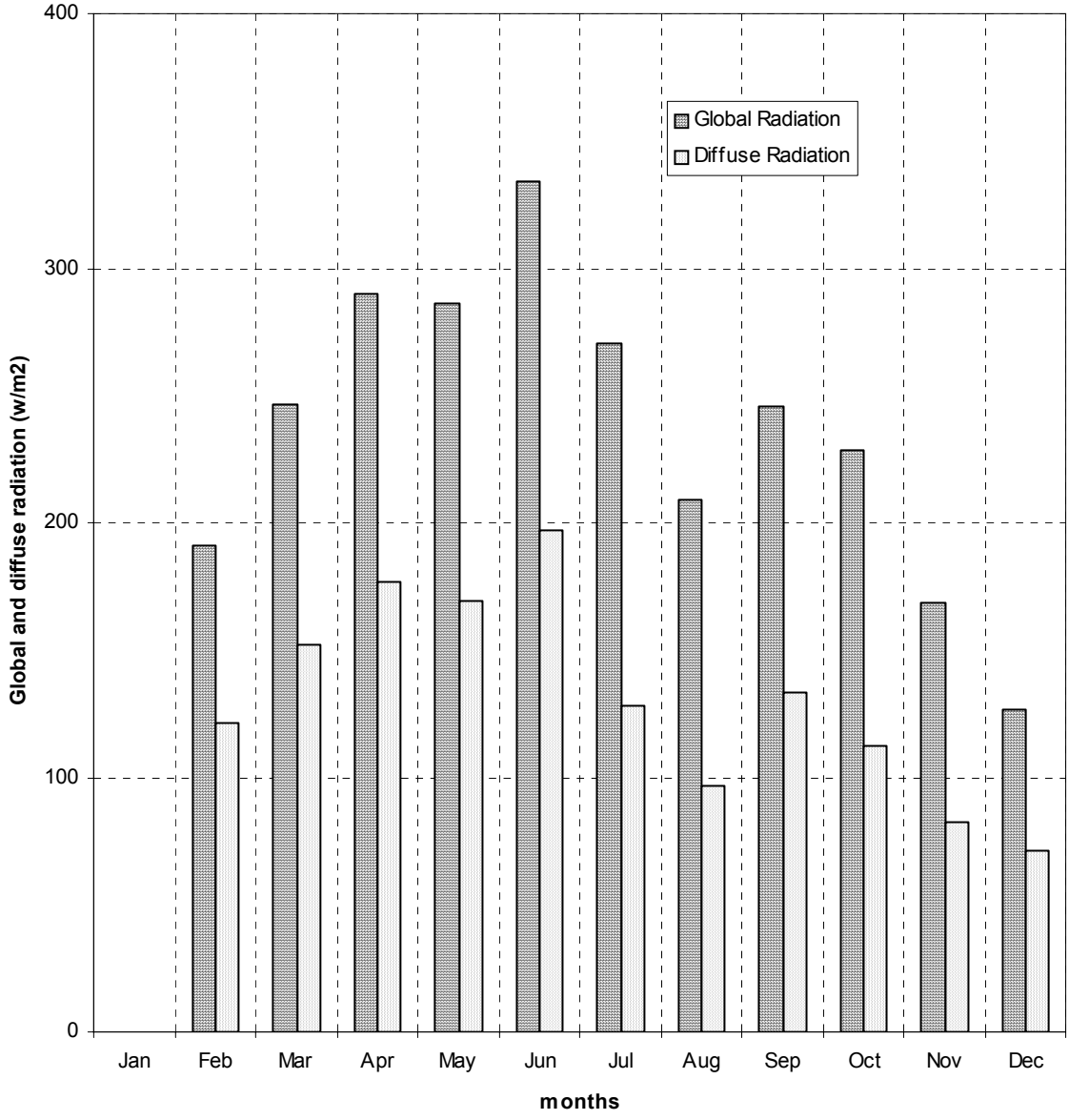

Figure 3. Monthly variation of global and diffuse solar irradiance at Gwnagju, Korea.

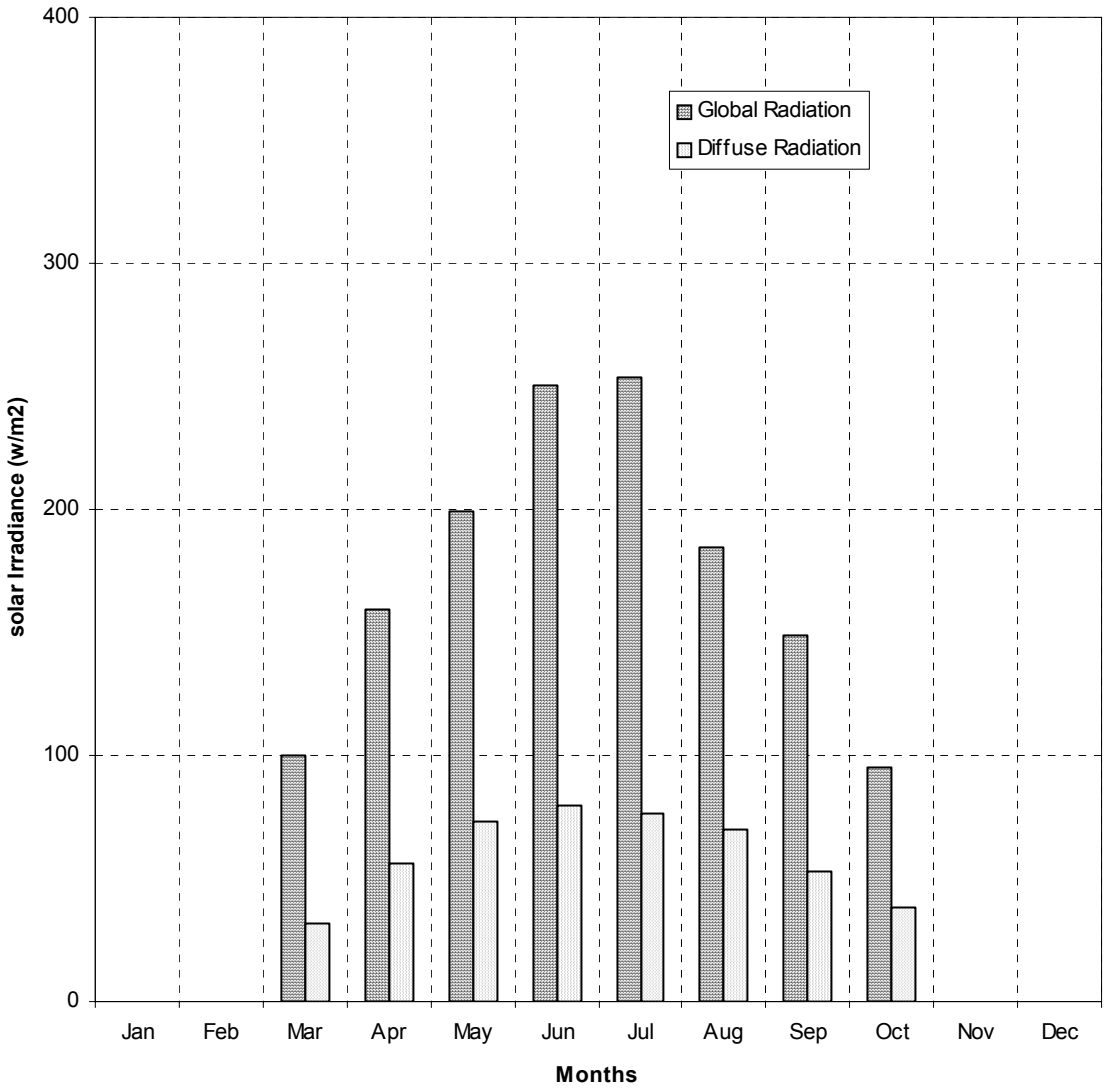

Figure 4. Monthly variation of global and diffuse solar irradiance at Ulaanbaatar, Mongolia.

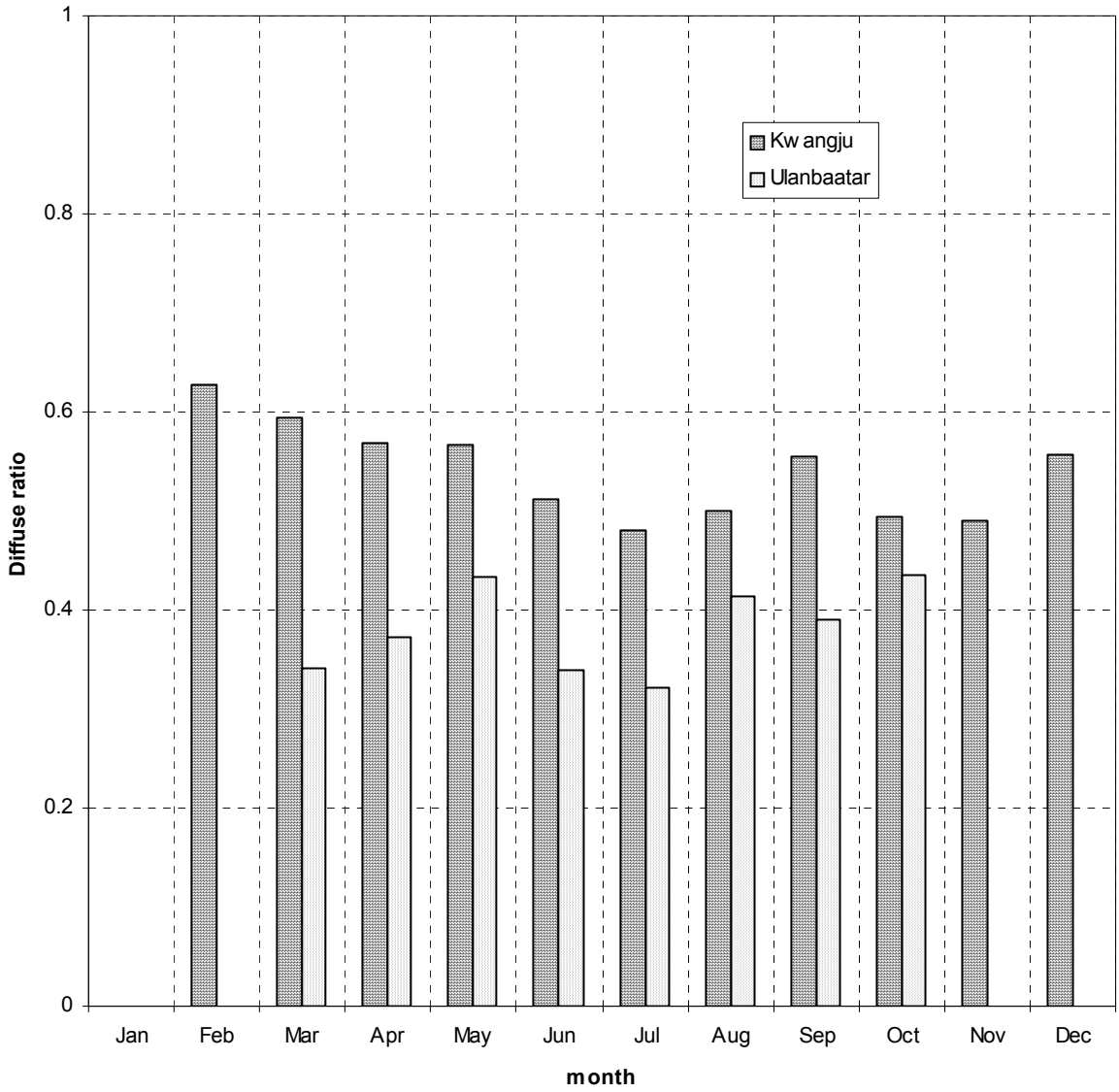

Figure 5. Seasonal diffuse ratio at Gwnagju, Korea and Ulaanbaatar, Mongolia.

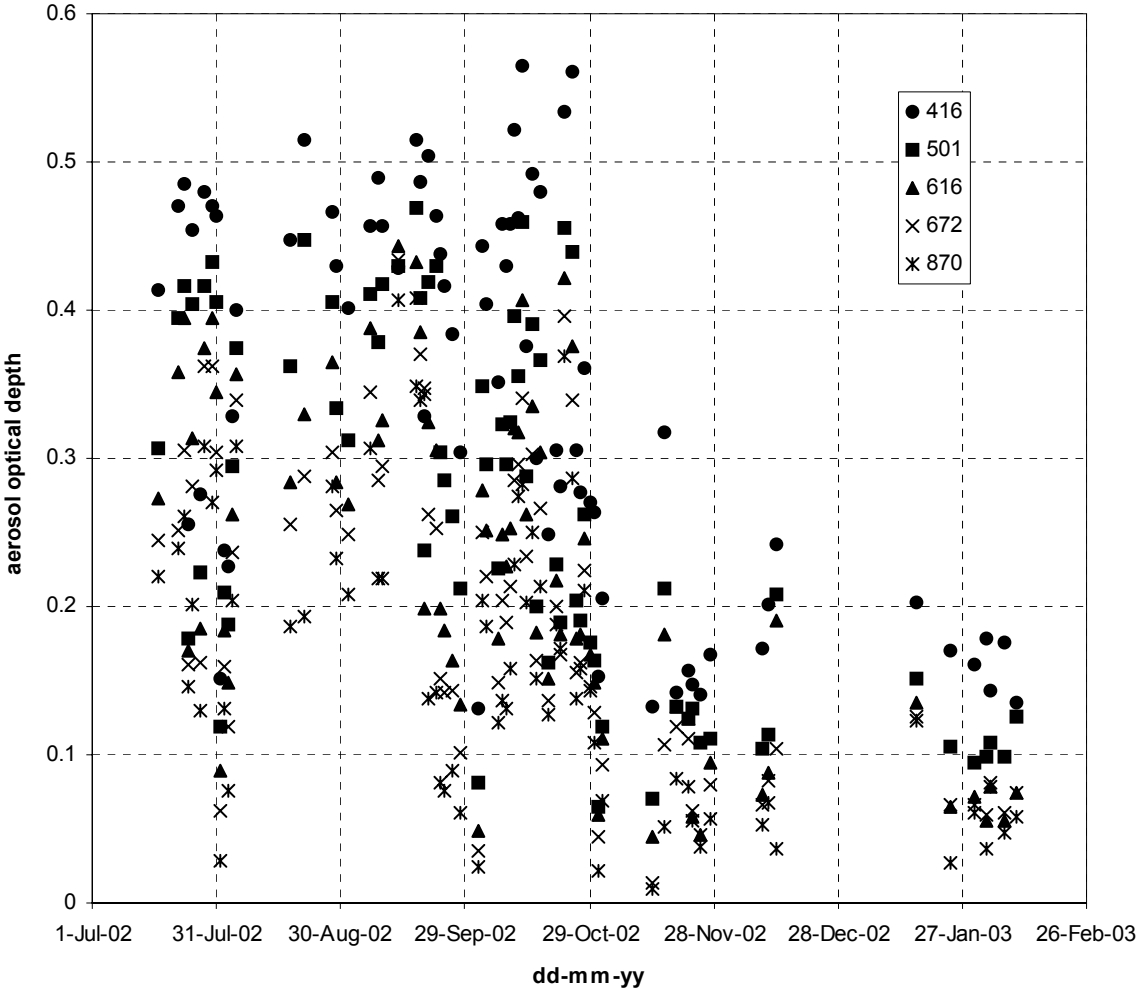

Figure 6. Spectral aerosol optical depth at 416nm, 501nm, 616nm, 672nm and 870nm wavelengths Gwnagju from July 2002 to February 2003.

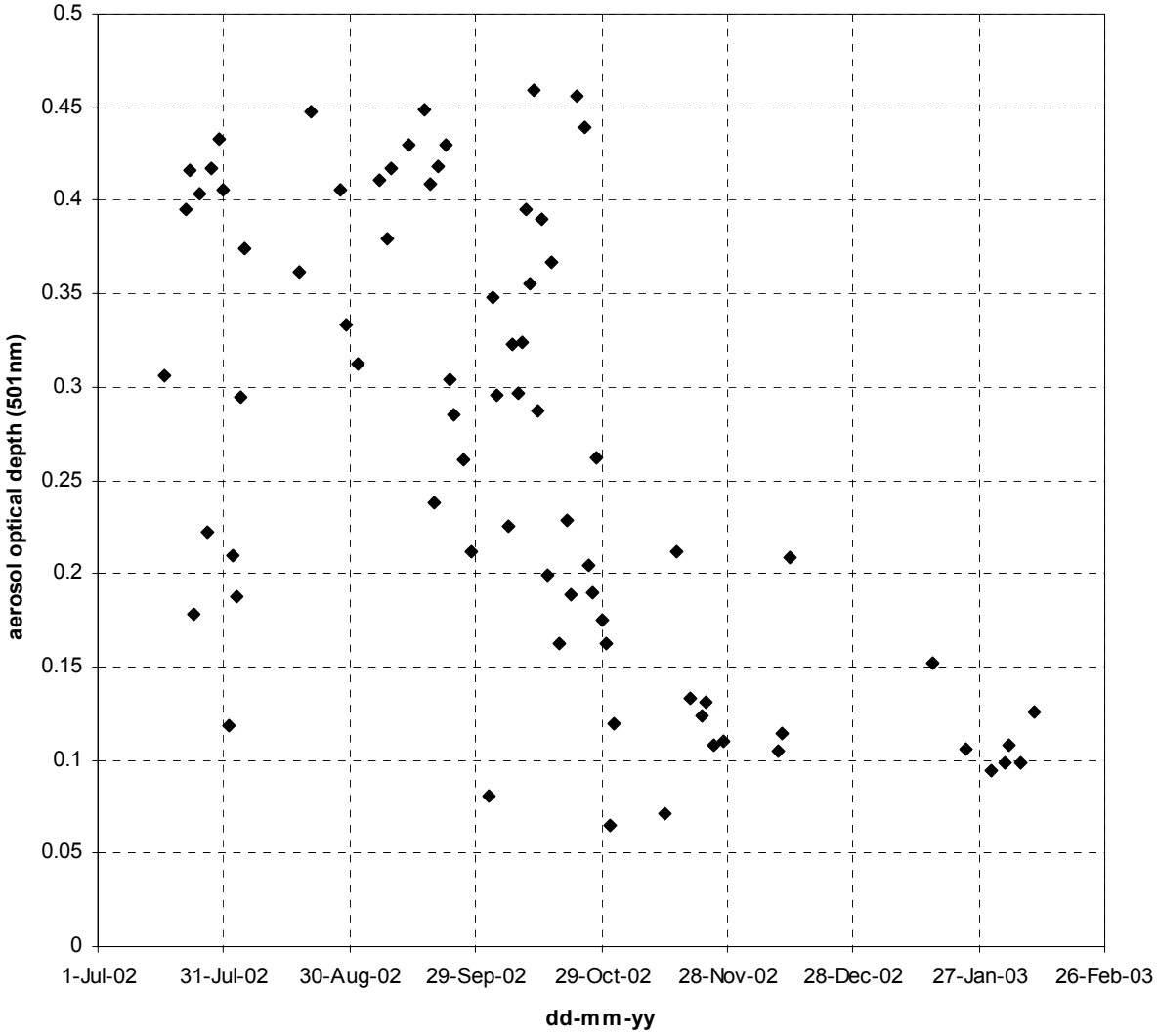

Figure 7. Aerosol optical depth at 501nm wavelength.

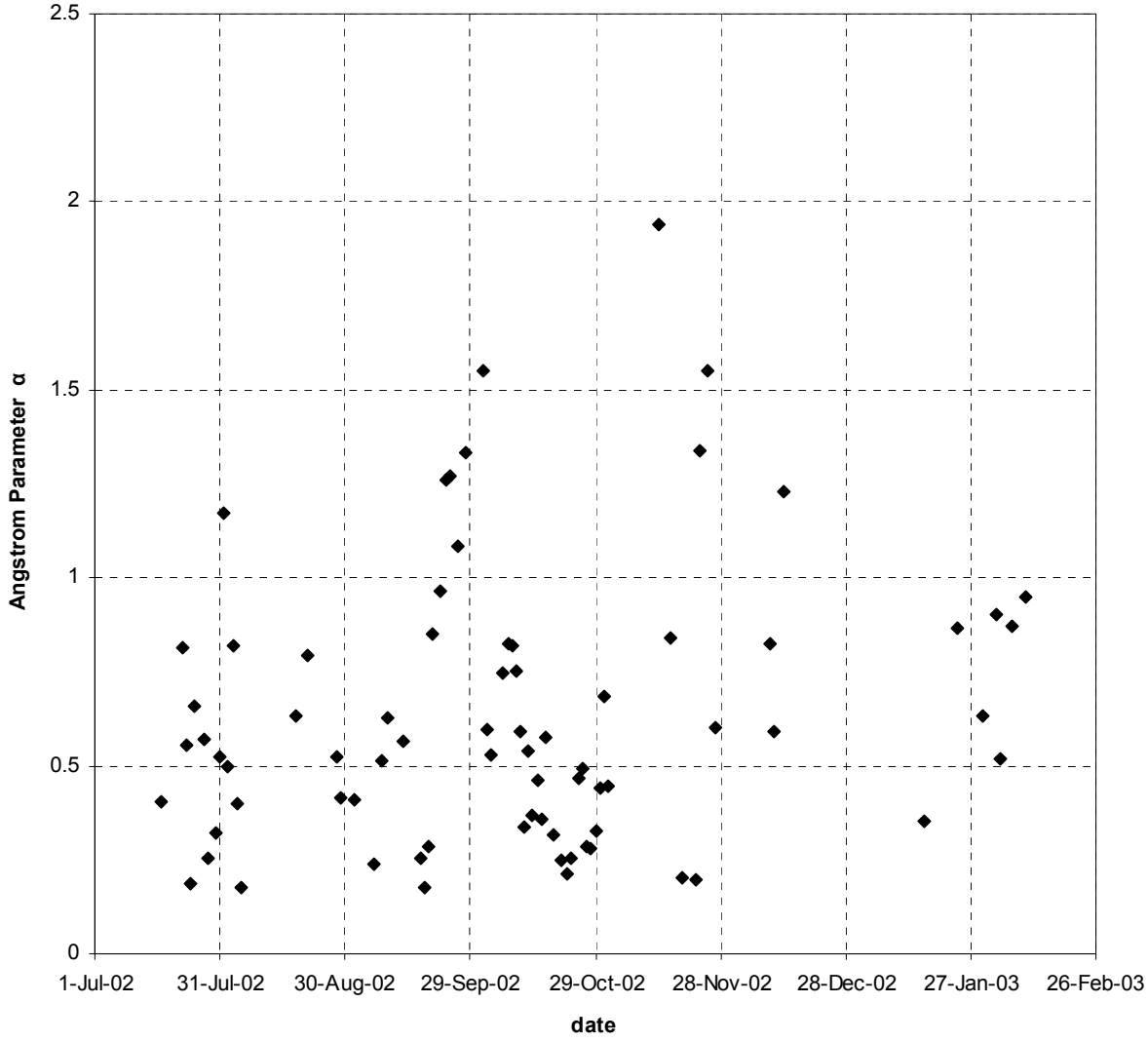

Figure 8. Computed Angstrom alpha parameter at Gwnagju from July 2002 to February 2003.

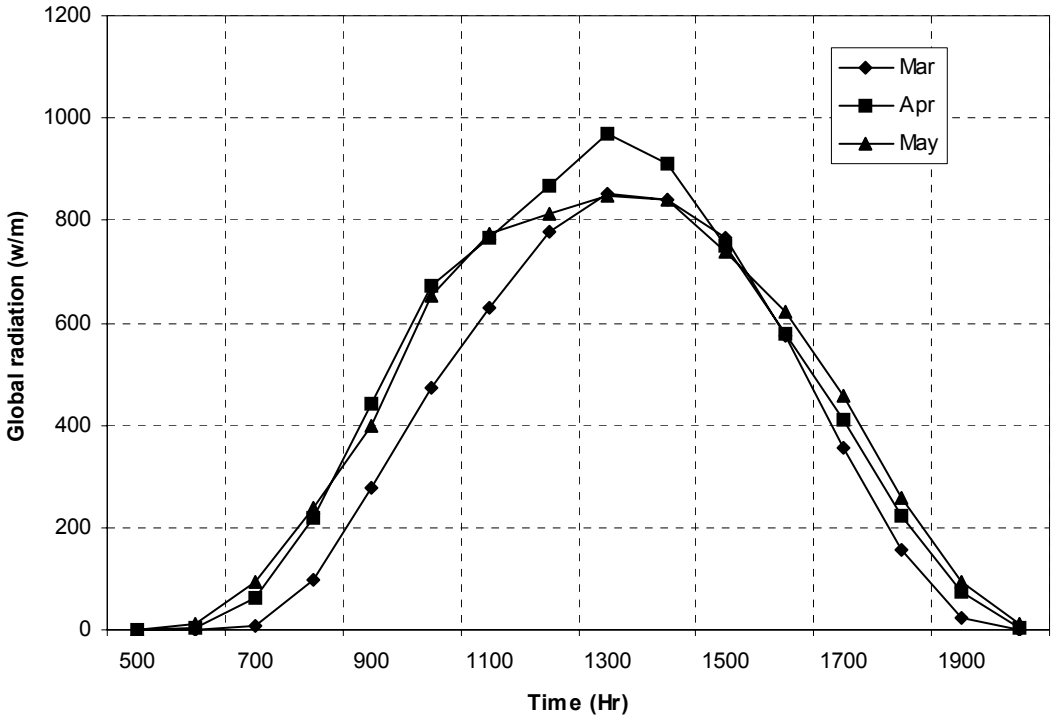

Figure 9a. Diurnal variation of global radiation during spring season, 2002 at Gwnagju, Korea.

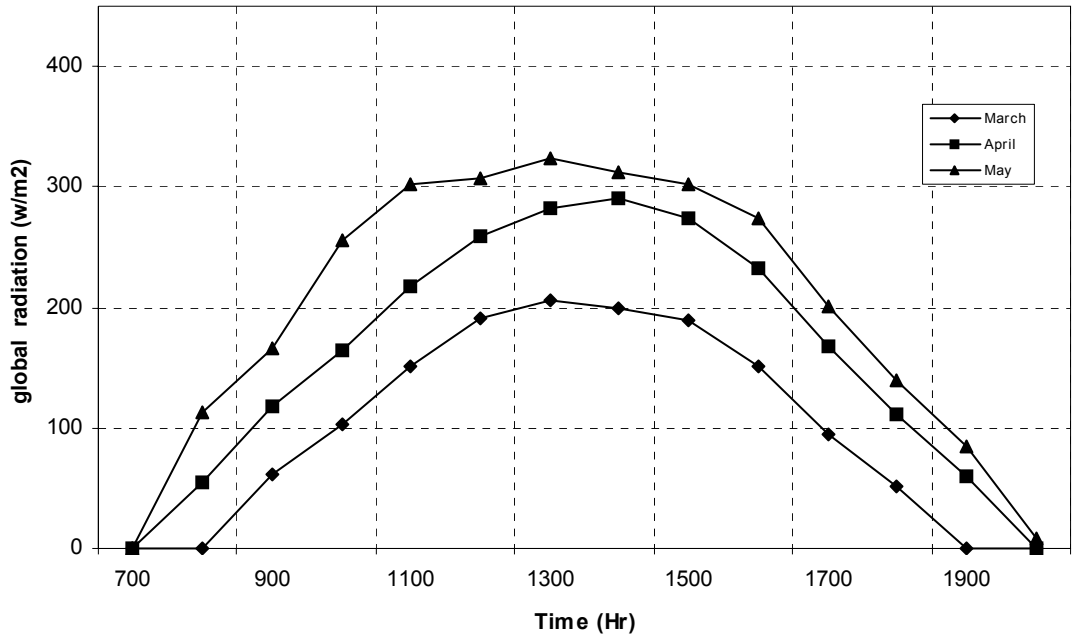

Figure 9 b. Diurnal variation of global radiation during spring season, 2002 at Ulaanbaatar, Mongolia.

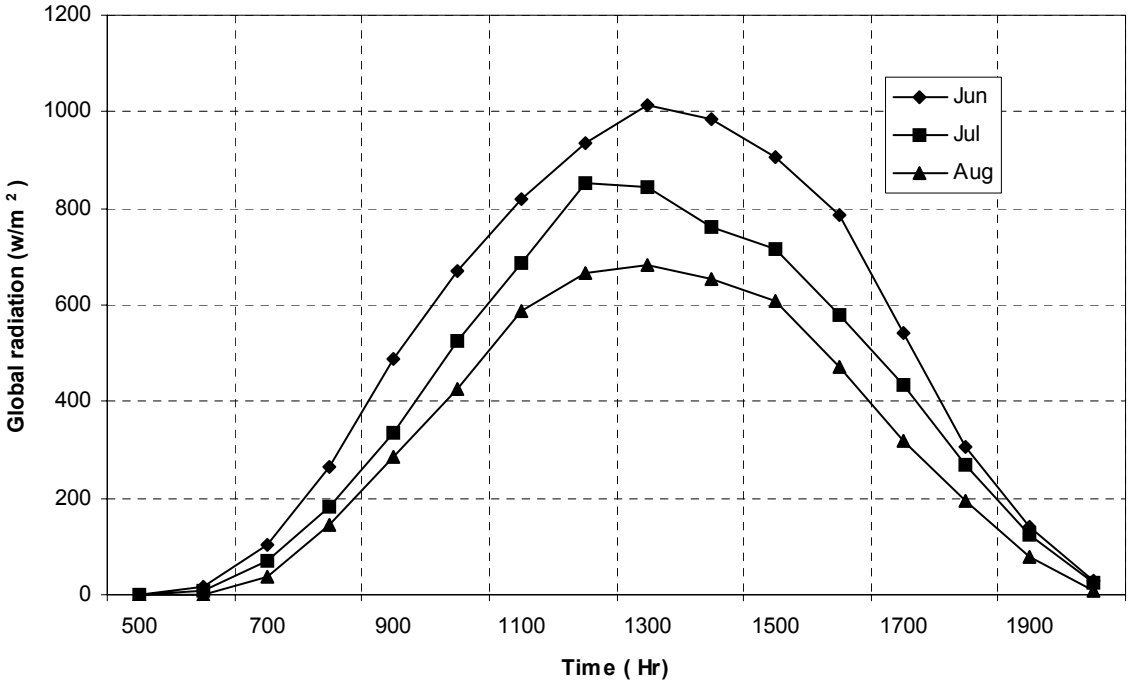

Figure 10a. Same as in Fig. 9a, but measurements are for summer season.

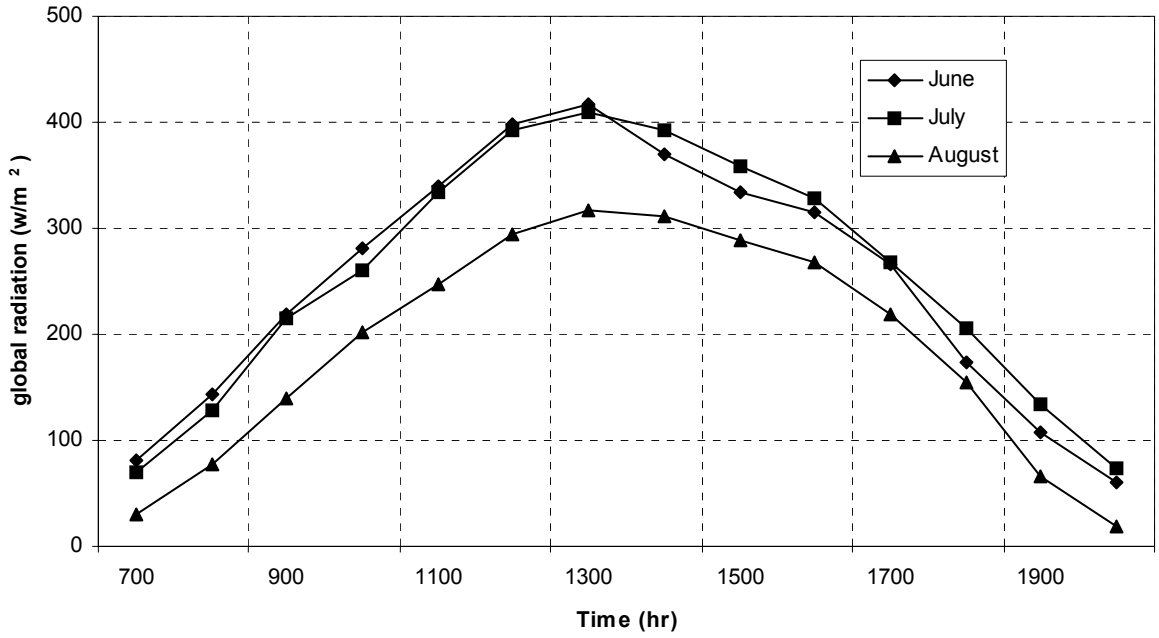

Figure 10b. Same as in Figure 9b, but measurements are for summer season.

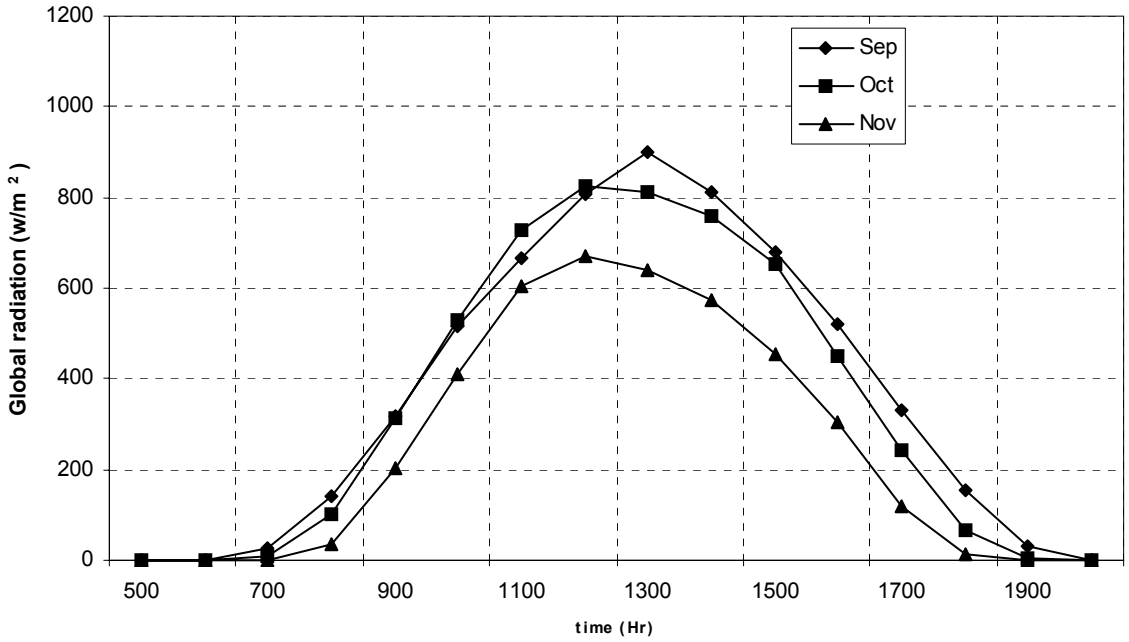

Figure 11a. Same as in Fig. 9a, but measurements are for fall season

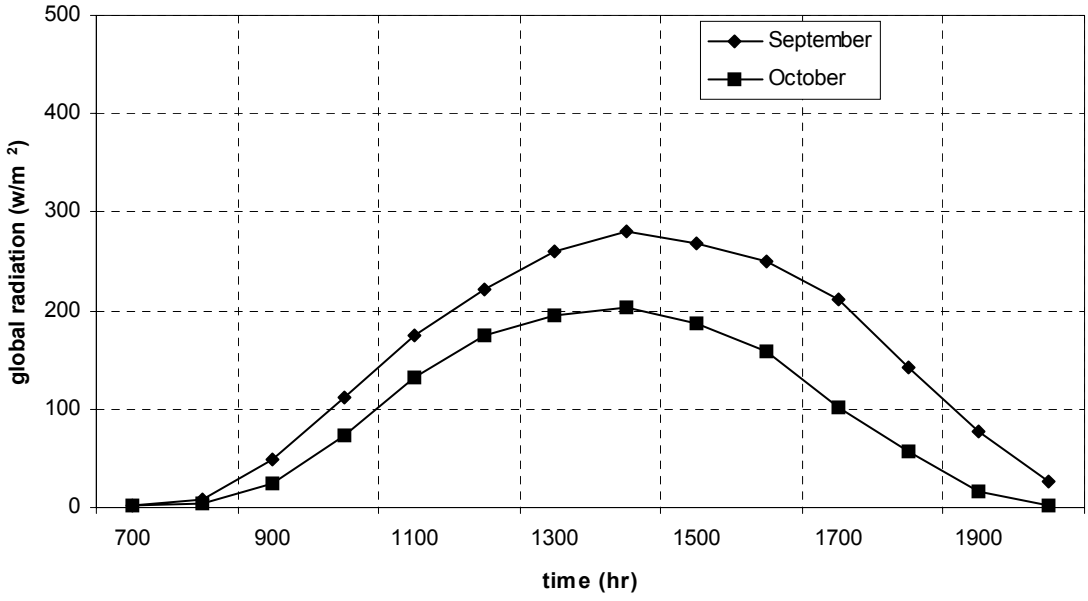

Figure 11b. Same as in Fig. 9b, but measurements are for fall season.

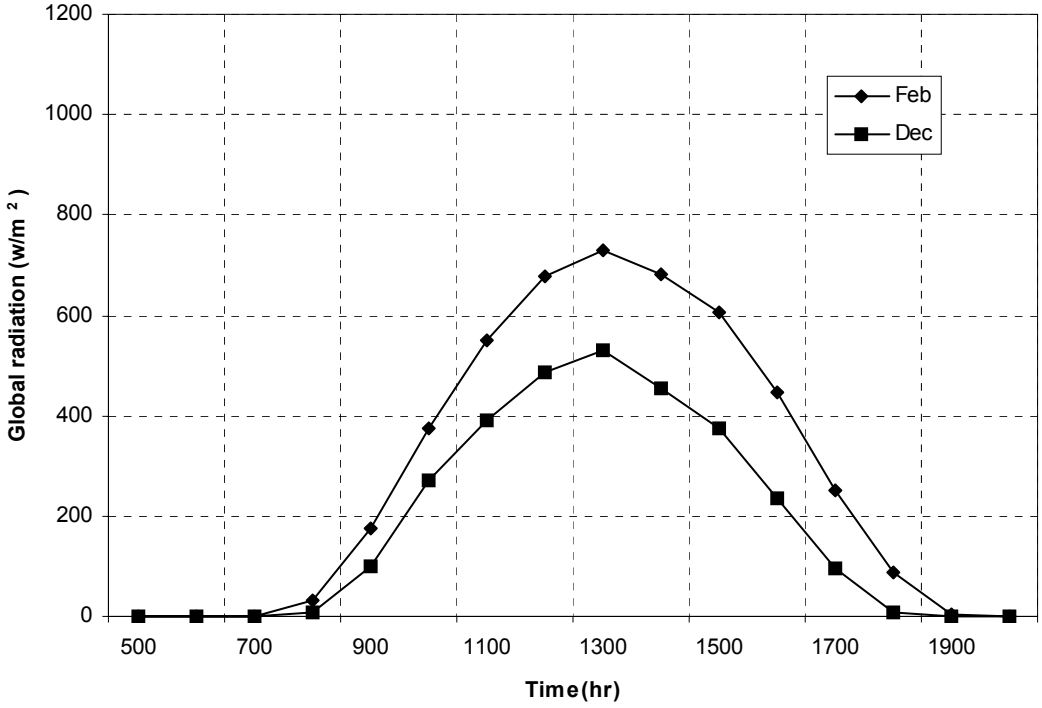

Figure12a. Diurnal variation of global radiation during winter season, Gwnagju, Korea.

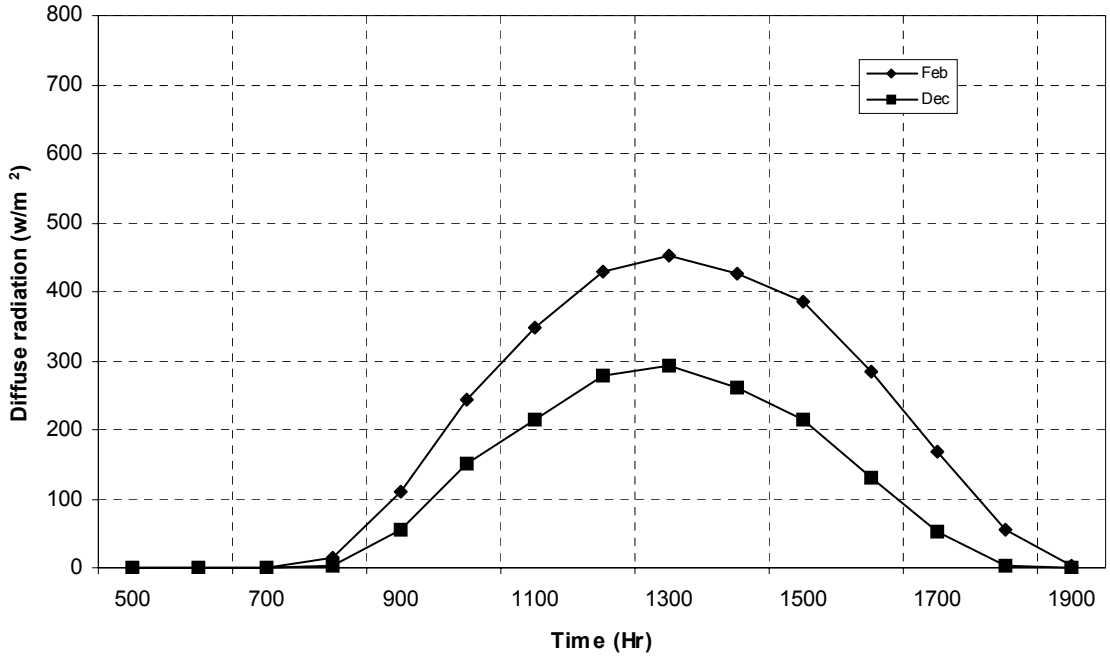

Figure12b . Diurnal variation of diffuse radiation during winter season, Gwnagju, Korea.

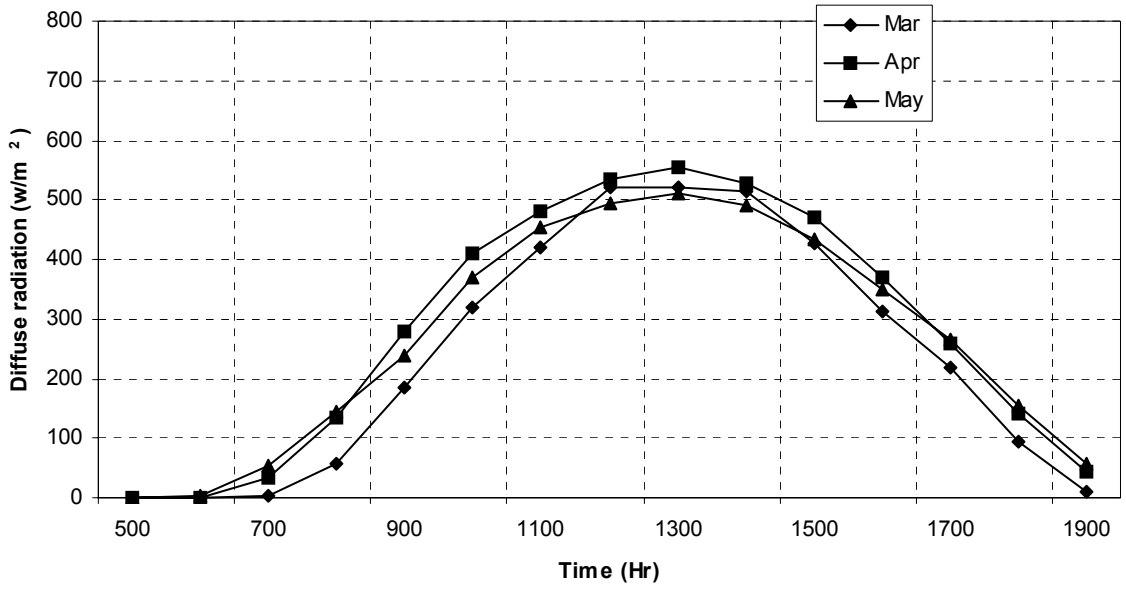

Figure 13a. Diurnal variation of diffuse radiation during spring season, 2002 at Gwnagju, Korea.

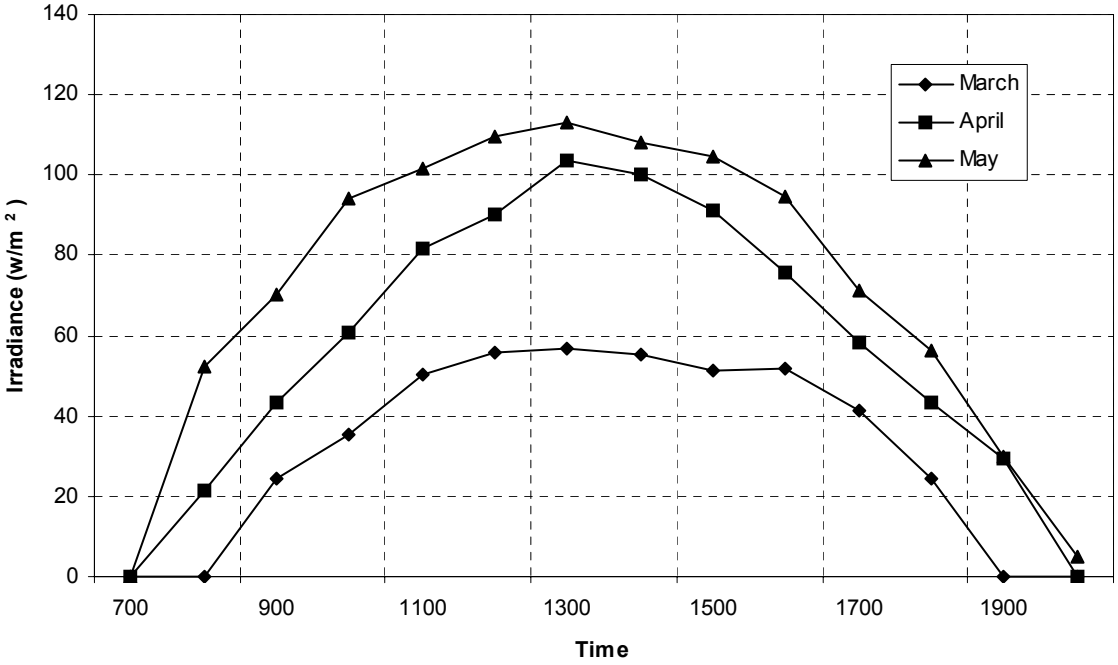

Figure 13b. Diurnal variation of diffuse radiation during spring season, 2002 at Ulaanbaatar, Mongolia.

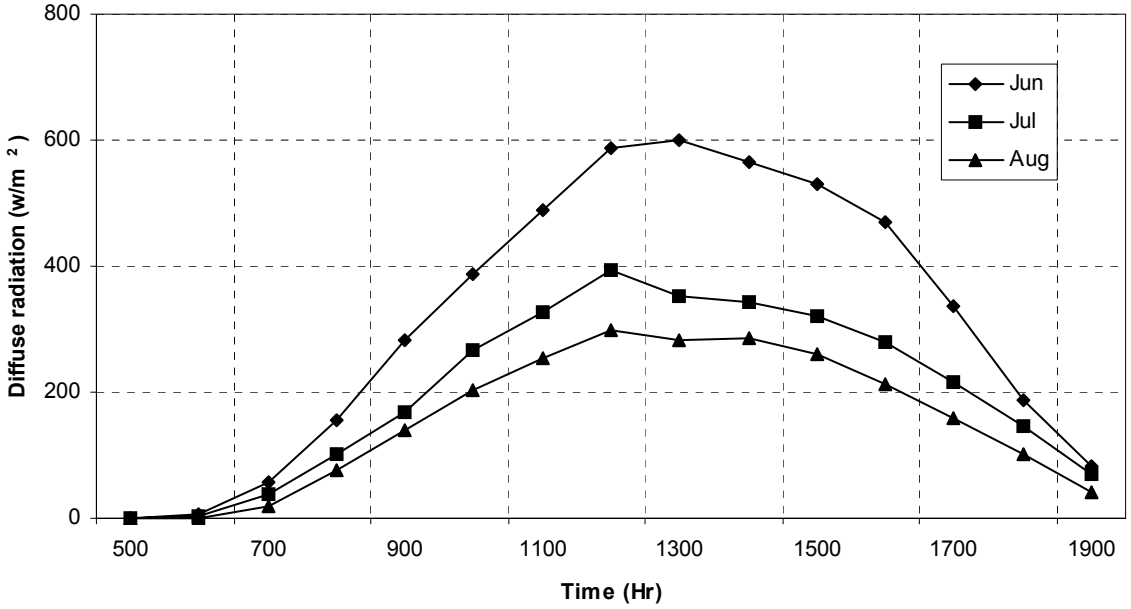

Figure 14a. Same as in Fig. 13a, but measurements are for summer season.

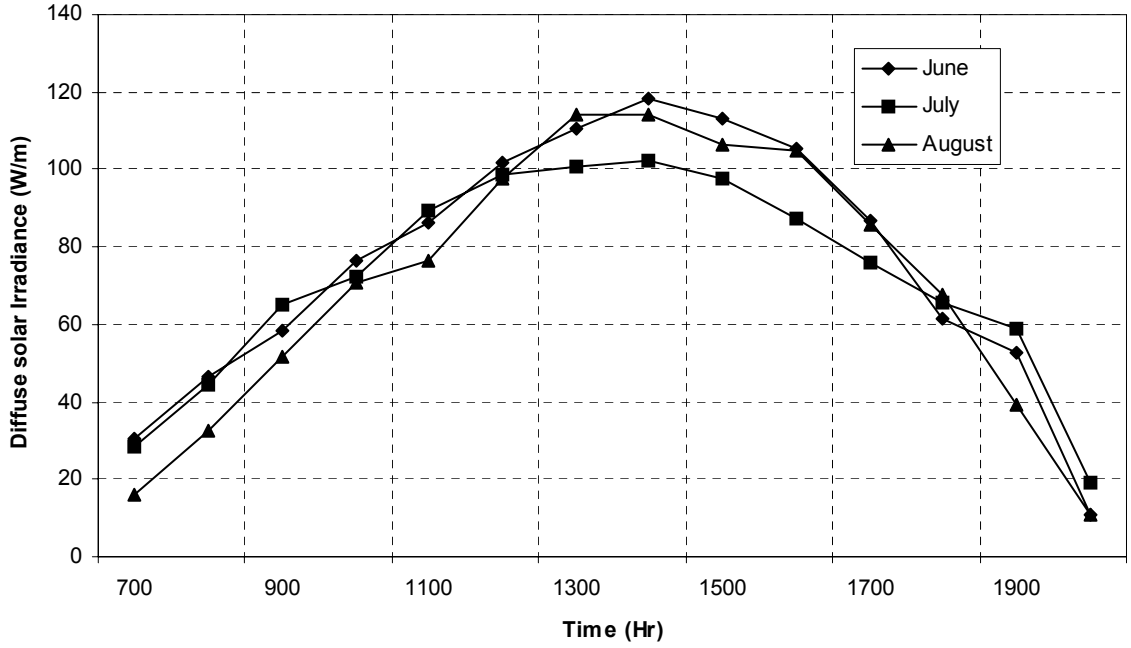

Figure 14b. Same as in Figure 13b, but measurements are for summer season.

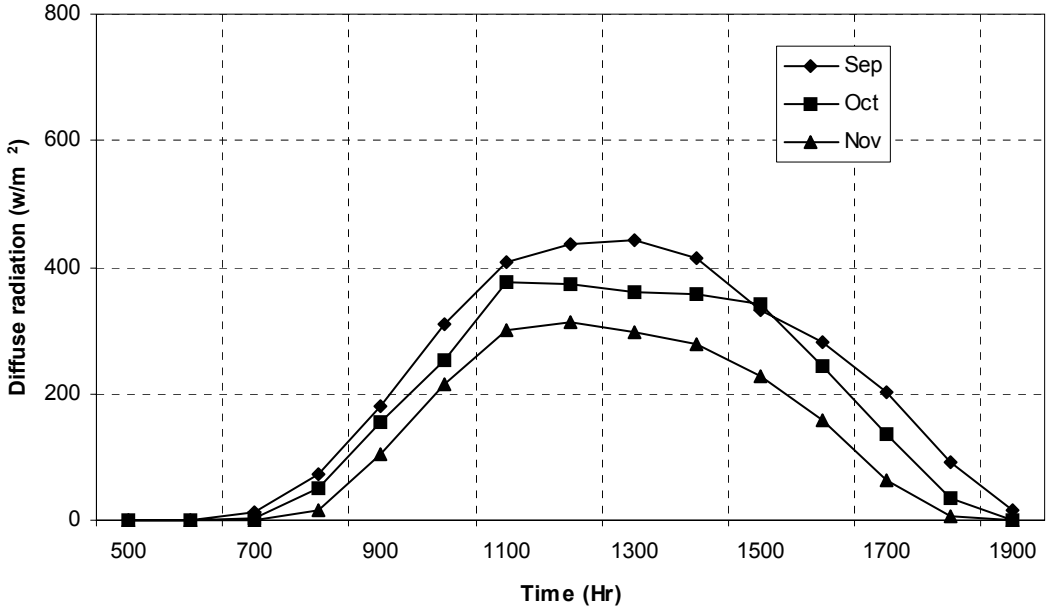

Figure 15a. Same as in Fig. 13a, but measurements are for fall season.

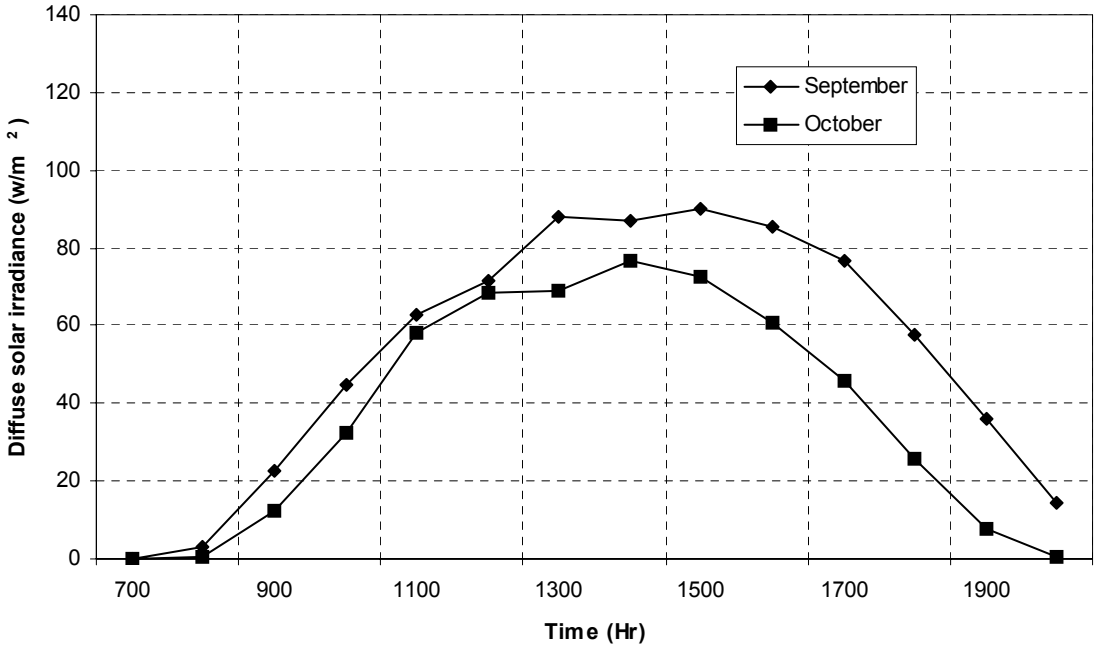

Figure 15b. Same as in Fig. 13b, but measurements are for fall season.

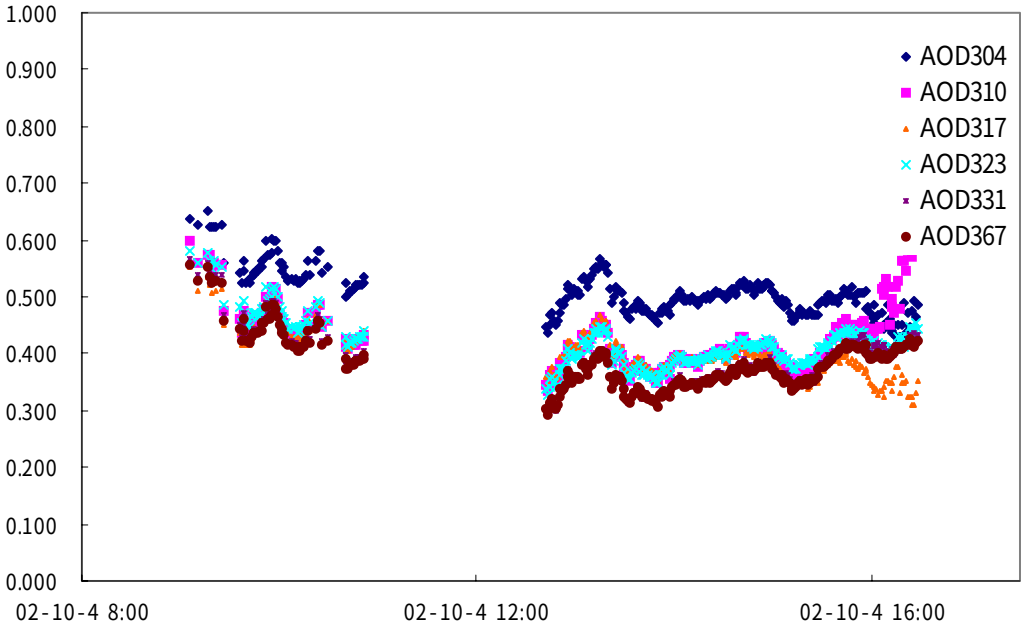

Figure 16. An example of daily AOD variation on October 4, 2002

Table 1. Monthly mean of spectral AOD for each each channel

Channel	Oct		Nov		Dec		Jan	
(nm)	mean	stdev	mean	stdev	mean	stdev	mean	stdev
304.5	0.65	0.20	0.75	0.25	0.70	0.17	0.74	0.24
310.6	0.60	0.20	0.64	0.28	0.66	0.20	0.69	0.25
317.1	0.54	0.19	0.57	0.27	0.55	0.18	0.54	0.19
323.9	0.53	0.17	0.57	0.23	0.47	0.16	0.50	0.17
331.7	0.50	0.18	0.55	0.24	0.46	0.19	0.49	0.17
367.4	0.49	0.17	0.44	0.23	0.37	0.18	0.47	0.16

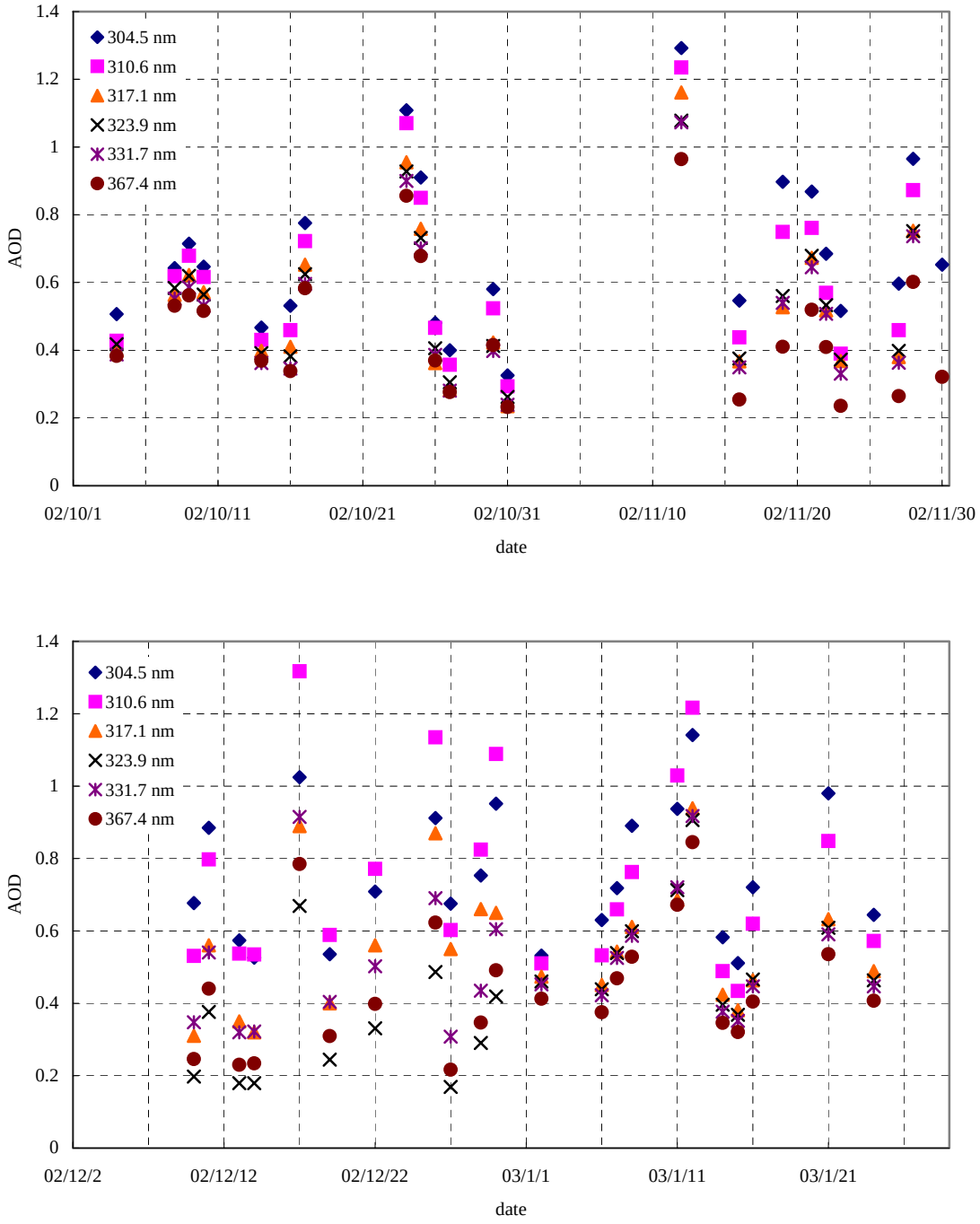

Figure 17. Daily AOD variation at UV wavelength range during the study period.

III. **Surface UV Radiation**

1 Introduction

The UV radiation constitutes very small portion of solar radiation, but it significantly affects on ecosystem as well as human health (e.g. cataracts, skin cancer). The ultraviolet radiation in the troposphere is referred to as radiation with wavelengths between about 290 and 400 nm. The UV radiation spectrum can be divided into three regions, named UV-A (315~400 nm) constituting most of the UV radiation received at the earth's surface, UV-B (280~315 nm) being partially absorbed or scattered in the atmosphere [*Al-Dhafiri et al., 2000*], and the most energetic UV-C (<280 nm) being completely absorbed by stratospheric ozone. Atmospheric ozone controls the amount of the most energetic ultraviolet radiation that reaches the troposphere, and total ozone amount and surface UV irradiance has an anticorrelation [*Cappellani et al.,* 2000 ; *Bais et al.,* 1997 ; *Bernhard et al.,* 1997 : *Weele,* 1996]. So, there has been a growing concern about increase in the surface UV radiation since ozone hole was observed in 1970s. While the largest changes in the surface UV radiation are due to the changes in the solar zenith angel, less is known about the impact by other parameters such as extraterrestrial solar radiation, cloud cover, extinction by aerosol [*Tsay et al*., 1992], the thickness of the atmosphere expressed by surface pressure (Rayleigh scattering), altitude, and surface reflectivity (albedo) [*Kylling et a*l., 1998 ; *Grobner et al*., 2000 ; *Tsay et al*., 1992]. Extraterrestrial solar radiation changes with Sun-Earth distance. Maximum and minimum values of extraterrestrial solar irradiance appear in January and July, respectively, because the Earth is at its closest point to the sun

(perihelion) on approximately 3 January, and at its farthest point (aphelion) on approximately 4 July [*Iqbal*, 1983]. Clouds scatter incident radiation and reduce the irradiance reaching the Earth's surface [*Tsay et al*., 1992]. Aerosol is important in that the size of aerosol is very similar to solar radiation wavelength.

Several studies have tried to investigate the effect of atmospheric aerosol on the surface UV radiation. *Kylling et al.* [1998] used measurement data and modeling results to investigate the effect of aerosol on UV irradiance by two instruments located at different two areas. The presence of aerosol is seen to reduce the UVB irradiance by a fraction ranging from 5% to 35% from the ratio between simulated UV spectra with and without aerosols. *Mayer et al*. [1997] studied the influence of several parameters such as aerosol on the ground level UV irradiance using spectral UV measurement and modeling results. Results of modeling without consideration of aerosol in the model input showed that the model clearly overestimated the measured results.

In this chapter we will monitor the variation of the surface UV irradiance over the Northeast Asia (Japan, and Mongolia). A simple statistical analysis of the data will be used to investigate the variability of surface UV irradiance.

2 Instrumentations

Measurements at Ulaanbaatar, Mongolia, are collected by UVB-1 pyranometer (Yankee Environmental Systems) at the ground of Ministry of Nature and the Environment, Institute of Geoecology. This instrument measures the integrated global UV-B irradiance at the wavelength of 280 to 320 nm, and shares CR10X (Campbell Scientific) data logger with RSR system. Measurement outputs from

the UV pyranometer are sampled and recorded every 10 minutes as a mean value into a data logger

UV-B radiometer (EKO, MS-212W) is located in Kyoto University at Kyoto, Japan, and measures the integrated global UV-B radiation (280 – 315 nm) every 10 minutes interval and recorded into data logger.

3 Methodologies and Measurements

The measured data are averaged each hour to plot the diurnal variation, and then the mean values for each month were computed. The UV radiation measurements were taken under all sky conditions. The measurement period are from April 2002 to October 2002 for Ulaanbaatar, and from April 2002 to Janyary 2003 for Kyoto.

Relationship between AOD and UV irradiance was investigated by scatter plot when the solar zenith angle is 60°, 70°, and 80° because AOD was calculated at the range from 60° ~ 80°. So, we don't need specific algorithm to filter out sky conditions because AOD was calculated under clear-sky condition.

4 Data Analysis and Results

Monitoring of UV radiation

Tables 4.4.1 and 4.4.2 show the diurnal variation of UV-B radiation at Ulaanbaatar and Kyoto, respectively for all sky conditions. Each month has its maximum hourly mean UVB irradiance between local noon and 2 PM as it can bee seen on Tables 4.4.1a ~ b. Figures 4.4.1 (a)~(c) are the plots of the diurnal

variation of Ulaanbaatar, Mongolia. In case of Ulaanbaatar, the maximum value of UVB irradiance of the measurement period was 222.4 mW/m^2 at local noon in July. From Table 4.4.2 and Figure 4.4.2, the diurnal variation at Kyoto is shown and the maximum hourly mean occur at noon for the period with a value of 932 mW/m^2 which is over 4 times larger than that of Ulaanbaatar. Seasonal variation for both sites were clear, highest in July and lowest in January (only for Kyoto).

Table 4.4.1a. Diurnal Variation of UVB irradiance at Ulaanbaatar, Mongolia (Apr 2002 – Oct 2002)

unit : mW/m^2

Time(h)	Apr	May	Jun	Jul	Aug	Sep	Oct
5.5		2.0	2.8	3.3			
6.5	2.7	3.7	4.9	4.4	3.5		
7.5	4.1	8.2	13.3	12.6	6.3	2.0	
8.5	8.8	19.7	33.1	30.4	13.7	3.6	2.6
9.5	19.0	45.9	68.4	56.3	26.5	8.5	4.2
10.5	36.9	66.9	97.9	95.5	46.6	17.1	8.4
11.5	62.5	106.5	165.3	163.2	60.0	30.3	14.6
12.5	74.1	100.5	192.3	**222.4**	64.6	43.6	17.2
13.5	103.6	121.9	168.4	216.2	93.5	79.2	27.5
14.5	87.4	128.0	148.4	167.7	92.3	63.4	18.9
15.5	58.4	91.9	133.5	144.8	80.8	55.0	16.5
16.5	27.2	38.7	66.0	82.1	48.3	35.2	10.5
17.5	11.5	20.5	30.9	43.0	25.6	17.0	6.0
18.5	4.5	7.8	12.7	16.6	10.6	7.7	3.4
19.5	3.1	4.0	4.8	6.2	4.2	3.7	
20.5		2.0	3.1	3.3	3.3		

Table 4.4.1b. Diurnal Variation of UVB irradiance at Kyoto, Japan (Apr 2002 – Jan 2003)

unit :mW/m^2

Time	Apr	May	Jun	Jul	Aug	Sep	Oct	Nov	Dec	Jan
5.5					6.6	5.8				
6.5	52.3	54.2	58.5	65.6	42.2	21.5	10.1	6.6		
7.5	105.7	133.3	128.8	352.3	168.2	104.2	58.4	21.3	8.7	7.0
8.5	250.1	340.0	252.3	477.5	404.5	271.4	176.5	87.4	42.4	37.1
9.5	438.3	518.3	364.4	614.8	631.4	464.7	328.1	194.4	104.8	102.1
10.5	607.2	680.0	429.5	806.8	830.4	614.0	459.2	299.4	171.5	187.2
11.5	705.6	748.3	518.2	**932.3**	873.9	693.0	516.0	332.6	231.3	237.4
12.5	719.4	706.7	522.0	888.1	856.9	683.0	483.4	322.4	234.8	229.7
13.5	566.8	660.0	512.9	833.7	788.7	570.0	375.9	251.8	170.4	196.0
14.5	425.0	503.3	379.5	675.3	558.0	386.1	237.8	142.1	97.4	116.9
15.5	251.6	305.0	225.8	519.3	374.2	219.4	108.0	53.3	34.9	49.1
16.5	107.7	131.7	129.5	373.0	193.5	85.4	26.7	10.6	8.1	12.8
17.5	51.4	55.0	61.3	86.8	54.5	18.0	6.6	6.6		
18.5		54.2	50.0	17.1	9.3	6.0				
19.5				65.6						
20.5										

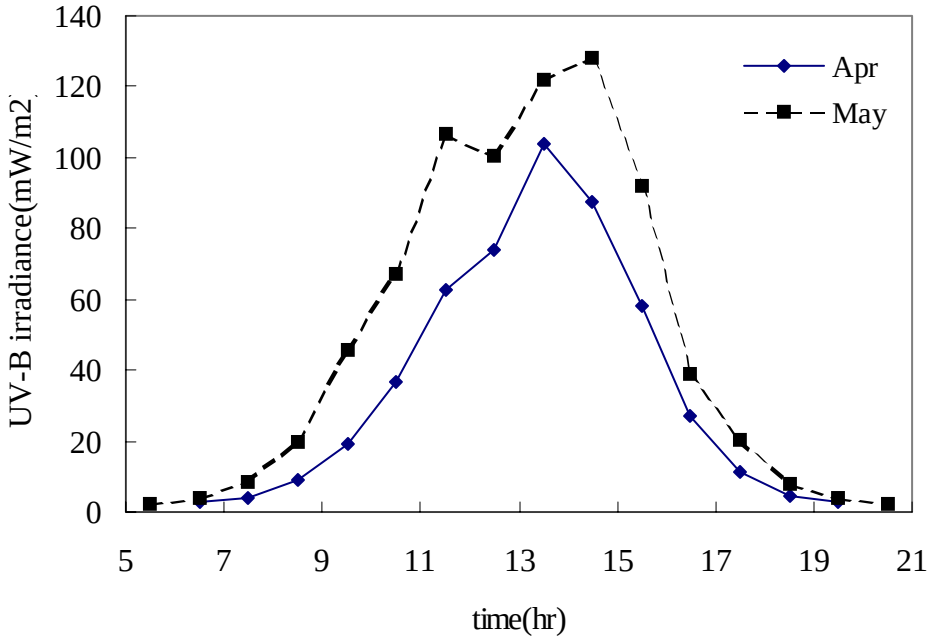

(a) Spring

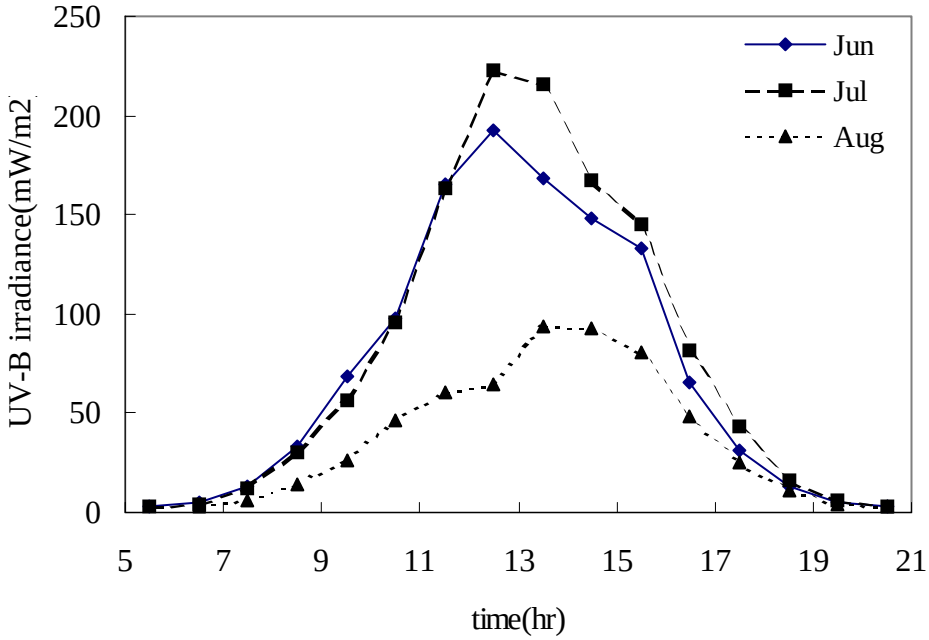

(b) Summer

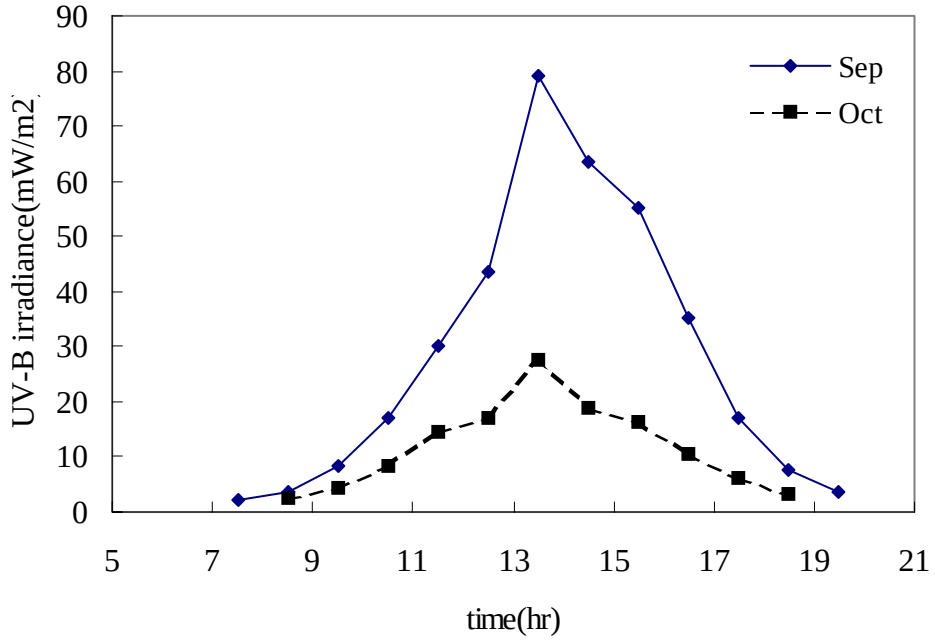

(c) Fall

Figure 1. Diurnal Variation of UVB radiation at Ulaanbaatar, Mongolia 2002

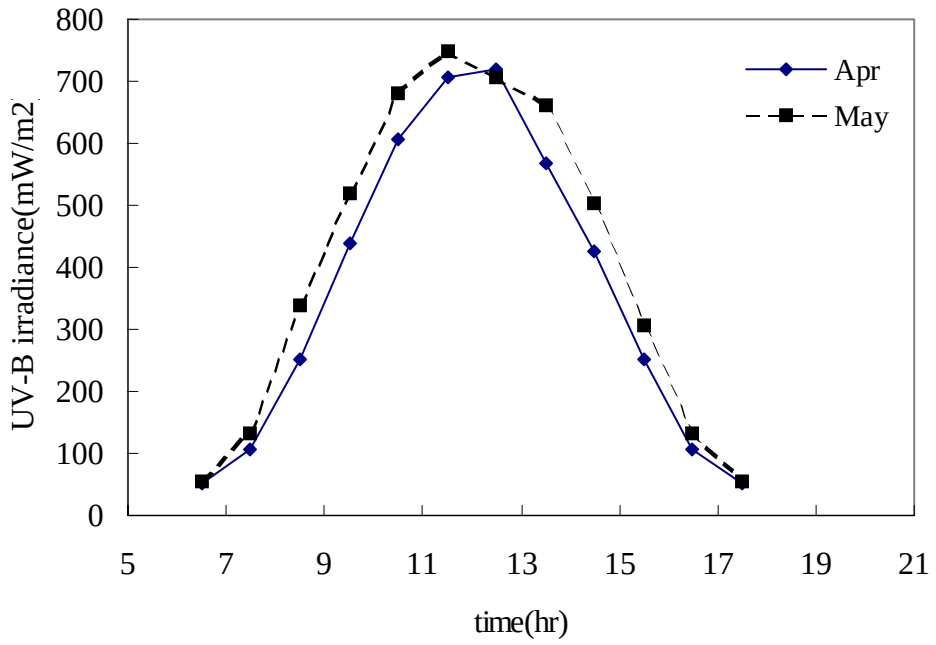

(a) Spring

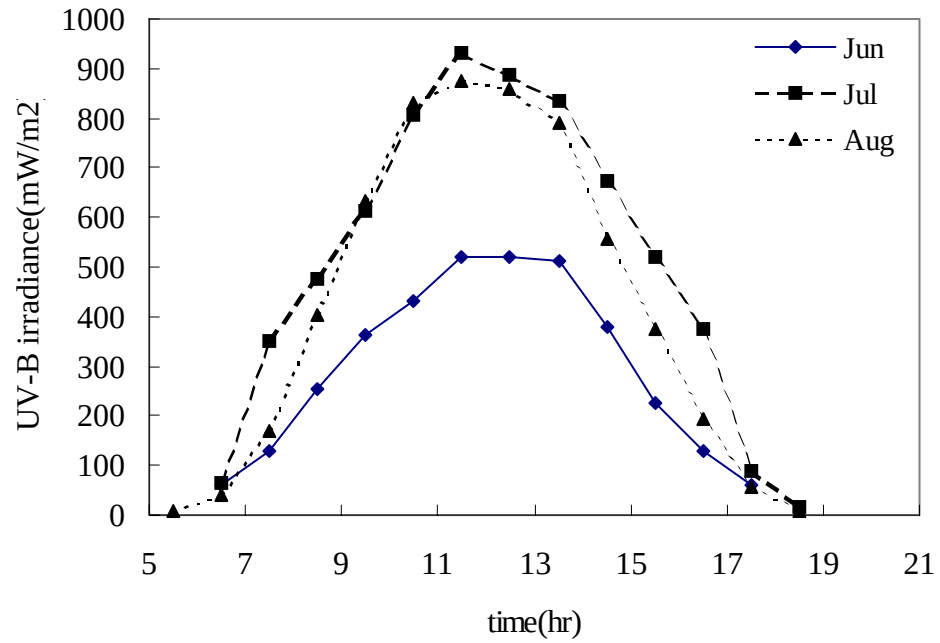

(b) Summer

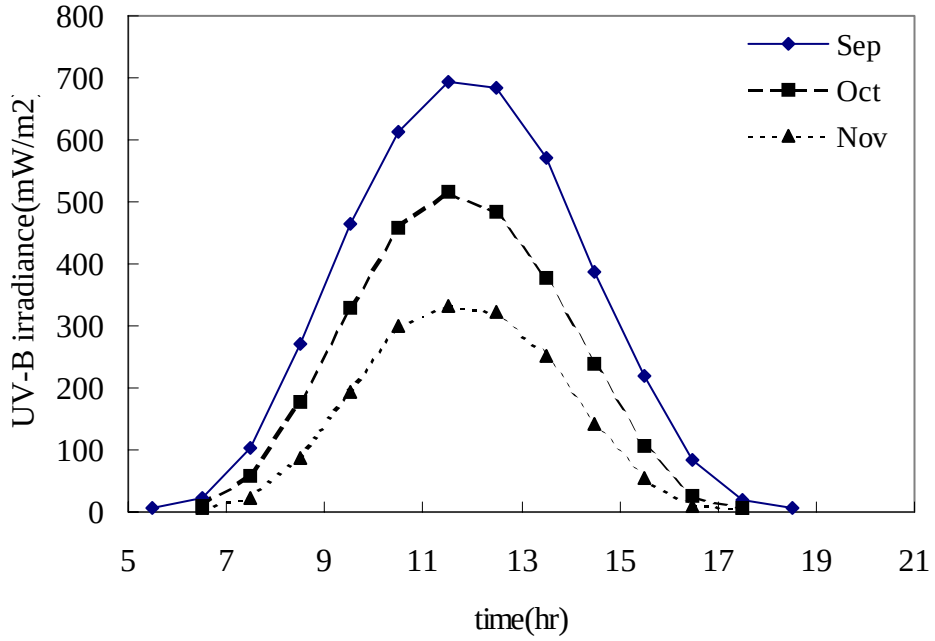

(c) Fall

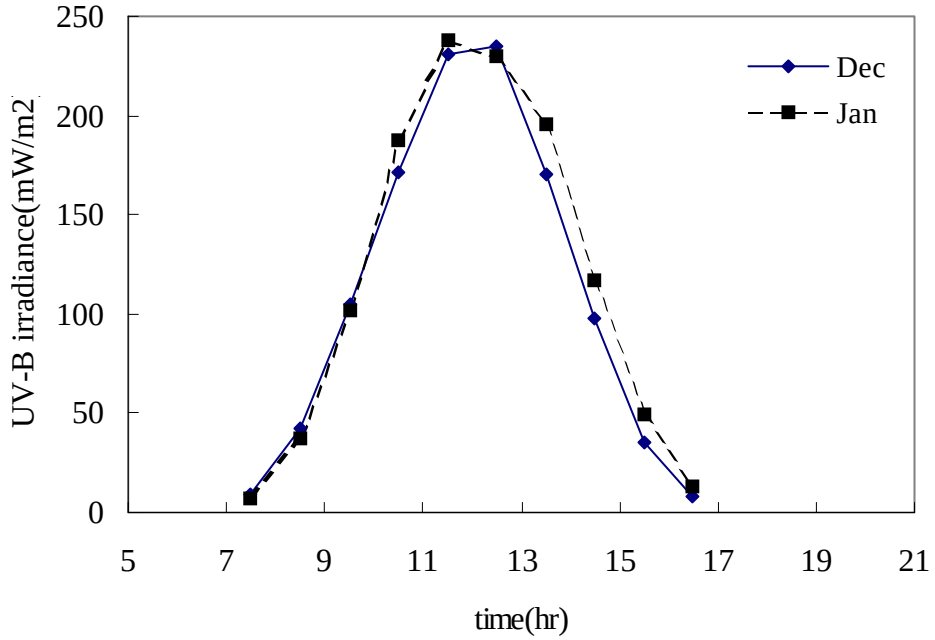

(d) Winter

Figure 2. Diurnal variation of UVB riadiation at Kyoto, Japan 2002-2003

5 Conclusions

Main goal of this chapter is to show and compare how the surface UV radiation varies through the year over the Northeast Asia (installed at Ulaanbaatar, and Kyoto).

This study will be continued to monitor and to characterize the surface UV radiation seasonally. The relationship between the surface UV irradiance and AOD has so many uncertainties because of inappropriate assumptions and insufficient data. Plenty of data and algorithm to determine cloudless conditions can reduce the uncertainties in estimating the surface UV irradiance.

6 References

Al-Dhafriri, A. M., M. S. Al-Ayed, and M. Bin Mahfoodh, Long-term Monitoring and Analysis of Hourly Solar UV Radiation in the 290~380 nm Range in the Middle Region of Saudi Arabia, *J. Air & Waste Manage. Assoc*., vol. 50, 1045~1049, 2000

Bais, A. F., M. Blumthaler, A. R. Webb, J. Groebner, P. J. Kirsch, B. g. Gardiner, C. S. zerefos, T. Svenoe, and T. J. Martin, Spectral UV Measurements over Europe within the Second European Stratospheric Arctic and midlatitude Experiment Activities, *J. of Geophys. Res*., vol. 102, No.D7, 8731-8736, 1997

Bernhard, G., B. Mayer, G. Seckmeyer, and A. Moise, Measurements of Spectral Solar UV Irradiance in Tropical Australia, *J. Geophys. Res*., vol.102, No.D7, 8719~8730, 1997

Cappellani, F., C. Kochler, Ozone and UV-B variations at Ispra from 1993 to 1997, *Atm. E*nv., 33, 3787~3790, 1999

Estupinan, Jeral G., Sethu Faman, Gennaro H. Crescenti, John J. Streicher, and Willian F. Barnard, Effects of Clouds and Haze on UV-B Radiation, *J. of Geophys. Res*., vol. 101, No.D11, 16,807-16,816, 1996

Grobner, J., A. Albold, M. Blumthaler, T. Cabot, A. De la Casiniere, J. Lenoble, T. Martin, D. Masserot, M. Muller, R. Philipona, T.Pichler, E. Pougatch, G. Rengarajan, D. Schmucki, G. Seckmeyer, C. Sergent, M. L.Toure, and P. Weihs, Variability of Spectral Solar Ultraviolet Irradiance in an Alpine Environment, *J. of Geophys. Res*., vol.105, No.D22, 26,991~27,003, 2000

Harrison, Lee, and Joseph Michalsky, Objective Algorithms for the Retrieval of

Optical depths from Ground-based Measurements, *Applied Optics*, vol.33, No.22, 5126-5132, 1994

Iqbal, Muhammad, *An Introduction to Solar Radiation*, Academic Press, 1983

Kim, Jeongeun, Seong Y. Ryu, and Young J. Kim, *Proceedings of the Third International Symposium on Advanced Environmental Mnitoring*, 255-256, 2000

Kylling, A., A. f. Bais, Blumthaler, J. Schreder, C. S. Zerefos, and E. Kosmidis, Effect of aerosols on Solar UV Irradiances during the Photochemical Activity and Solar Ultraviolet Radiation Campaign, *J. of Geophys. Res*., vol.103, No.D20, 26,051-26,060, 1998

Kwon, H. J., Variations of the Surface Ultraviolet-b radiation with Changes in the Ozone Layer, MS Dissertation, 1996

Mayer, B., G. Seckmeyer, Systematic Long-term Comparison of Spectral UV measurements and UVSPEC Modeling Results, *J. Geophys. R*es., vol. 102, No.D7, 8755~8767, 1997

Meleti, C., Cappellani, F., Measurements of Aerosol Optical Depth at Ispra : analysis of the Correlation with UV-B, UV-A, and Total Solar Irradiance, *J. Geophys. Res*., vol. 105, No.D4, 4971~4978, 2000

Min, Hee-Kyoung, A Study on Variation of Aerosol Optical Depth (AOD) in the Atmosphere using RSR (Rotating Shadowband Radiometer) data, MS Dissertation, 2000

Park, Ji Yong, Sensitivity of Surface UV Radiation due to Changing Total Ozone in the Frederick Model, MS Disseration, Yonsei University, 1998

Reid, E. Basher, X. Zheng and S. Nichol, Ozone-related Trends in Solar UVB series, *Geophys. Res*. Lett., 21, 2719-1716, 1994

Sabziparvar, Ali A., Piers M. de F., and Keith P. Shine, Changes in Ultraviolet Radiation due to Stratospheric and Tropospheric Ozone Changes since Preindustrial times, *J. Geophys. Res*., vol.103, No.D20, 26,107~26,113, 1998

Tsay, Si-Chee, Ultraviolet Radiationin the Arctic ; The Impact of Potential Ozone Depletion and Cloud Effects, *J. Geophys. Res,.*vol.97, No.D8, 7289-7840, 1992

UVB-1 Ultraviolet Pyranometer Installation and User Guide, ver.2.0, Yankee Environmental Systems, Inc., 1997

Weele, Michale Van, Effect of Clouds on Ultraviolet Radiation : photodiss-ociation rates of chemical species in the troposphere, 1996

IV. Air mass backward trajectories during APN intensive sampling periods (07/23-08/02, 11/05-11/14/2002) at Beijing, Gwnagju, Kyoto and Ulaanbaatar

Lagrangian trajectory, which were used to identify pathways of the air mass transport or establish source-receptor relationships of air pollutants, have enjoyed considerable popularity as an approach to determine the potential source regions of pollutants. Trajectories could reflect the large-scale atmospheric transport characteristics of air mass arriving at Taean. They were not only necessary for estimating the long-range transport of pollutants, other chemical species, but also provided a better understanding of airflow patterns.

Three-day back-trajectories at three levels (500, 1000 and 2000m above ground level) with 1-hr interval during APN intensive sampling periods (07/23-08/02, 11/05-11/14/2002) were calculated using HYsplit model （NOAA/ARL; Draxler, 1996, 1997, 1998） with the framework of Final Run (FNL) meteorological data, which was six hourly archive data from NCEP's GDAS (Global Data Assimilation System). Northern Hemisphere FNL data have 129x129 polar stereographic grids and 190.5km grid spacing. FNL data include four times (0000, 0600, 1200, 1800UTC) output and upper level FNL data include thirteen mandatory pressure surfaces: 1000, 925, 850, 700, 500, 400, 300, 250, 200, 150, 100, 50, and 20hPa.

A computed trajectory is representative for the path of an air parcel only for a limited period. The uncertainty for the computation of trajectories can be induced by truncation errors, interpolation errors, errors resulting from certain assumptions regarding the vertical wind, wind field errors, and starting position

errors, amplification of errors, and ensemble methods (Stohl, 1998). To estimate of the divergence and confluence of the flow near the site, four different trajectories were computed simultaneously by a spatial displacement of ±0.5° of latitude and longitude from the sampling site. When all four trajectories were converged, the trajectories is considered valid, otherwise it was discarded (He et al., 2003).

<Trajectory patterns >

The back-trajectories that satisfied convergence condition during intensive sampling periods lasted 72-hr with 1-hr time interval. All trajectories in one specific time were also discarded if at least one back-trajectory at three-level ended in those time crashed into the surface or because of lack of meteorological data, or didn't satisfy convergence condition.

Figs. 1-8 exhibits the pattern for all available three-day back trajectories at 500, 1000 and 200m agl (above ground level) during the intensive APN sampling periods.

Figure lists:

- Figs. 1-4 exhibit back-trajectory patterns at 500, 1000 and 2000m agl. at 01:00UTC, 07:00UTC, 13:00UTC and 19:00UTC during the period of

07/23-08/02/2002.

- Figs. 5-8 exhibit back-trajectory patterns at 500, 1000 and 2000m agl. at 01:00UTC, 07:00UTC, 13:00UTC and 19:00UTC during the period of 07/23-08/02/2002.

Site	UTC	Local Time
Beijing & Ulaanbaatar	01:00	09:00a.m.
	07:00	03:00p.m.
	13:00	09:00p.m.
	19:00	03:00a.m.
Gwangju & Kyoto	01:00	10:00a.m.
	07:00	04:00p.m.
	13:00	10:00p.m.
	19:00	04:00a.m.

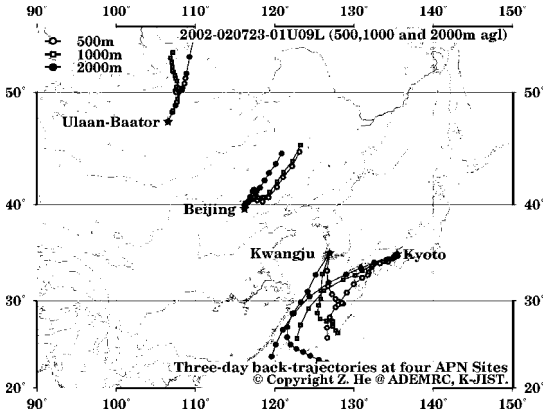

01:00 UTC Time, 07/23/2002

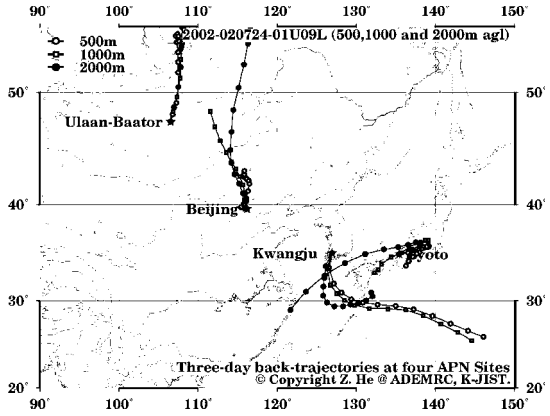

01:00 UTC Time, 07/24/2002

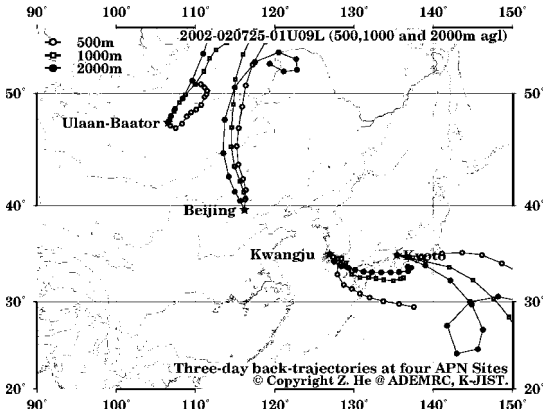

01:00 UTC Time, 07/25/2002

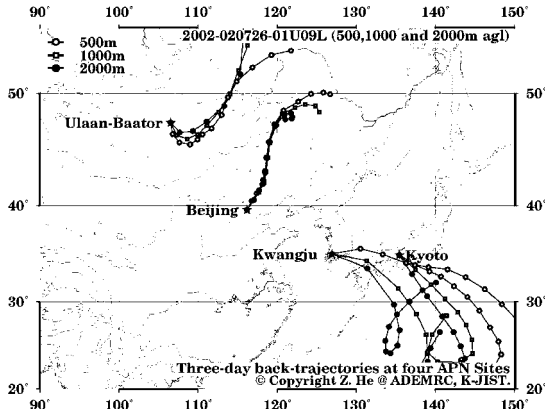

01:00 UTC Time, 07/26/2002

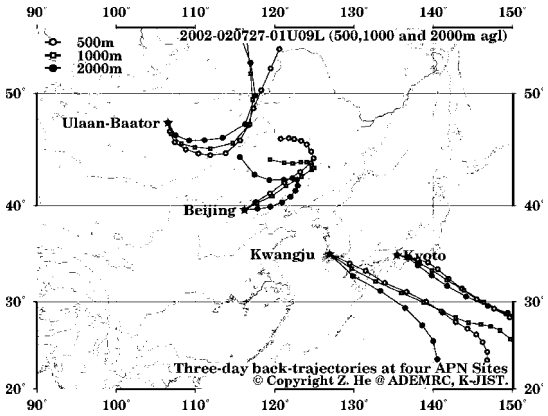

01:00 UTC Time, 07/27/2002

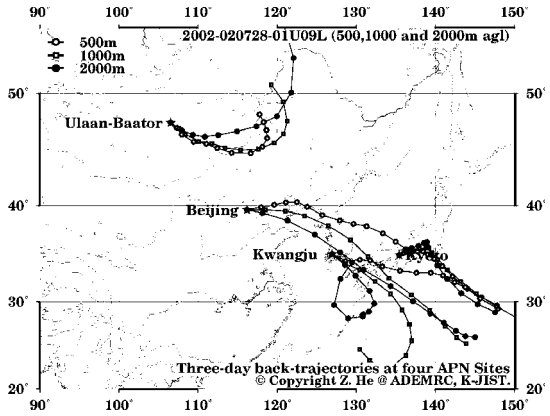

01:00 UTC Time, 07/28/2002

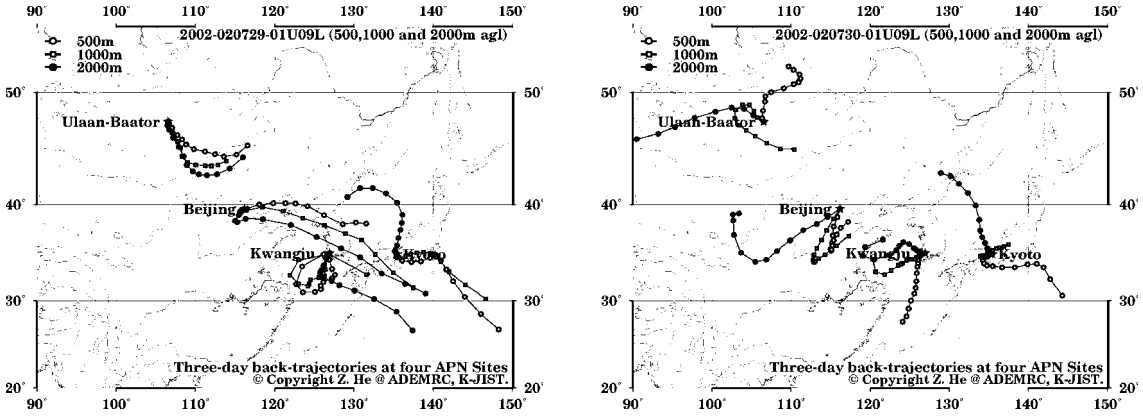

01:00 UTC Time, 07/29/2002

01:00 UTC Time, 07/30/2002

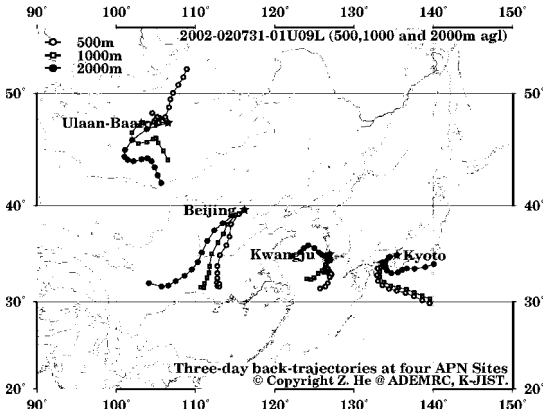

01:00 UTC Time, 07/31/2002

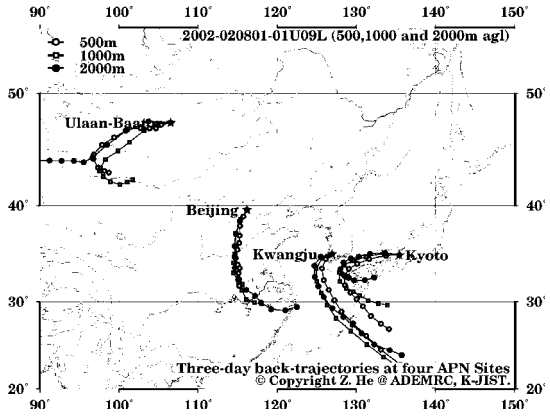

01:00 UTC Time, 08/01/2002

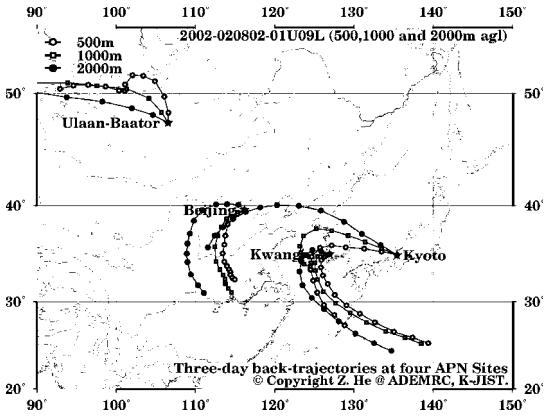

01:00 UTC Time, 08/02/2002

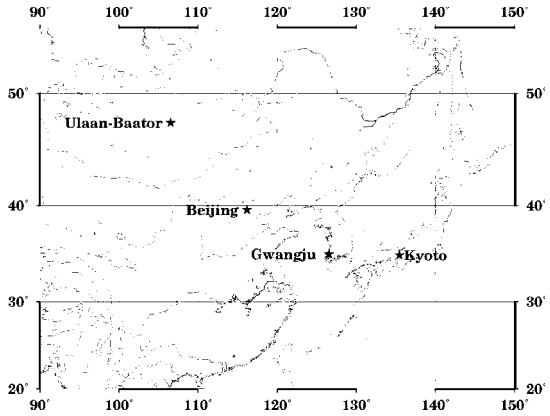

01:00 UTC Time, 08/03/2002

Fig. 1. Back-trajectory patterns at 500, 1000 and 2000m agl during the period of 07/23-08/02/2002. All trajectories ended at 01:00 UTC time, which is local time 08:00a.m., 09:00a.m., 09:00a.m. and 08:00a.m. of Beijing, Gwnagju, Kyoto and Ulaanbaatar, respectively.

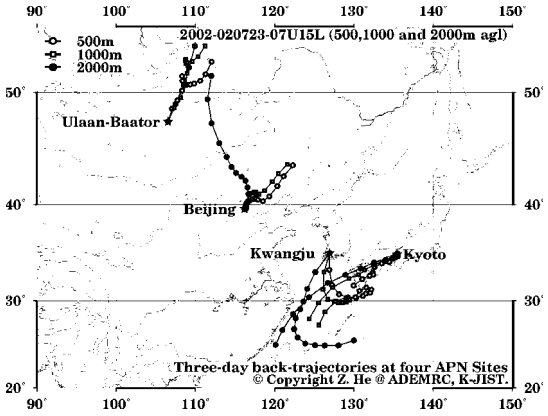

07:00 UTC Time, 07/23/2002

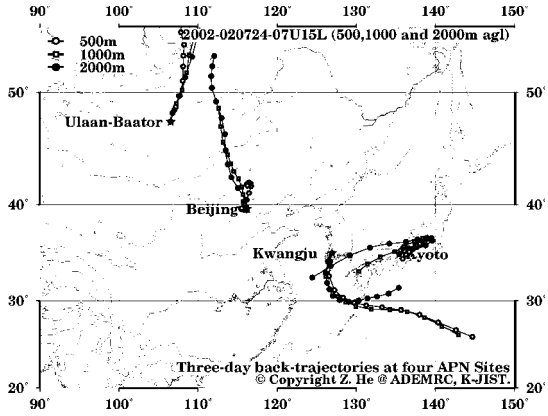

07:00 UTC Time, 07/24/2002

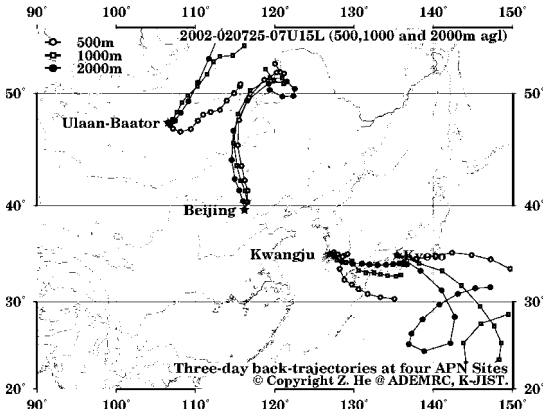

07:00 UTC Time, 07/25/2002

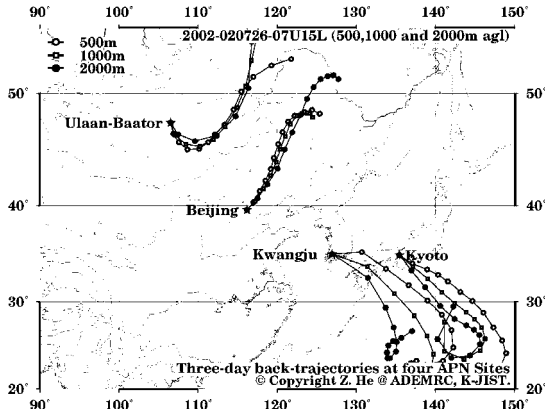

07:00 UTC Time, 07/26/2002

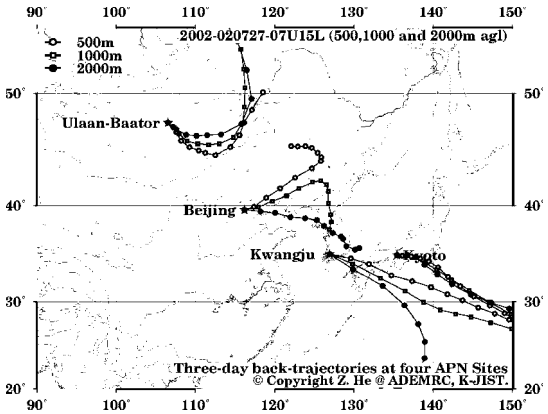

07:00 UTC Time, 07/27/2002

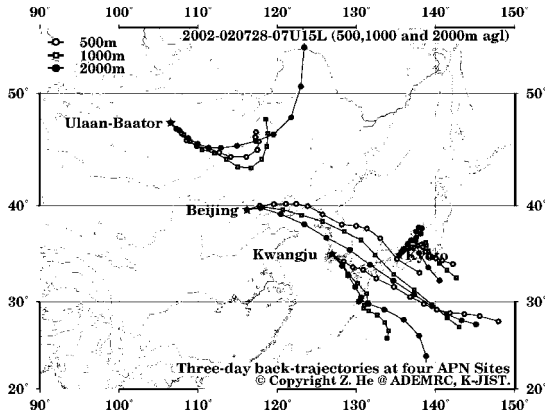

07:00 UTC Time, 07/28/2002

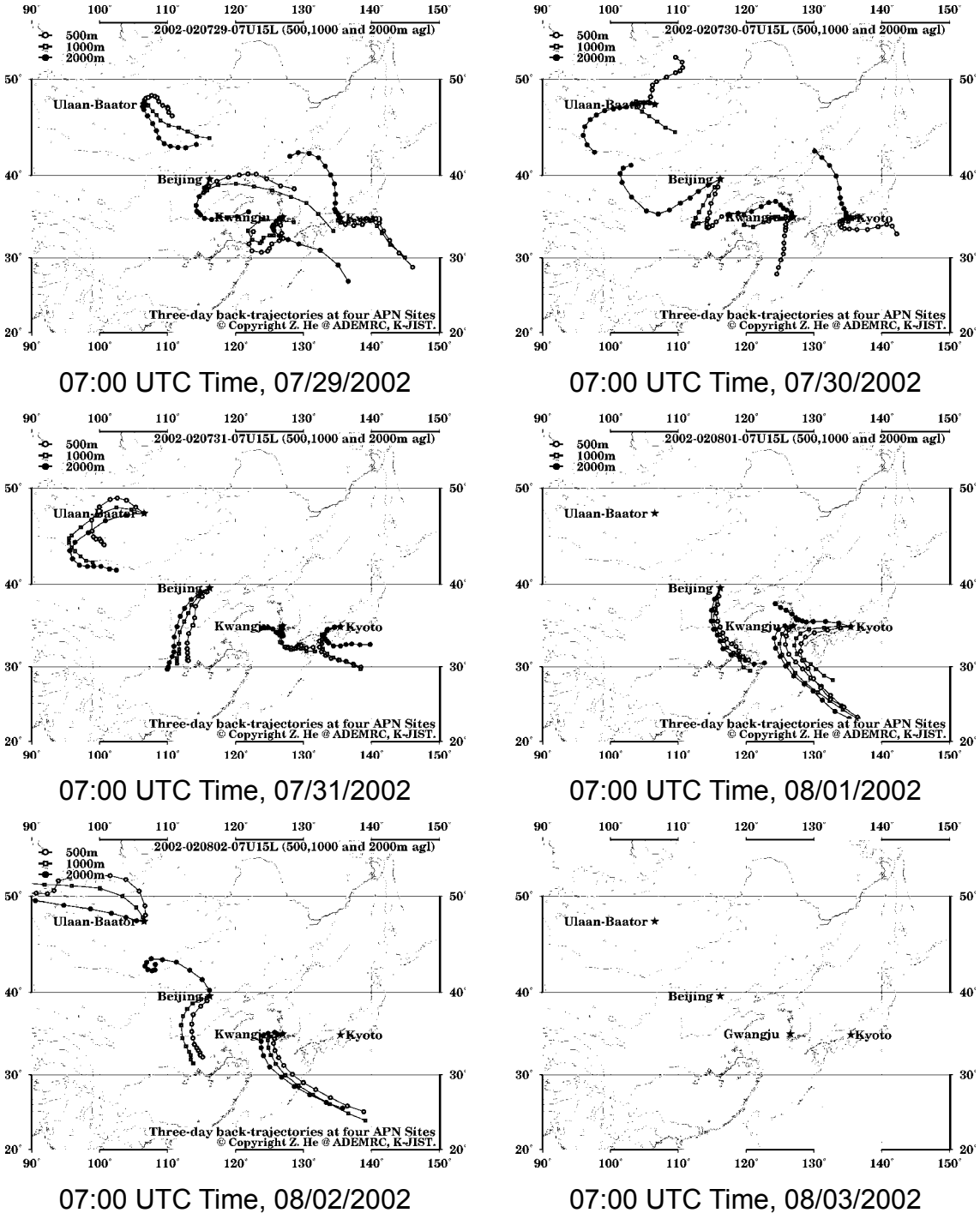

Fig. 2. Back-trajectory patterns at 500, 1000 and 2000m agl during the period of 07/23-08/02/2002. All trajectories ended at 07:00 UTC time, which is local time 03:00p.m., 04:00p.m., 04:00p.m. and 03:00p.m. of Beijing, Gwnagju, Kyoto and Ulaanbaatar, respectively.

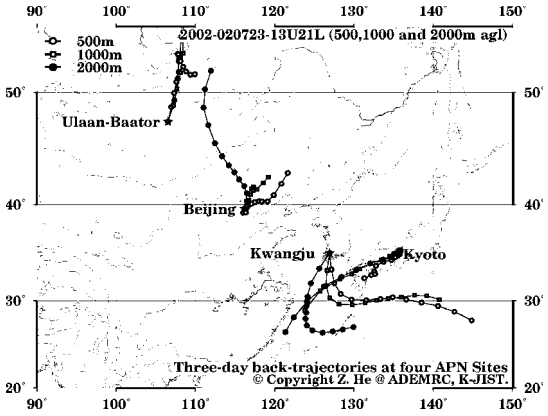

13:00 UTC Time, 07/23/2002

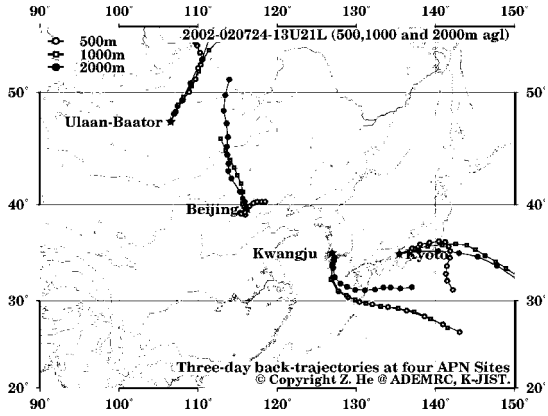

13:00 UTC Time, 07/24/2002

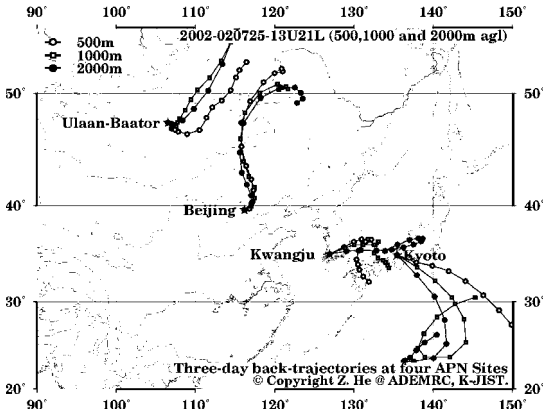

13:00 UTC Time, 07/25/2002

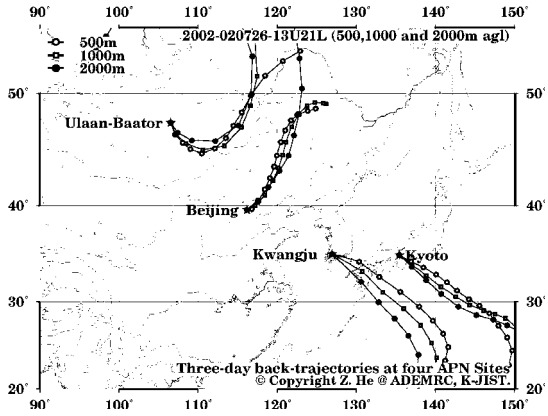

13:00 UTC Time, 07/26/2002

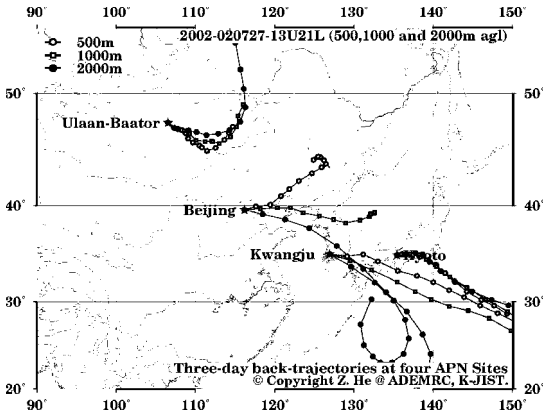

13:00 UTC Time, 07/27/2002

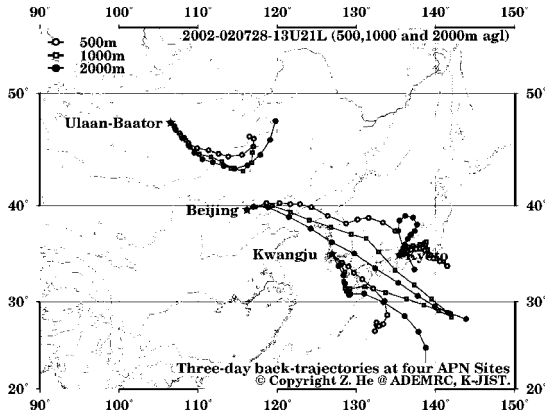

13:00 UTC Time, 07/28/2002

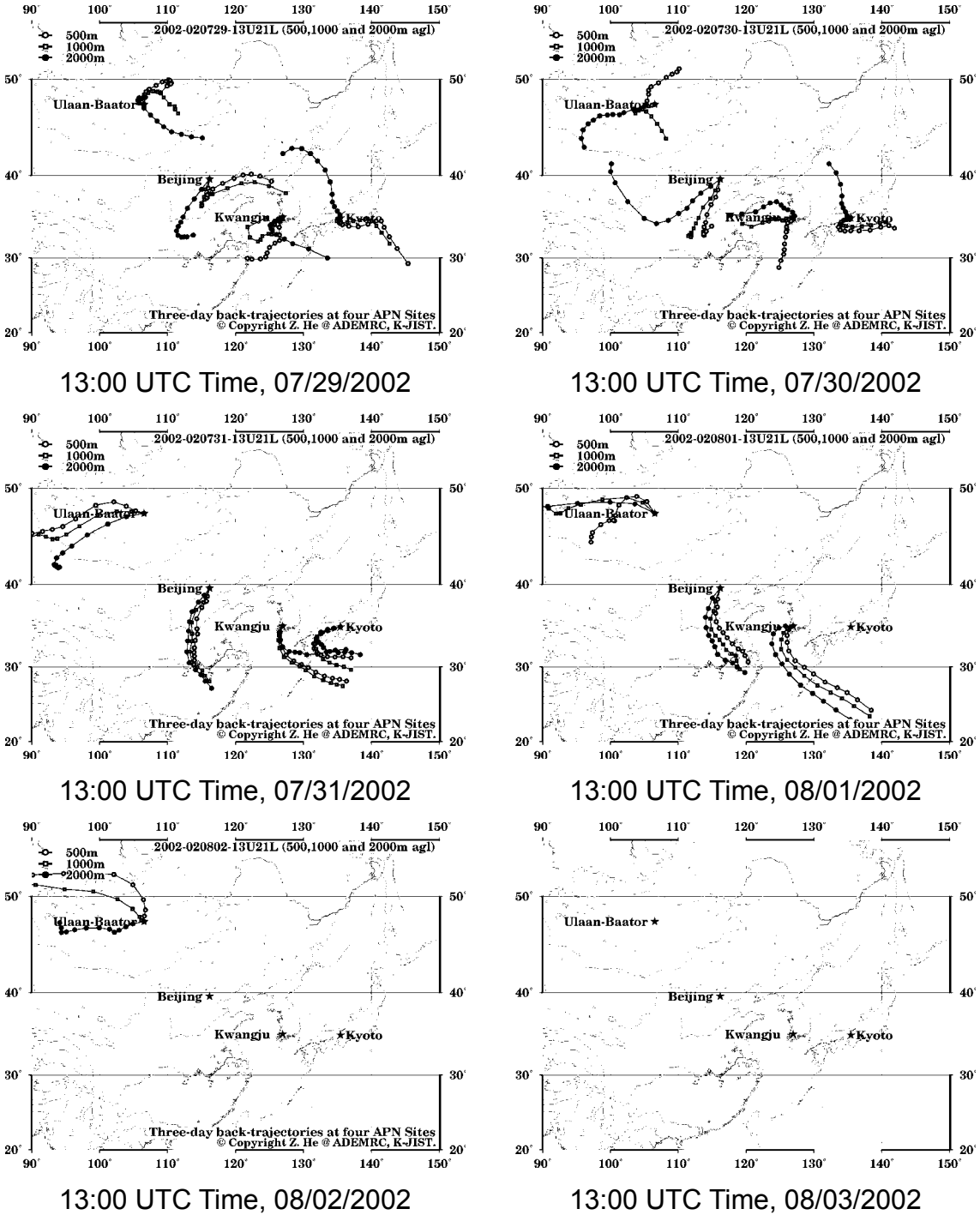

Fig. 3. Back-trajectory patterns at 500, 1000 and 2000m agl during the period of 07/23-08/02/2002. All trajectories ended at 13:00 UTC time, which is local time 09:00p.m., 10:00p.m., 10:00p.m. and 09:00p.m. of Beijing, Gwnagju, Kyoto and Ulaanbaatar, respectively.

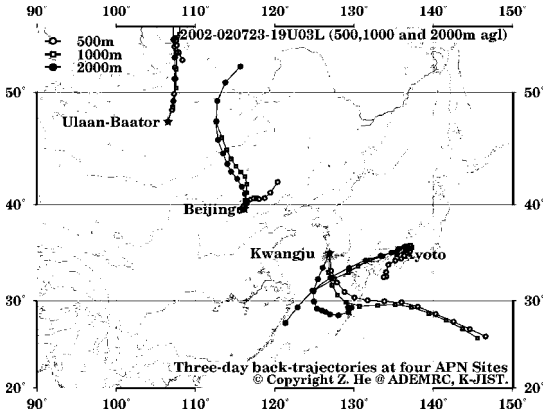

19:00 UTC Time, 07/23/2002

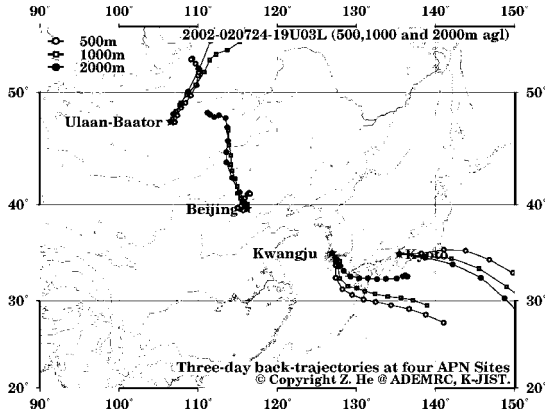

19:00 UTC Time, 07/24/2002

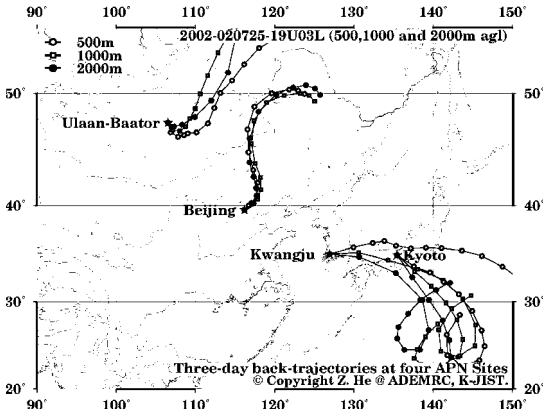

19:00 UTC Time, 07/25/2002

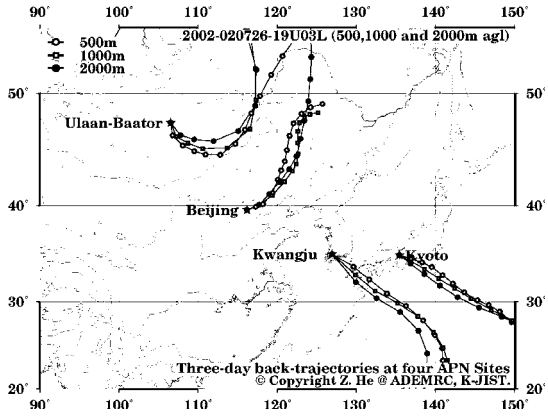

19:00 UTC Time, 07/26/2002

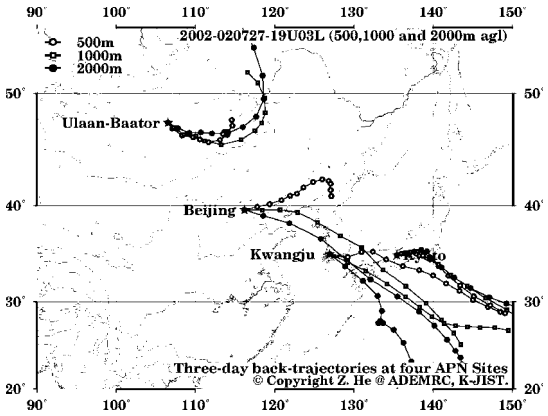

19:00 UTC Time, 07/27/2002

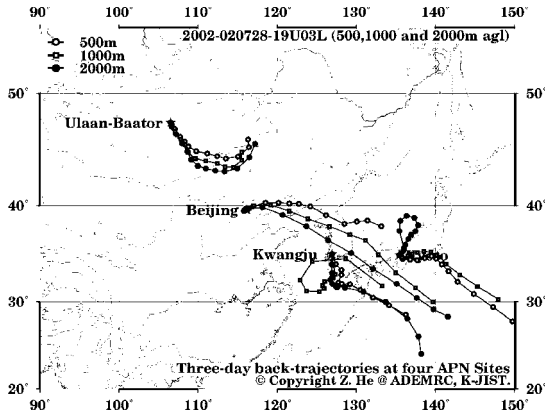

19:00 UTC Time, 07/28/2002

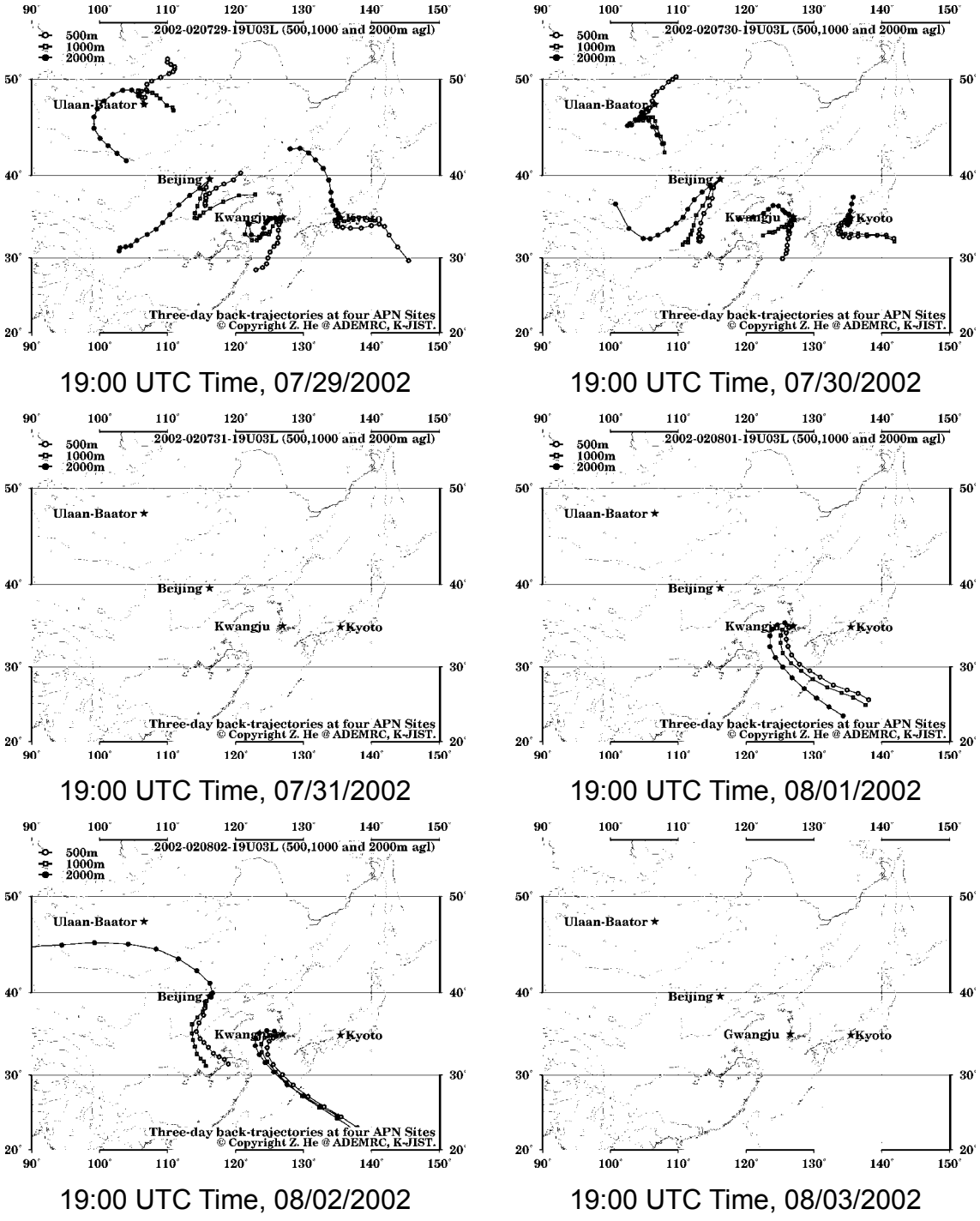

Fig. 4. Back-trajectory patterns at 500, 1000 and 2000m agl during the period of 07/23-08/02/2002. All trajectories ended at 19:00 UTC time, which is local time 03:00a.m., 04:00a.m., 04:00a.m. and 03:00a.m. of Beijing, Gwnagju, Kyoto and Ulaanbaatar, respectively.

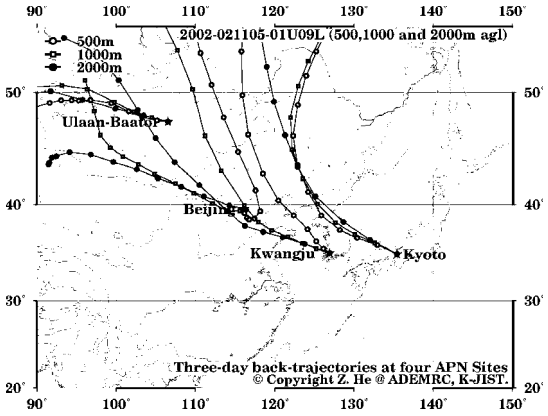

01:00 UTC Time, 11/05/2002

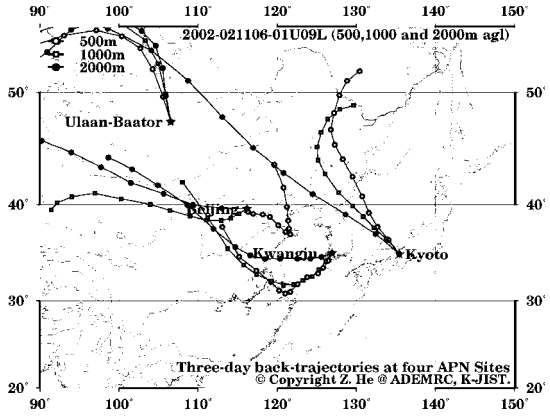

01:00 UTC Time, 11/06/2002

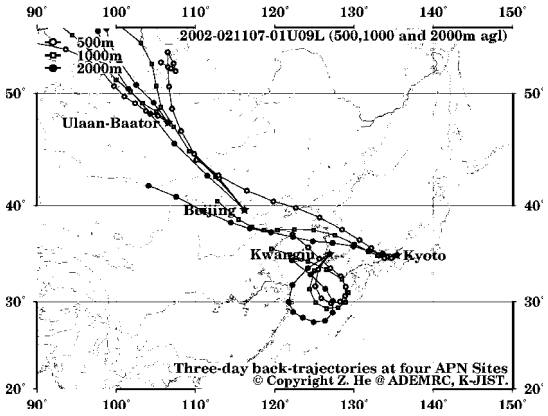

01:00 UTC Time, 11/07/2002

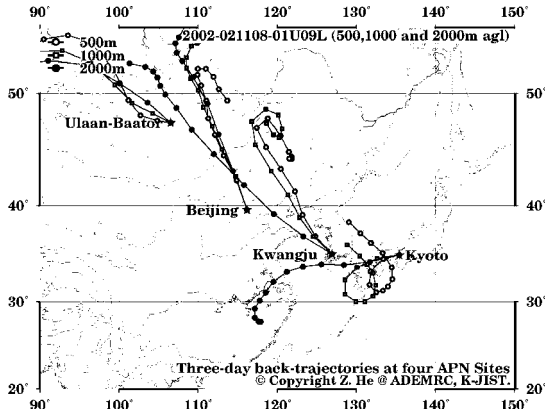

01:00 UTC Time, 11/08/2002

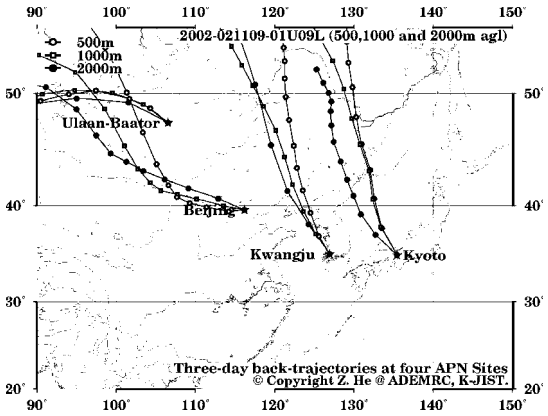

01:00 UTC Time, 11/09/2002

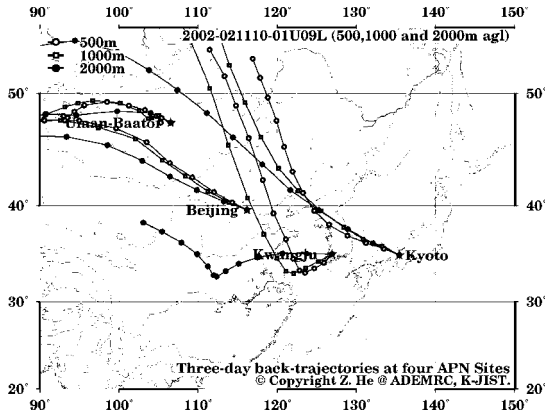

01:00 UTC Time, 11/10/2002

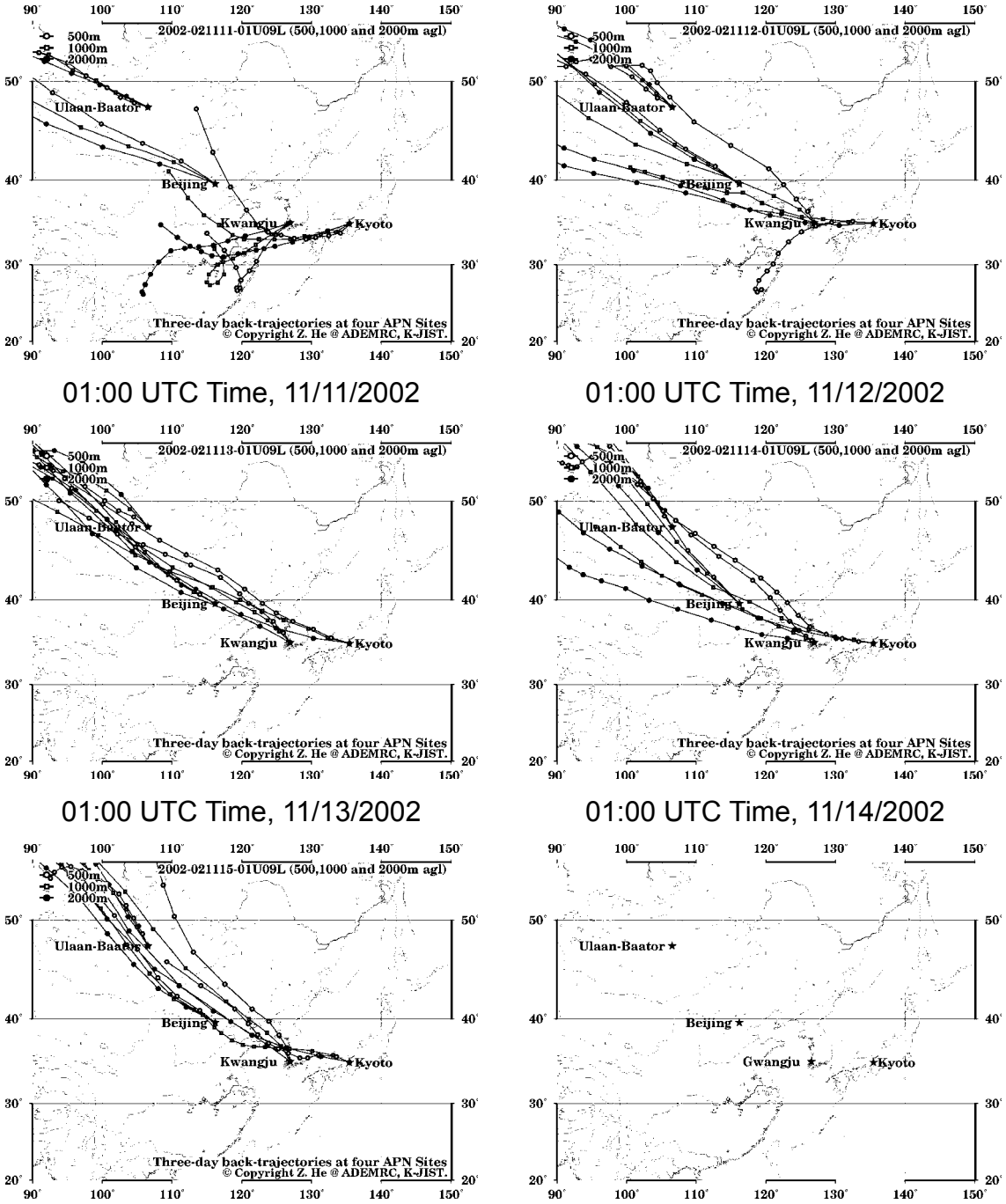

Fig. 5. Back-trajectory patterns at 500, 1000 and 2000m agl during the period of 11/05-11/15/2002. All trajectories ended at 01:00 UTC time, which is local time 09:00p.m., 10:00p.m., 10:00p.m. and 09:00p.m. of Beijing, Gwnagju, Kyoto and Ulaanbaatar, respectively.

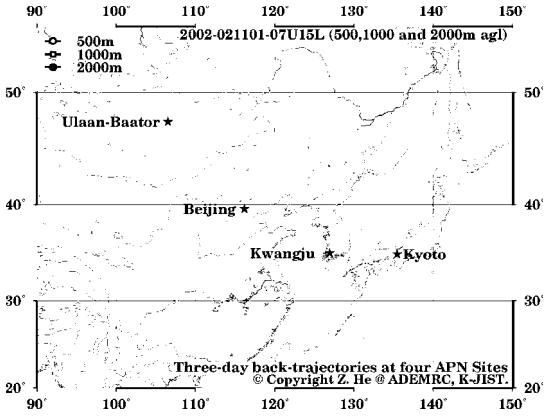

07:00 UTC Time, 11/05/2002

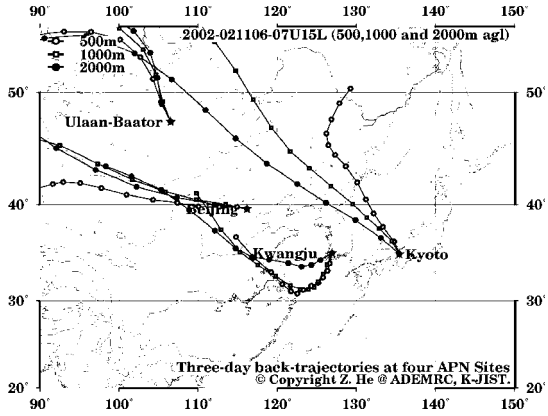

07:00 UTC Time, 11/06/2002

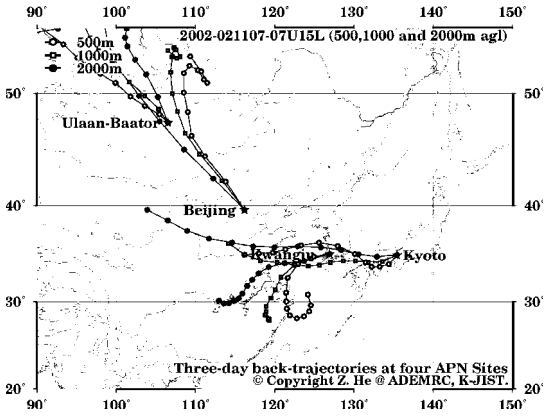

07:00 UTC Time, 11/07/2002

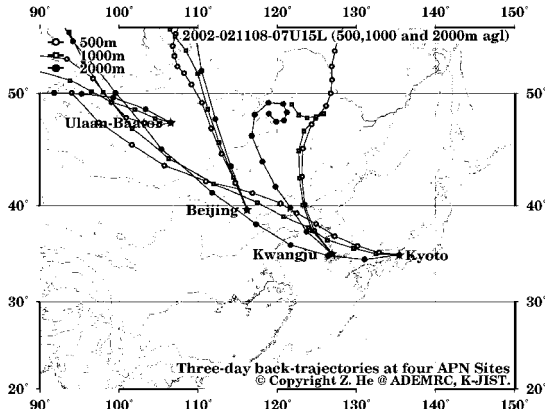

07:00 UTC Time, 11/08/2002

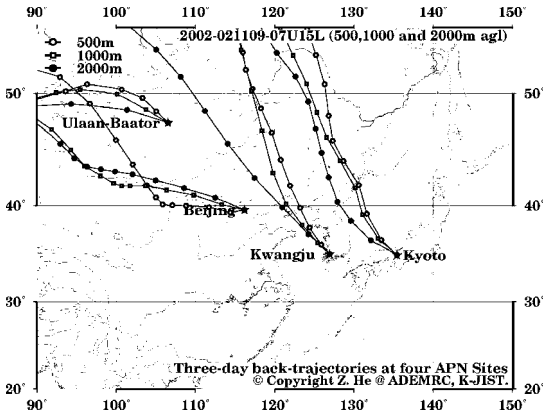

07:00 UTC Time, 11/09/2002

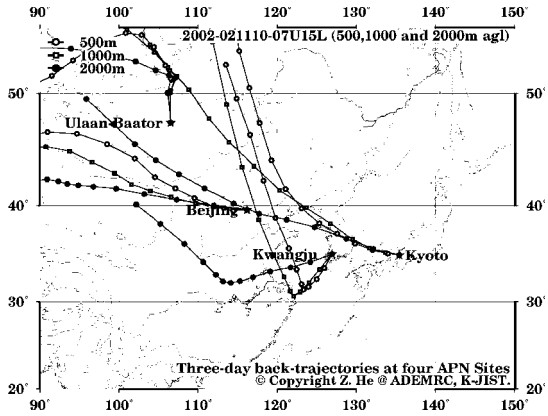

07:00 UTC Time, 11/10/2002

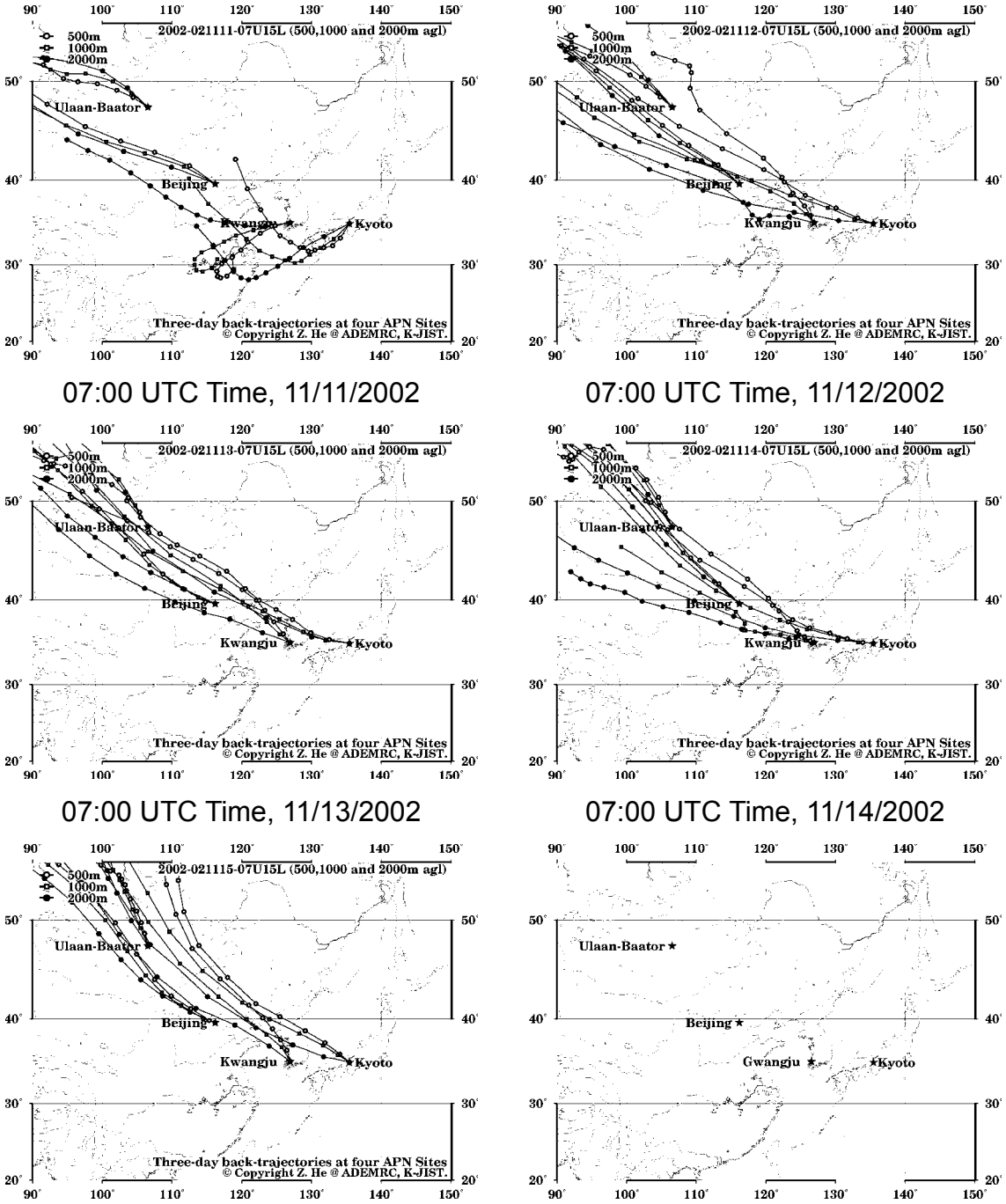

Fig. 6. Back-trajectory patterns at 500, 1000 and 2000m agl during the period of 11/05-11/15/2002. All trajectories ended at 07:00 UTC time, which is local time 15:00p.m., 16:00p.m., 16:00p.m. and 15:00p.m. of Beijing, Gwnagju, Kyoto and Ulaanbaatar, respectively.

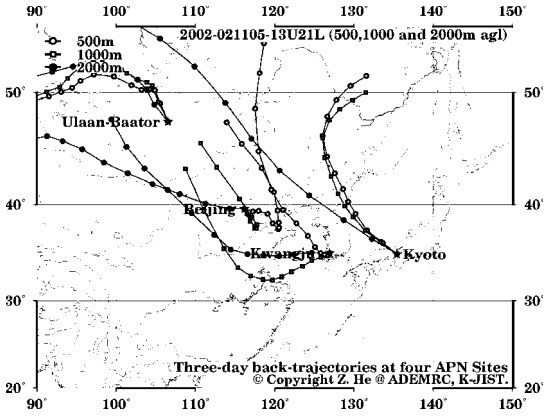

13:00 UTC Time, 11/05/2002

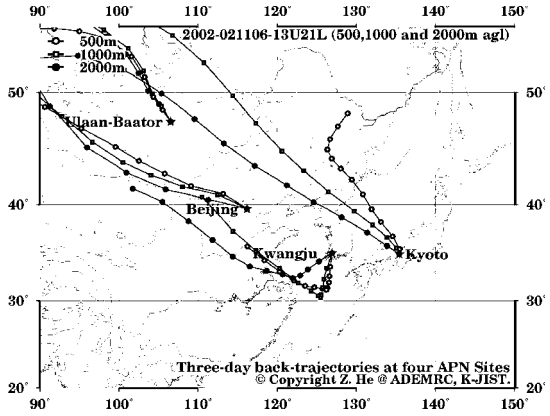

13:00 UTC Time, 11/06/2002

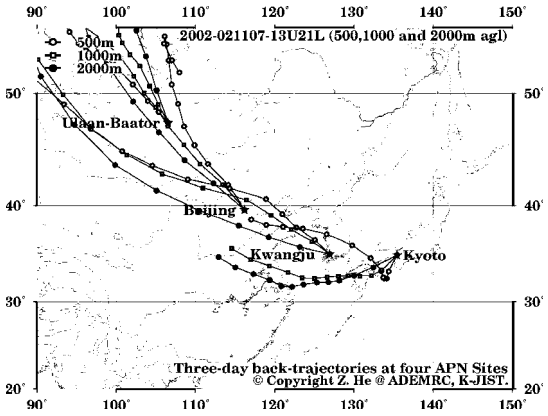

13:00 UTC Time, 11/07/2002

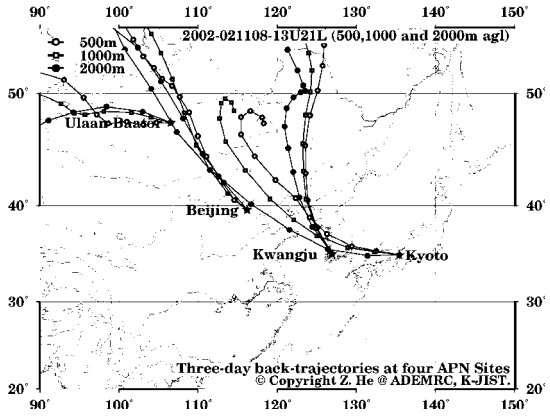

13:00 UTC Time, 11/08/2002

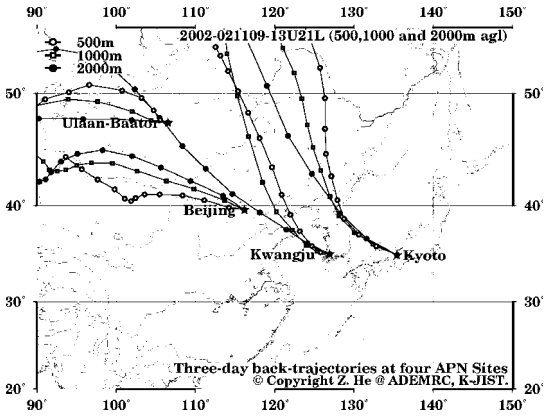

13:00 UTC Time, 11/09/2002

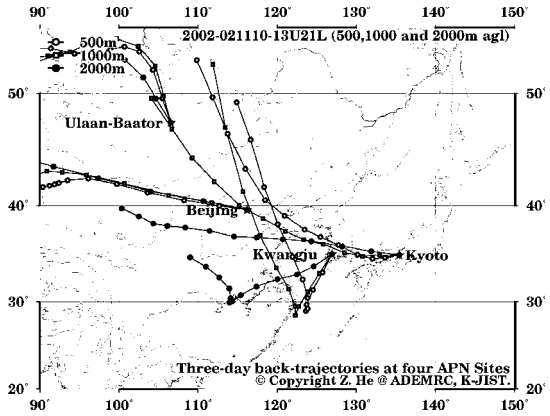

13:00 UTC Time, 11/10/2002

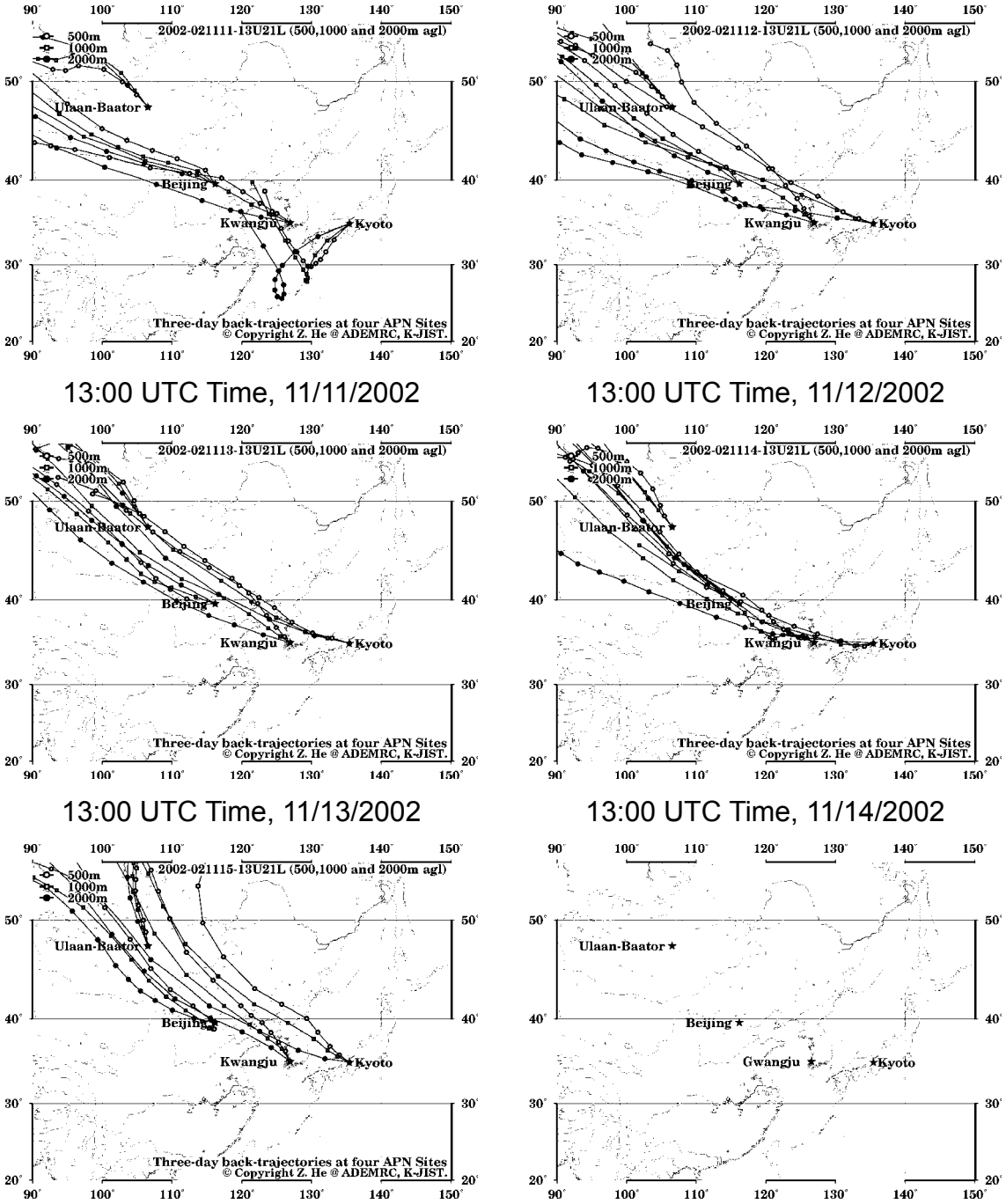

Fig. 7. Back-trajectory patterns at 500, 1000 and 2000m agl during the period of 11/05-11/15/2002. All trajectories ended at 13:00 UTC time, which is local time 21:00p.m., 22:00p.m., 22:00p.m. and 21:00p.m. of Beijing, Gwnagju, Kyoto and Ulaanbaatar, respectively.

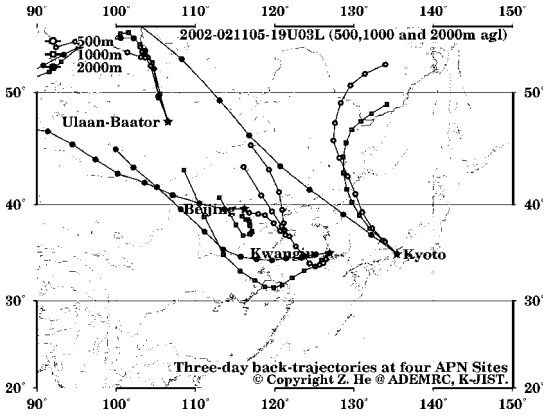

19:00 UTC Time, 11/05/2002

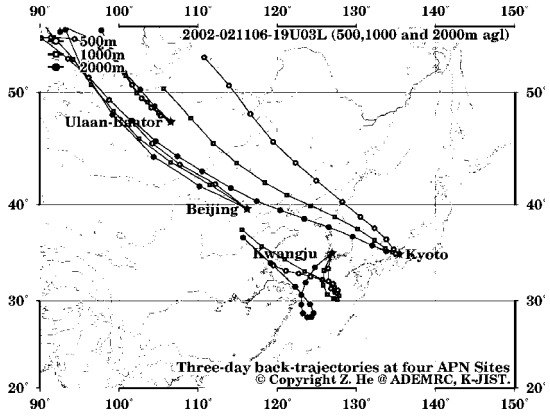

19:00 UTC Time, 11/06/2002

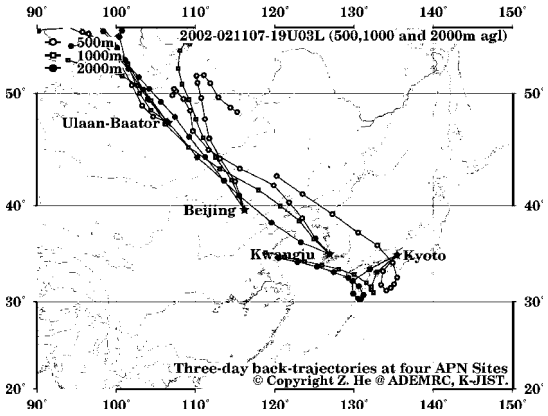

19:00 UTC Time, 11/07/2002

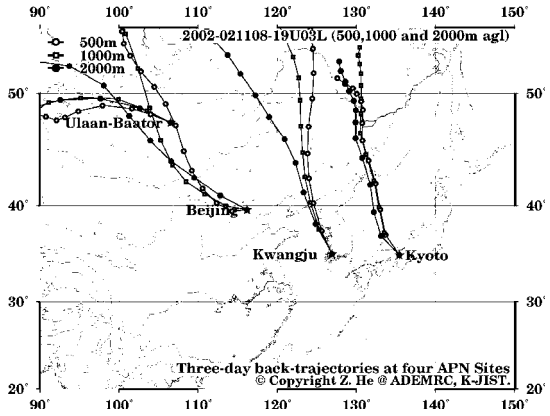

19:00 UTC Time, 11/08/2002

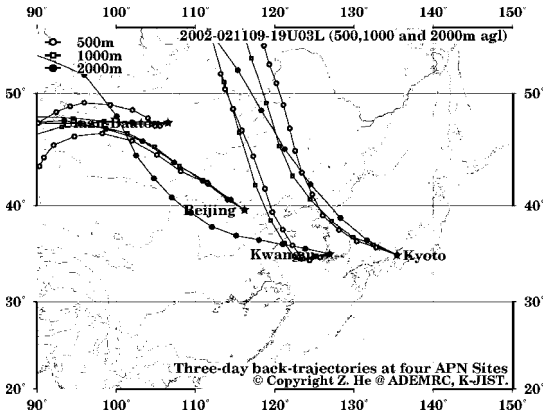

19:00 UTC Time, 11/09/2002

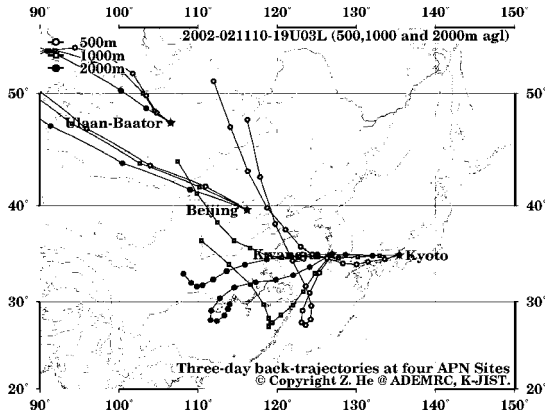

19:00 UTC Time, 11/10/2002

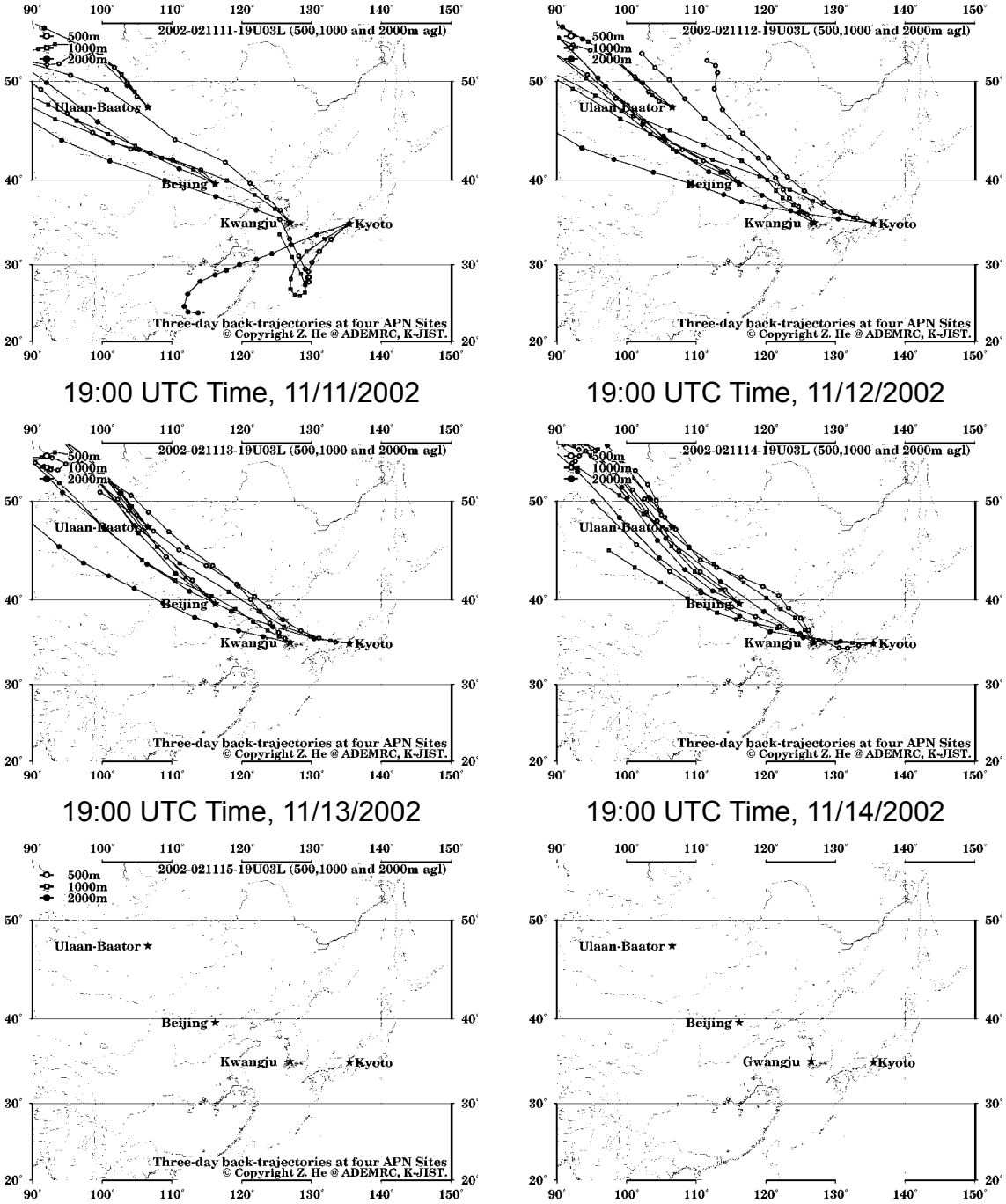

Fig. 8. Back-trajectory patterns at 500, 1000 and 2000m agl during the period of 11/05-11/15/2002. All trajectories ended at 19:00 UTC time, which is local time 03:00a.m., 04:00a.m., 04:00a.m. and 03:00a.m. of Beijing, Gwnagju, Kyoto and Ulaanbaatar, respectively.

Draxler, R.R., 1996. Boundary layer isentropic and kinematic trajectories during the August 1993 North Atlantic Regional Experiment Intensive. Journal of Geophysical Research 101 (D22), 29255-29268.

Draxler, R.R., Hees, G.D., 1997. Description of the HYsplit_4 Modeling System. NOAA Technical Memorandum ERL ARL-224.

Draxler, R.R., Hees, G.D., 1998. An overview of the HYsplit_4 modeling system for trajectories, dispersion, and deposition. Australian Meteorological Magazine 47, 295-308.

He, Z., Kim, Y.J., Ogunjobi, K.O., Hong, C.S., 2003. Characteristics of PM2.5 species and long-range transport of air masses at Taean background station, South Korea. Atmospheric Environment 37, 219-230.

HYSPLIT4 Model, 1997. (http://www.arl.noaa.gov/ready/hysplit4.html). NOAA Air Resources Laboratory, Silver Spring, MD.

NOAA/ARL, 1997, HYSPLIT4 model (http://www.arl.noaa.gov/ready/hyslit4.html), NOAA Air Resources Laboratory, Silver Spring, MD.

Stohl, A., 1998. Computation, accuracy and applications of trajectories- A review and bibliography. Atmospheric Environment 32 (6), 947-966.

V. Radiative Transfer Model

The Tropospheric Ultraviolet and Visible (TUV) model was used to corroborate the aerosol impact on UV radiation and the results were compared with measurement data. TUV model was developed by *Madronich* [1993] at NCAR (National Center for Atmospheric Research). The latest pc version 4.2 (for windows) of the TUV model is available via http://www.acd.ucar.edu/TUV/TUV.zip. Since the optical properties of the atmosphere vary with altitude or optical depth, the atmosphere is divided into 80 adjacent (1 km interval, 80 km altitude) and homogeneous layers in TUV model. In each of the layers, there is an assumption that scattering and absorbing properties are constant, but allowed to be different from layer to layer. Wavelength grids are set from 280 to 420 nm (delta = 1 nm)

Inputs to the radiative transfer model are the time and the location of the measurement, total column ozone, aerosol optical depth, vertical profiles of ozone, temperature and air density profile, the surface albedo, single-scattering albedo of aerosols, asymmetry factor of aerosols, and sea-level pressure.

For total column ozone, TOMS daily data were used. US standard atmosphere (1976) profiles for 45°N and annual mean were applied for temperature, air density, and ozone profile. Surface albedo was set to 0.1. Single scattering albedo and the asymmetry factor of aerosols were set to 0.96 and 0.66 independent of day, respectively, selected from literature [d'*Almeida et al*., 1991]. They show single scattering albedos and asymmetry factors with aerosol types as functions of 8 humidity classes. This study uses 50 % humidity class for ultraviolet wavelength range of average-continental aerosol type. Since calculated AOD values existed from UVMFR, AOD at 331 nm was used to make an aerosol profile

following Elterman aerosol distribution which was provided by TUV model.

In this study, two case were analyzed by using TUV model – one during Asian Dust event and the other during non Asian dust event. On November 12 Asian dust occurred and cloud cover was almost zero. AOD at 331 nm was calculated from UVMFR data and this value was converted to Elterman aerosol profile so that TUV model could read that. It was very clear and clean on November 16, 2002, AOD value at 331 nm was 0.35. Model calculation was conducted for UV-B region (280-315 nm) with aerosol profile from real AOD data and without aerosol condition. The ratios of UV irradiance without aerosol to that with aerosol were 0.84 and 0.94 for Nov 12, and Nov 16, respectively. With aerosol loading due to Asian dust, the surface UV-B radiation decreased to 84 % compared to that without aerosol loading (see Table 1). But for less aerosol loading condition (AOD of 0.35 at 331 nm) the UV-B radiation decreased only 6 %. The comparisons between the daily plot of irradiance for aerosol loading and no aerosol condition are shown in Figure 1.

Table 1. The comparisons of calculated irradiances without aerosol loading and with aerosol loading, their ratio and % decrease of irradiance with aerosol loading compared to the irradiance without aerosol (top : November 12, bottom : November 16).

local time (hr)	no aerosol	aerosol	no aerosol/aerosol	% decrease due to aerosol loadings
8.5	0.06	0.05	0.89	0.11
9.5	0.21	0.18	0.84	0.156
10.5	0.42	0.35	0.83	0.17
11.5	0.58	0.48	0.84	0.16
12.5	0.62	0.52	0.84	0.16
13.5	0.52	0.44	0.84	0.16
14.5	0.34	0.28	0.84	0.16
15.5	0.14	0.12	0.86	0.14
16.5	0.03	0.02	0.93	0.07

local time (hr)	no aerosol	aerosol	no aerosol/aerosol	% decrease due to aerosol loadings
8.5	0.05	0.05	0.96	0.04
9.5	0.19	0.18	0.94	0.06
10.5	0.39	0.36	0.94	0.06
11.5	0.54	0.51	0.94	0.06
12.5	0.58	0.55	0.94	0.06
13.5	0.49	0.46	0.94	0.06
14.5	0.32	0.30	0.94	0.06
15.5	0.13	0.12	0.95	0.05
16.5	0.02	0.02	0.98	0.02

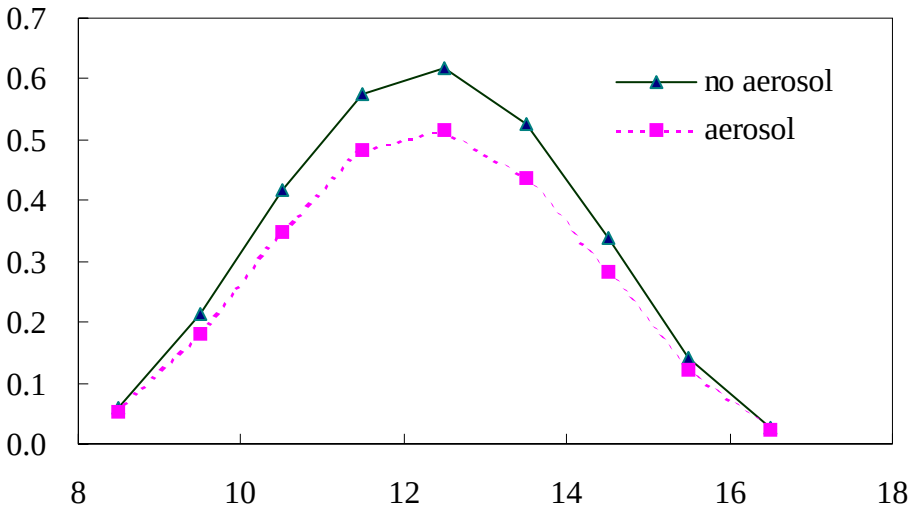

Figure 1. The comparison of daily plot of calculated irradiance on Nov 12, 2002 (AOD = 1.07)

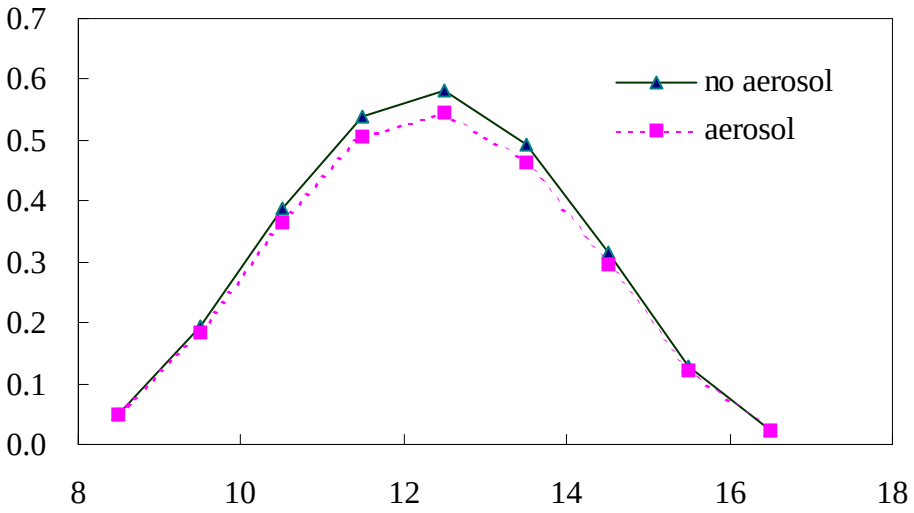

Figure 1. The comparison of daily plot of calculated irradiance on Nov 12, 2002 with AOD of 1.07 (top), and Nov 16, 2002 with AOD of 0.35 (bottom.)